INFORMATION TO USERS

This manuscript has been reproduced from the microfilm master. UMI films the text directly from the original or copy submitted. Thus, some thesis and dissertation copies are in typewriter face, while others may be from any type of computer printer.

The quality of this reproduction is dependent upon the quality of the copy submitted. Broken or indistinct print, colored or poor quality illustrations and photographs, print bleedthrough, substandard margins, and improper alignment can adversely affect reproduction.

In the unlikely event that the author did not send UMI a complete manuscript and there are missing pages, these will be noted. Also, if unauthorized copyright material had to be removed, a note will indicate the deletion.

Oversize materials (e.g., maps, drawings, charts) are reproduced by sectioning the original, beginning at the upper left-hand corner and continuing from left to right in equal sections with small overlaps.

Photographs included in the original manuscript have been reproduced xerographically in this copy. Higher quality 6" x 9" black and white photographic prints are available for any photographs or illustrations appearing in this copy for an additional charge. Contact UMI directly to order.

Bell & Howell Information and Learning
300 North Zeeb Road, Ann Arbor, MI 48106-1346 USA

UMI®
800-521-0600

UNIVERSITY OF OKLAHOMA

GRADUATE COLLEGE

DIRECT ANALYSIS OF TYPE Ia SUPERNOVAE SPECTRA

A Dissertation

SUBMITTED TO THE GRADUATE FACULTY

in partial fulfillment of the requirements for the

degree of

Doctor of Philosophy

By

ADAM K FISHER
Norman, Oklahoma
2000

DIRECT ANALYSIS OF TYPE Ia SUPERNOVAE SPECTRA

A Dissertation APPROVED FOR THE
DEPARTMENT OF PHYSICS AND ASTRONOMY

BY

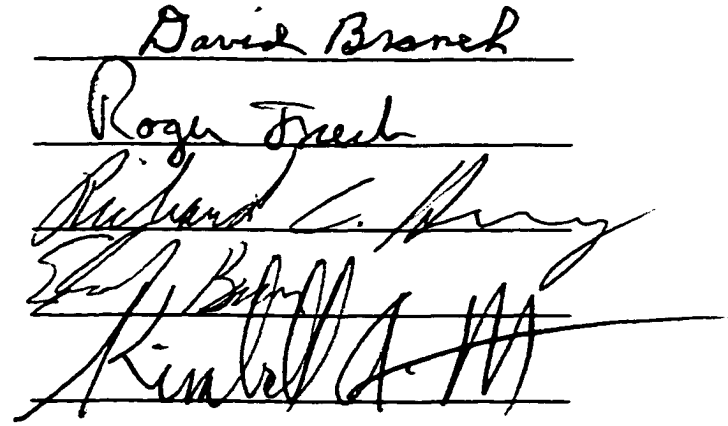

Acknowledgements

The Fishers
(Corrine,
David, Andrew, Samuel,
Mom, Dad)

Dr. David Branch,

Alston and Beatrice Reed,

Olen Boydstun,

Dr. Herczeg,
My Committee,
Thomas E. Vaughan,
and Peter Nugent.

Sonnet XIV by Shakespeare

Not from the stars do I my judgment pluck;
And yet methinks I have astronomy,
But not to tell of good or evil lcuk,
Of plagues, of dearths, or season's quality;
Nor can I fortune to brief minues tell,
Pointing to each his thunder, rain and wind,
Or say with princes if it shall go well,
By oft predict that I in heaven find:
But from thine eyes my knowledge I derive,
And, constant stars, in them I read such art
As truth and beauty shall together thrive,
If from thyself to store thou wouldst convert;
Or else of thee this I prognosticate:
Thy end is thruth's and beauty's doom and date.

Table of Contents

Page	Chapter	
1	1	Introduction
3	2	Supernovae in general
8	3	SYNNEW
36	4	Spectral Diagnostics
55	5	The Minimum Ejection Velocity of Calcium in Type Ia Supernovae and the Value of the Hubble Constant.
68	6	Evidence for a High Velocity Carbon-Rich Layer in the Type Ia Supernova 1990N
82	7	On the Spectrum and Nature of the Peculiar Type Ia Supernova 1991T
112	8	Conclusions
113	9	References
115	Appendix 1	The SYNNEW code
130	Appendix 2	Flow charts and variable lists
146	Appendix 3	Example SYNNEW input files
150	Appendix 4	Auxiliary programs

Chapter 1. Introduction

How old is the universe? What is its fate? Mankind has been searching for the answers to these cosmological questions for thousands of years. Searching for these answers has led to an intense study of supernovae and, in particular, the brightest, most regular class of supernovae (Type Ia). Type Ia supernovae (SNe Ia) have several properties that encourage their use in answering cosmological questions: brightness, distinctiveness, uniformity, frequency, and a basic theoretical understanding. Their brightness at maximum light rivals the light of an entire galaxy. This allows them to be discovered out to redshifts approaching 1 (Perlmutter et al. 1998, Garnavich et al. 1998). Their distinctiveness allows SNe Ia to be easily separated from all other astronomical occurrences with a small amount of information. Their uniformity allows for a statistical treatment permitting their use in determining the Hubble constant (Branch, 1998). Their frequency has two effects. First, they are common enough that they are found relatively nearby for us to study in detail (about 1 per year in the Virgo supercluster). Second, they are common enough to allow a large number of them to be discovered at cosmologically interestings redshifts. Their brightness has allowed their evolution to be followed through various phases of their development. Their distinctiveness has allowed us to trim away other phenomena. Their uniformity was the first key to unlocking their puzzle. And their rate of occurrence also puts constraints on what progenitor systems are responsible for SNe Ia. The purpose of this work is to increase the basic theoretical understanding of SNe Ia by

extracting information about the compositions and velocities of the matter that they eject into space.

This work presents the results of an intense analysis of near maximum light spectra of SNe Ia. This stage of a SN Ia's development is important for several reasons. First, this is the only phase at which the most distant supernovae can be observed. It is when the SN is the brightest, thus making the identification of peculiarities in this phase essential to avoid cosmological pitfalls. Second, it is only at early times that the outer layers of the SNe dominate the spectral formation. This produces strong constraints upon explosion models. Third, this phase shows the most variation in SNe Ia, as at later times iron peak elements dominate the spectrum, in all subclasses. It is this variation in SNe Ia that is both the dilemma and salvation of SNe Ia. It provides us with varations on a theme that need to be explained, resulting in a better model for all SNe Ia. It provides us with the daunting task of removing the effects of distinctiveness from cosmologically interesting samples of SNe Ia.

Chapter 2 - Supernovae in general.

Supernovae and novae are classes of variable stars that greatly increase their luminosity for a time. The difference between a nova and a supernova is that a supernova results in the ejection of a large fraction (if not all) of the mass of the precursor, whereas a nova results in the ejection of a small amount of surface material.

There are several effects that cause a supernova to change its appearance. The dominant effect is that the supernova is becoming more and more transparent as it ages. This allows us to see deeper and deeper into the supernova (in mass coordinates). The other effect is that the temperature of the supernova is a strong function of time. This effect is caused by the decreasing radioactive energy being deposited and the increasing transparency of the supernova atmosphere. Figure 1 shows the spectral evolution of SN 1994D, a well observed SN Ia. Initially the spectra are dominated by the features caused by elements Carbon through Calcium, towards the end of graph iron peak elements become dominant, with a few notable exception such as the sodium dip near 5700 Angstroms. Figure 2 shows the spectral variation among SNe Ia near maximum light.

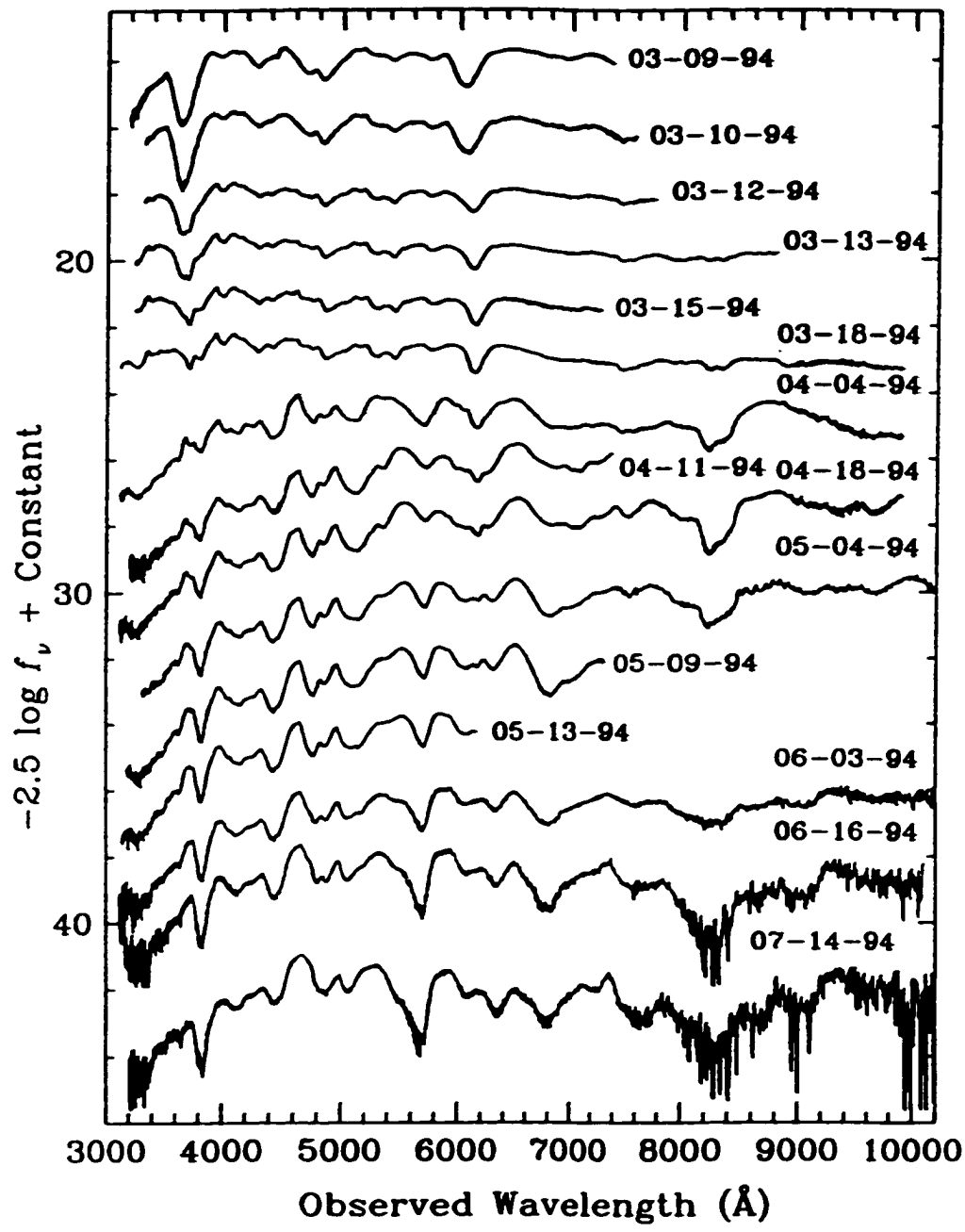

Figure 1. This figure shows the spectral evolution of the well observed SN 1994D. (from page 5 of "Type Ia Supernovae: Observational Overview" by Alexei Filippenko in **Thermonuclear Supernovae** edited by P. Ruiz-Lapuente, R. Canal and J. Isern.

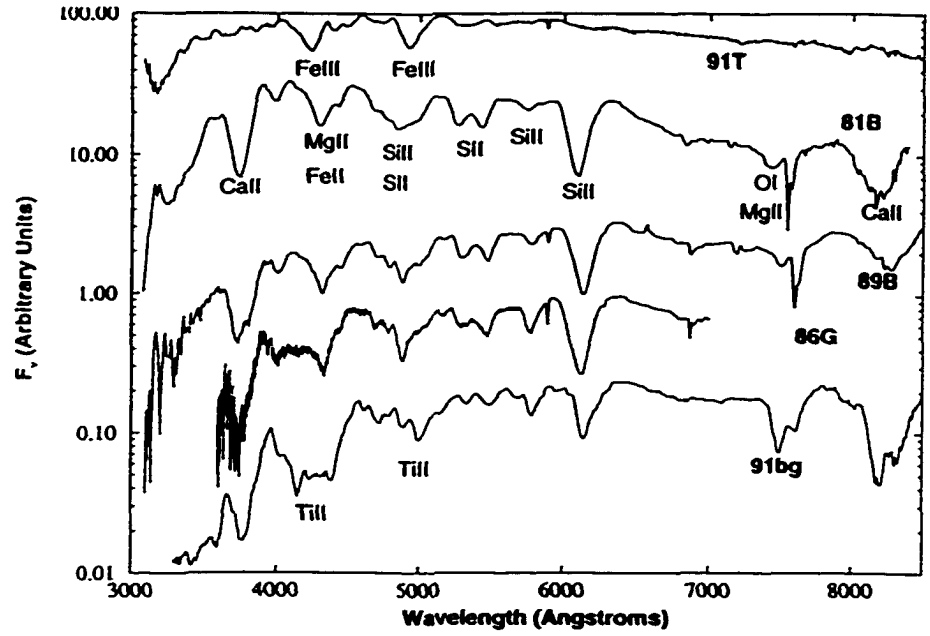

Figure 2. A comparison of near-maximum light spectra of two normal SNe Ia (SN 1981B: Branch et al. 1983; SN 1989B: Wells et al. 1993) and three peculiar SNe Ia (SN 1991T: Filippenko et al 1992; SN 1986G: Cristiani et al. 1992; SN 1991bg: Filippenko et al. 1992b). From Branch, Fisher, Nugent (1993).

Instead of these effects hampering the study of supernovae, they greatly enhance our ability to do so. As we observe a supernova again and again, layer after layer becomes transparent allowing us to see what is closer towards the center, much like the peeling of an onion. Also the temperature variation can allow us to solve problems that have two comparable solutions at a single temperature. The most obvious problem that can be solved this way is the problem of telling the difference between helium and sodium. The strongest optical lines of these elements are close enough together that the presence of sodium could be misdiagnosed as helium and vice versa. Luckily, sodium tends to strengthen in intensity as the supernova cools while helium tends to weaken in intensity. This difference can aid us in determining whether the feature is produced by sodium, helium or a combination of both.

Supernovae are currently being studied using several different approaches. One approach is the pure statistical method. This is the favorite method of most observers in the supernovae community. Observations are made, correlated, and extrapolated (or interpolated) with little need for theoretical backing. This approach is exemplified by the recent high-z supernova searches. A second approach is the pure theoretical or *ab initio* approach. While being the only approach that can convincingly produce a complete understanding of supernovae, (or even some types of supernovae), the *ab initio* approach is currently too daunting a task for the supernova theoreticians. Thus the dominant approach to studying supernova, theoretically, is the phenomenological approach. In this method, theoretical ideas are compared to actual observations. This is the

method that is favored and used by the author. There is quite a range of variability in this approach, from methods close to *ab initio* to methods close to the statistical methods. In the next chapter, I will describe the mechanics of a program that has been used to study the phenomena that are supernovae.

Chapter 3 -- SYNNEW

SYNNEW is a highly parameterized spectrum synthesis program. The program used for this work is a second generation program based upon one developed by Branch (Branch et al. 1983, 1985, Jeffery & Branch 1990). The goal of this program is to allow us to extract information directly from spectral observations of supernovae in the photospheric phase. This is different from the purely observational approach, where simple relationships are sought between measurable properties of spectra and/or light curves. It is also different from the *ab initio* approach, where the goal is to first model the explosion in a sophisticated hydrodynamic code and then to calculate its spectra (Baron et al 1996, Nugent et al 1997, Höflich 1995, Eastman & Pinto 1993). These approaches are complementary. The first method provides information that acts as a guide to more sophisticated calculations as well as providing direction to this and other works. The *ab initio* approach is also essential, as only it can provide an acceptably complete theory explaining supernovae. In order to meet the goal of having a quick program, capable of calculating spectra as realistic as possible, several important assumptions have been made. For the benefit of those who will use SYNNEW, in the years to come, it is described in some detail, in this chapter. Those who are not interested in how the program works may choose to move on to Chapter 4, which illustrates how SYNNEW can be used to diagnose the physical conditions and composition structures of SNe Ia. Chapters 5,6, and

7 present analyses of individual SNe Ia (as already published in refereed journals).

First, I assume that the supernova is spherical and in homologous expansion. This means that the radial velocity (V) of a mass element is proportional to its radius (R). This assumption is easily justified as the forces of pressure and gravity become negligible soon after the explosion. After that point the mass element is in constant linear motion,

$$R = Vt + R_0$$

where t is the time since explosion and R_0 is the effective displacement of that element during the hydrodynamic phase. The R_0 term becomes negligible soon after the explosion, leaving R proportional to V.

Second, I approximate continuum transport with a sharp photosphere at a parameterized velocity (v_{phot}). This photosphere is a blackbody with a parameterized temperature (Tbb). This approximation is partially justified by the success of the program in modeling spectra, but the caveat is given that this approximation basically nullifies any information on the absolute flux being emitted, as this sensitiveity depends on the details of continuum transport. An important consequence of this assumption is the supernova can be subdivided into five regions based on the observers point of view. The first region is inside the photosphere, since the photosphere is completely opaque this region is completely obscurred. The second

region is the photosphere itself, since we are assuming spherical symetry the photosphere is located at a constant velocity relative to the center of the explosion. The photosphere's emits light like a blackbody and absorbs all light incident apon it. The third region lies between the photosphere and the observer. This region is called the absorption region, as the material in this region can interact with light traveling from the photosphere directly towards the observer. The forth region lies on the opposite side of the photosphere from the observer. No light from this region can directly reach the observer, so it is called the occulted region. The fifth region lies to the side of the photosphere and is shaped like a doughnut, this is called the emmission region. The matter in this region cannot interact with light traveling from the photosphere directly towards the observer, but it can scatter light from the photosphere towards the observer (see figure 3). It should be noted that although the supernova is assumed to be spherically symetric the addition of the observer defines an axis,therefore all calculations that are internal to the supernova are calculated with spherical symetry, but all calculations relating to what the observer sees (i.e. the output spectrum) must be calculated using cylindrical symetry.

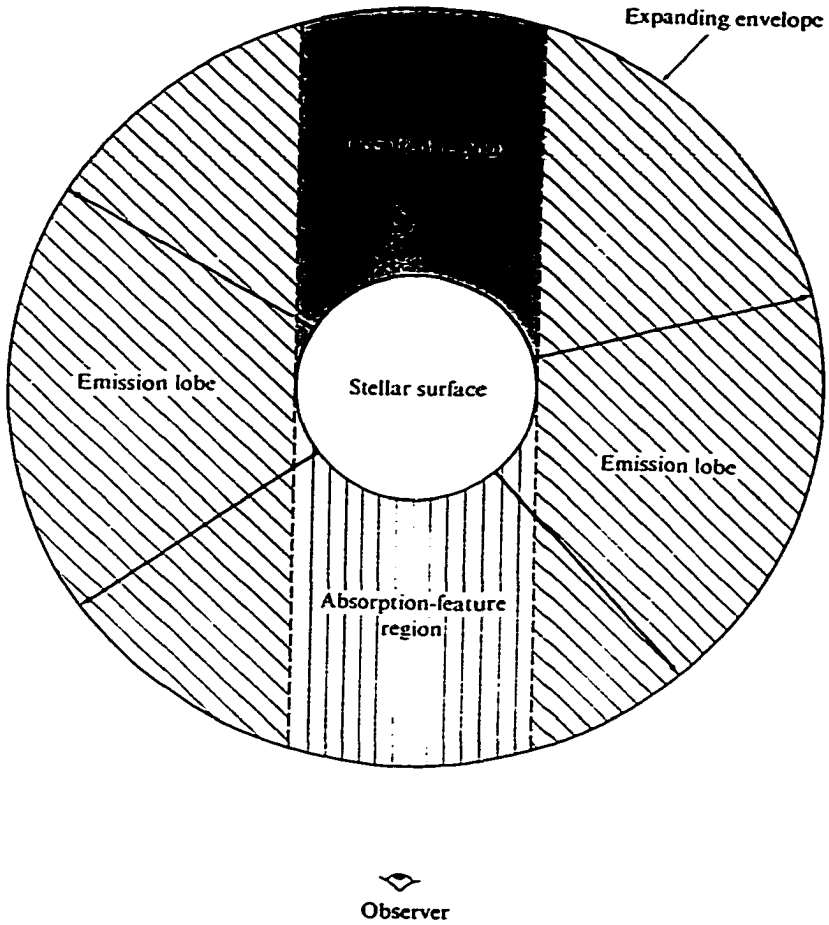

Figure 3. (From *Stellar Atmospheres* by D. Mihalas, page 473) This figure is a schematic diagram of an expanding envelope surrounding a stellar surface (in this case the photosphere). The material in the occulted region is blocked from view by the stellar disk, and cannot be seen by an external observer.

Third, I use the Sobelev approximation to include the effect of atomic transitions on the spectrum (Mihalas,1978, Jeffery & Branch 1990). The Sobelev approximation, simply put is the assumption that the rapid expansion of the atmosphere dominates radiative transport. Imagine a photon that has the same wavelength as a spectral line, as this photon travels it is constantly being redshifted relative to the material it is flying through. After it travels a certain distance, it will have redshifted so much, it will no longer be able to interact with that spectral line. Thus the problem of radiative transport problem switches from a global problem to a local problem. Instead of having to simultaneously solve the radiative transfer equation for all locations in the supernova, the radiative transfer problem reduces down to two local problems. The first is determining the probability of escape for a photon at this location. The negative log of the probability of escape is called the optical depth. My parameterization of the optical depths of various transitions allows me to set the optical depth of a reference line for each ionization stage of each element. I then determine the relative optical depths, of other transitions, in that ionization stage of that element, by assuming that the ratios of the populations of the lower levels of the transitions are in local thermodynamic equilibrium at some parameterized temperature (T_{ex}), and by taking into account the difference in the oscillator strength of each line, and then by including the corrections for stimulated emission. The second problem that is required to solve the radiative transfer equation has to do with the quantity of light that is at this location. This is called the source function. In my model the source function is set equal to the amount of light that arrives at

this location. This simply means that the number of photons that come into a location is the same as the number that depart that location. This ignores several processes that are included in more sophisticated models (photon creation by collisional excitation of a state, photon spliting where one photon is absorbed and two or more less energetic photons are emmitted, and photon distruction by collisional de-excitation). A short hand way of saying this is that I assume that each transition is in complete resonant scattering. Another important assumption that is required for this model is that when a photon is scattered by being absorbed and quickly re-emmitted by an atom, the angle at which the new photon is departs is independent of the angle at which the original photon arrived. This assumption is called complete angular redistribution.

Another assumption used in the calculations is that the radial dependence of the optical depth of a transition is characterized by an exponential function. The basis for this assumption came from the approximately exponential behavior of the density in several hydrodynamic calculations. This assumption is not of great importance here, as other parameterizations (such as a power law) produce similar results, but it will be tested in future works that probe deeper into the supernovae.

Combining these assumptions with the extensive database of 40 million atomic transitions provided by Kurucz (1994) is the basis of this work. Now I will describe the way each of these routines works. For further detail, the code itself is provided as Appendix 1 and annotated flow chart diagrams and variable lists are presented in Appendix 2. Sample input files are contained in Appendix 3.

Appendix 4 provides a description of several auxiliary programs used during the spectrum fitting process.

Section 1 - SYNNEW

SYNNEW begins by initializing the input variables, reading in the reference line data and user inputs in a subroutine called INITIALIZE. Several small routines are executed next. BB loads the appropriate blackbody function into an array named black. For each radial zone, THETA calculates the geometrical dilution factor (which is the fraction of the sky subtended by the photosphere) and then divides the solid angle subtended by the photosphere and the remaining solid angle into ten parts each, selecting twenty rays to represent these regions.

In order to avoid reading unused portions of the linelist, the linelist was split into thirty sections by wavelength. SYNNEW calculates the starting and stopping files that will be used. If these files are out of the range of the available files, the program terminates with an error message.

The principle loop of SYNNEW is the loop over wavelength files. Inside this loop SYNNEW calls FILE to set up file information. Then the GETBIN routine reads in the optical depths for each wavelength bin at each radial zone. Each wavelength bin corresponds to a velocity width of three hundred kilometers per second. The secondary loop of SYNNEW loops over wavelength bins. SYNNEW uses the routine SOURCE to calculate the source function of one wavelength bin at a time. After each source function is calculated, SYNNEW checks to see if it can calculate a portion of the output spectrum. If it can, it will do so using the routine SPECTRUM, which not only calculates the output spectrum, but also keeps track of the bluest line that can interact with the current

transition. Photons redshift with respect to the matter as they propagate through the supernova (see section 7). All lines to the blue of this transition can be discarded in order to conserve computer memory. Once SYNNEW completes as much of the spectrum as it can, it repeats the process with the next wavelength bin, until all the wavelength bins that were read in have been used. Once there are no more known wavelength bins SYNNEW checks to see if it can read in the next wavelengths without running out of memory. If it cannot, it will recycle or shuffle memory. In this process the known lines are moved from near the end of the data arrays to the front and future wavelength bins will fill in after them. See Figure 4(a,b) for a graphical representation of this procedure. The main goal of this routine is to trade off a little bit of calculation time in order to use less memory. This hopefully allows the program to run, on most machines, without paging. Then the program loops back to the loop over wavelength files and continues until the final wavelength files have been used. Then, just to tidy things up a little, the last portion of output spectrum is calculated by the routine SPECTRUM, at which time the program terminates.

SYNNEW works through the first wavelength region
GETBIN loads the optical depths for the first species.

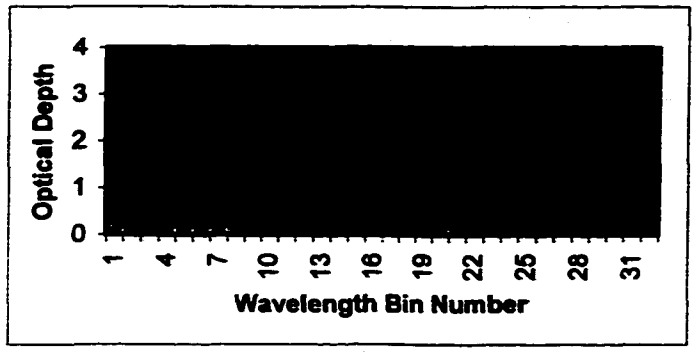

GETBIN loads each species one at a time.

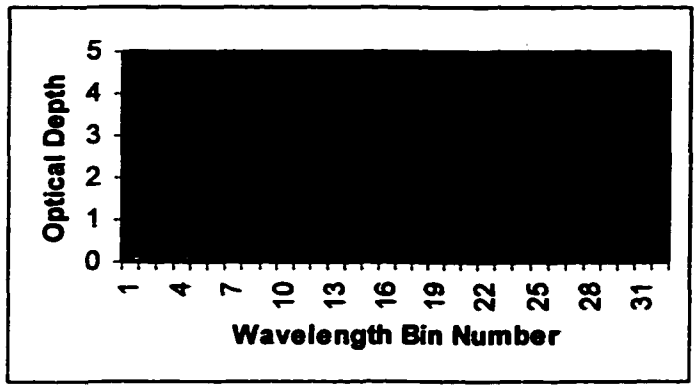

GETBIN then removes bins with insignificant optical depth.

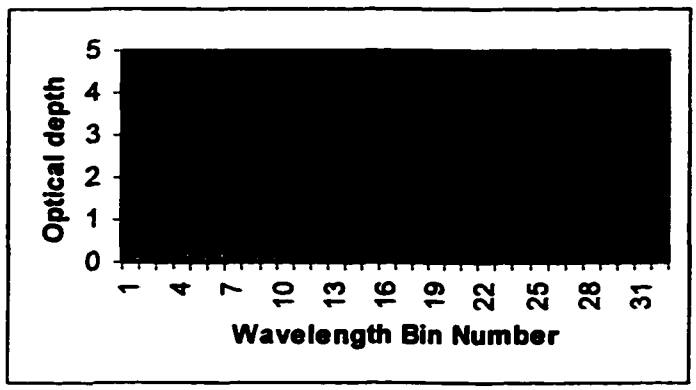

Figure 4a - Shuffling

GETBIN then returns to SYNNEW, which calculates the source function for each wavelength bin and as much of the output spectrum as it can. SYNNEW then calls GETBIN to read in the next wavelength region. GETBIN goes through the same procedure resulting in something like the figure below.

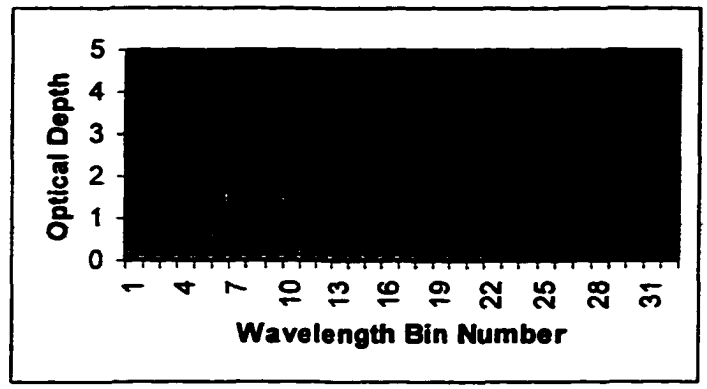

GETBIN returns to SYNNEW, which calculates more source functions and more of the output spectrum. Eventually GETBIN is invoked when there are not enough wavelength bins remaining to accomplish GETBIN's task, so it determines the smallest (bluest) wavelength bin that might be needed in future calculations and discards all bins smaller (bluer) than that one. GETBIN shuffles the remaining wavelength bins so that the first bin has a wavelength bin number of one. GETBIN is now capable of loading the next wavelength region.

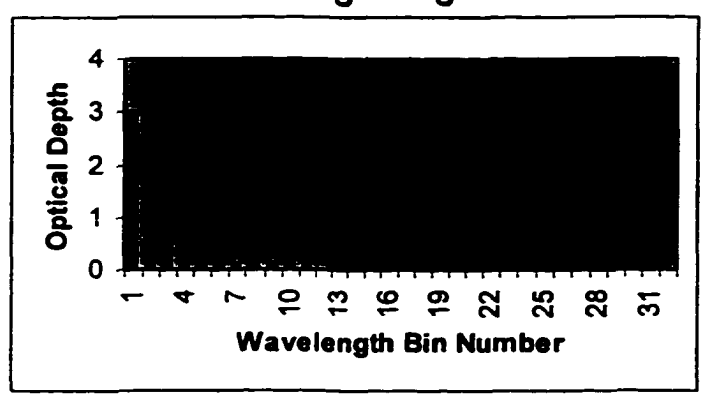

Figure 4b- Shuffling

Section 2- INITIALIZE

The routine INITIALIZE begins by reading in the wavelengths, log(gf)'s and lower level energy of a reference line for each species. This information is found in the file "ref.dat". The reference line for each species was usually chosen to be the most prominent line in the optical region.

After the reference data has been loaded INITIALIZE loads the user inputs from the file "in.dat". This file contains following variables:

- vphot (the photospheric velocity)
- vmax (the maximum velocity included in the calculation)
- tbb (the blackbody temperature of the photosphere)
- ea (the bluest wavelength considered)
- eb (the reddest wavelength considered)
- grid (the number of zones per photospheric radius)
- taumin (the minimum optical depth included in the calculation)
- flambda (a logical variable that is true for f_λ and false for f_ν)
- numref (the number of reference optical depths considered)
- zeta (the dilution factor of the photosphere)
- nlam (the number of wavelength points for the output spectrum)
- stspec (the bluest wavelength where the output spectrum will be calculated; this was inserted to allow the effects of u-v line blanketing to be included in the line interactions, but to not waste time calculating the region of the spectrum that was not observed)
- pwrlaw (a logical variable that is true if the optical depth profiles are supposed to follow a power law and false if the they are to follow an exponential decay)

- pwrlawin (the index of that power law).

This file also has several arrays which contain information specific to each species. These arrays are:

- an (atomic number)
- ai (ionization stage, 0 for neutral, 1 for singly ionized, etc.)
- vmine (minimum velocity in units of Mm/s)
- vmaxe (maximum velocity in units of Mm/s)
- ve (e-folding velocity in units of Mm/s)
- temp (the excitation temperature in units of kK).

The arrays are arranged so that each index represents a different species, i.e. an(1) contains the atomic number of species one, ai(1) contains the ionization stage of species one and temp(5) contains the excitation temperature of species 5. One note about the optical depth profile is, that if the variable pwrlaw is true, then the ve array is overridden and is meaningless.

Note to future SYNNEW programmers: INITIALIZE uses the Fortran 77 namelist construct. If SYNNEW is upgraded to a later version of Fortran, several changes will need to be made to INITIALIZE and the file in.dat. The read command will need to have the form READ (5, NML=parms) instead of READ (5,parms). The in.dat file will have to be modified to begin with &parms and end with a backslash (\) instead of begining with $parms and ending with $END.

After the user inputs are loaded, INITIALIZE sets up the radial profiles for each species. Care is taken to anit-correct for the effect of stimulated emission on the optical depth of the reference line so that when the correction for stimulated emission is applied to the

reference line during the main portion of the calculation it will have the user defined optical depth. If the user trys to use a species that does not have a proper reference line the program terminates, allowing the user to correct the problem.

Finally INITIALIZE deletes species that have zero optical depth and packs the remaining species to the front of the arrays. The routine then returns back to SYNNEW.

Section 3- BB (Blackbody)

The subroutine BB is about as simple as it gets. It loads the array xplot with the wavelength points for which the output spectrum will be calculated. These wavelengths are selected to span from ea to eb, in such a way as to make the change in wavelength proportional to the wavelength itself. Also, the array black is loaded with a normalized blackbody function of a temperature tbb at each of those wavelengths. The blackbody is normalized so that black is set to 1.0 for the first wavelength. The routine then returns to SYNNEW.

Section 4- THETA

THETA is a rather cryptic subroutine that performs several angular tasks. THETA chooses the rays which are going to be used to calculate the average intensity in the SOURCE subroutine. Most of the effort here is to load the array ctheta with various information. For each radial zone, THETA divides the whole sky into two portions. The first is the region of the sky subtended by the photosphere. THETA then samples each of these regions, with ten rays distributed equally in solid angle. For each radial zone, the cosine of these angles are loaded into the first ten elements of the array ctheta. Next THETA samples the remaining portion of the sky with ten rays and stores the cosine of these angles in the next ten elements of the array ctheta. Finally THETA loads the dilution factor as the last element in the array ctheta. Special care is made to assure that the first radial zone is taken care of properly. The routine then returns to SYNNEW.

Section 5- FILE

FILE reads in several parameters that are used in reading in the wavelength files. This information is stored in the file linelist.info. The first thing FILE does is to initialize the filparm array, where all the information will be stored. For each species, present in the calculation, filparm contains five pieces of information. The first two elements contain parameters used in the compression of the oscillator strengths for each wavelength region of each species. The next two elements contain parameters relating to the excitation energy of the lower level of the transitions. The fifth element in filparm stores the number of transitions each species has in that wavelength interval. This routine then returns to SYNNEW.

Section 6- GETBIN

GETBIN is the subroutine responsible for reading in the linelist. The principle loop of GETBIN is over the species in use. For each species, GETBIN determines which file is to be read and how many lines are in that file. Then GETBIN reads in those lines and writes their optical depth profiles into the appropriate portions of the array t.

In order to save disk space, network traffic and access time, the linelist has been stored in a compressed form. Each transition is stored as a four byte integer. The eight most significant bits store the wavelength bin the transition is in. These bits are transferred to the variable iwl. The wavelength can be extracted from this integer using

$$\lambda = \left(1.001^{(256(i-1)+iwl)}\right)90nm$$

where i is the wavelength region currently being loaded. The next twelve bits contain the compressed data for the gf value of the transition, igf. The remaining twelve bits contain the compressed data for the excitation energy of the lower level of the transition. The atomic data that is used by SYNNEW was derived from the atomic data distributed by Robert Kurucz. His data is distributed in two formats, a 160 character format, or a 32 byte binary format. SYNNEW uses a 4 byte binary format to improve network and hard drive performance. The optical depths as a function of radius are then calculated and stored in the array t. After all the lines have been read in for this wavelength region, GETBIN removes empty wavelength bins from t. This routine then returns to SYNNEW.

Section 7- SOURCE

SOURCE is the subroutine responsible for calculating the source function of a line. In the form that I am describing, the source function is set equal to the angle averaged intensity, J. Therefore, SOURCE has to calculate J at each radial zone. Aside from the numerics, the trickiest thing to remember is that we need to calculate J from the point of view of an observer moving with the material in that particular radial zone. Imagine yourself sitting at a particular point, facing radially outward, in an atmosphere that is expanding radially with the velocity of expansion being proportional to its radius. Relative to the center of the explosion, the things behind you are moving slower than you are and are thus moving backward relative to you. The things in front of you are moving faster than you are and are thus moving forward relative to you. Actually, we are all familiar with a system that works this way, the Hubble expansion of the Universe. From any point in either system, the velocity of an object is proportional to the distance it is away from that point. Another way to picture this is; that the surface of constant speed, relative to a mass element, is the surface of a sphere centered on that mass element. Care must be taken to include the effects of relativistic Doppler shifts and changes in frame of reference. An important consequence of this is that only lines located blueward from the current transition need to be considered in calculating the average intensity at this frequency, since only they can emit or absorb photons that would be redshifted into the line. This is the reason that the calculation begins with the bluest line and ends with the reddest line. Another benefit of this is that only lines located within a band from $\lambda\,(1 - 2\,V_{max}/c)$ to λ

can effect the source function for a line with wavelength λ. This means that lines bluer than $\lambda(1 - 2 V_{max}/c)$ cannot affect this line or any line to the red of λ. Thus, we can save memory by discarding the old line information, after we make sure that we don't need it for calculating the output spectrum.

For the first portion, we approximate the intensity using ten rays that begin on the photosphere and terminate at the point of interest. For each of these rays the initial intensity is set to the blackbody function taking care to correct for the fact that the location where the intensity is being calculated is moving away from the photosphere with a relativistic velocity. As the rays approach the radial point of interest, they continuously redshift relative to the mass elements that they are in. As they do so, they will have the same wavelength as other lines. These lines contribute in two ways; first, they decrease the incoming beam by $\mathrm{Exp}[-\tau]$, and second, they contribute to the beam by means of their source function. For the second portion, the same treatment occurs with the exception that the initial flux in each ray is zero. The ten rays are averaged for each portion and those averages are weighted with the dilution factor (the fraction of the solid angle that is subtended by the photosphere) and one minus the dilution factor.

Section 8- SPECTRUM

The subroutine SPECTRUM is responsible for figuring out what the supernova looks like for a distant external observer located on the positive z axis. The first thing SPECTRUM does is to determine if the source function of the reddest line, that can effect the output spectrum at the current wavelength, has been calculated. If it has SPECTRUM will calculate a portion of the spectrum. If it has not, SPECTRUM exits back to SYNNEW. If the source function of that line has been calculated, then all the source functions that can effect the output spectrum, at the current wavelength, have been calculated.

After it has been determined that all the required source functions have been calculated, SPECTRUM begins a loop over rays starting on the opposite side of the supernova from the observer, traveling towards the observer. These rays are parallel to the z axis and are spaced linearly in their impact parameters, p. It is important to realize that surfaces of constant velocity with respect to the observer are planes of constant z. This comes from the fact that the atmosphere is expanding radially with a speed proportional to the distance from the center of the explosion. $v = v_{phot}/R_{phot} * r$. If we want to calculate the z component of this velocity, $V_z = v_{phot}/R_{phot} * r^* \cos(\theta)$, but $r * \cos(\theta)$ is simply z. This leaves $V_z = v_{phot} * (z/R_{phot})$, thus a surface of constant V_z is a plane perpendicular to the z-axis.

If p is less than one photospheric radius, the ray intersects the photosphere. The ray begins at the photosphere with an intensity equal to the intensity of the photosphere, with care being taken to assure that the photosphere is moving with a speed of $v_{phot}* (1 - p^2)^{0.5}$

relative to the observer. If p is greater than one, the ray does not intersect the photosphere and its intensity is set to zero on the side of the supernova away from the observer.

Now SPECTRUM begins a loop over lines, from the bluest line to the reddest line, watching out to avoid wasting time on lines that are too blue or too red to affect the spectrum at this wavelength. Each line is located in z so that photons emitted or absorbed at the rest wavelength of the line will be doppler shifted to the wavelength at which the output flux is being calculated. This means that lines to the blue of the wavelength of interest will be located at negative z (away from the observer) and lines to the red of the wavelength of interest will be located at positive z (towards the observer). Now the effect of the lines is calculated on the rays moving toward the observer. Each ray encounters line after line constantly moving redder in wavelength and towards the observer. If the p value is less than one, lines that are located inside or behind the photosphere are ignored as the photosphere is assumed to be opaque. The values for the source function and optical depth of each line are then interpolated for the coordinates of p (for the ray) and of z (of the line). The effect of the line on the ray is then included.

After all the lines are included, SPECTRUM adds the flux of this ray to the flux of the previous rays, noting that each ray represents a hollow cylinder with a cross sectional area proportional to $2\pi p\ dp$. If the output spectrum is desired to be in f_λ instead of f_ν the output flux is converted next. Then the output is written in a three column format easy for graphing. The first column is the wavelength

in Angstroms, the second column is the output spectrum, and the third column is the blackbody function of the underlying photosphere.

SPECTRUM then cleans up a little. It advances the blueline counter up to the bluest line that actually affected the current output flux. Finally SPECTRUM terminates the program if it calculates the last wavelength point, or loops back to the beginning of the subroutine to see if any more of the spectrum can be calculated.

Section 9- in.dat

The file in.dat contains the user controlled inputs. An example of an in.dat file is given in Appendix 3. The user interfaces with SYNNEW using the in.dat file. It contains all of the model parameters used in fitting spectra, including the photospheric velocity, the continuum temperature, the wavelength range of interest, the optical depths of the reference lines for each species and their radial behavior. In addition to this, the user is encouraged to maintain some kind of history or notes about past runs at the end of the file.

Section 10- ref.dat

The file ref.dat contains the atomic data for each reference line. An example ref.dat file is contained in Appendix 3. Reference lines were usually chosen to be the strongest optical transition for each species at a temperature of 10,000 K, with some exceptions. When the user inputs an optical depth for this line, the data provided in the ref.dat file are combined with the atomic data on the other transitions of that same species to calculate all the optical depths of that species.

Section 11- linelist.info

In order to speed up SYNNEW, the linelist was fragmented into 10470 files. These files each contain atomic data on all of the transitions in a particular wavelength band for each species. This allows SYNNEW to easily avoid reading unneeded data. This is especially thrifty when some of the iron peak elements, which have the most numerous lines, are included in the calculation.

Section 12- REDD

REDD is an independent program that reddens the output spectrum and normalizes it to a value set by the user. This makes comparing the synthetic spectrum to the observation significantly easier than having to normalize the output spectrum by hand every time. The reason that the synthetic spectrum is reddened rather than the observed spectrum being dereddened, is that the amount of interstellar reddening suffered by the supernova is always in some doubt.

Section 13- shell scripts.

An example of each shell script is given in Appendix 4. The shell script *run* does much of the busy work included in spectral fitting. Quite simply, it keeps track of the previous run's output spectrum and input parameters. This helps considerably in spectral fitting by allowing the user to compare the previous fit to the current fit directly. This script then runs SYNNEW, which calculates the synthetic spectrum. It then reddens the synthetic spectrum by running REDD. Subsequently, it launches a graphics program to compare the current spectrum, the old spectrum, and the observed spectrum. If a run is going to take a very long time, the user can include a command in *run* to beep or send an e-mail when the program terminates.

The shell script *runmore* allows the user to move through a batch of spectra efficiently. For each set of spectra, I have a *runmore* script set up to allow the user to easily go through viewing the current fit for each observed spectra, modifying the file in.dat, and

running SYNNEW. This makes working on a series of spectra much easier to manage.

Cmaster is another shell script that allows me to optimize my computer usage. During high usage periods, the user can rapidly generate a large number of input files that need to be run. If computers are not immediately available for these runs, *cmaster* can run them when a machine becomes available. *Cmaster* consists of two lists. The first is a list of computers organized from the fastest to the slowest. The second is a list of directories where there is an in.dat file ready to be run. Whenever a computer becomes available, *cmaster* runs SYNNEW remotely with the parameters contained in the first in.dat file in the list. This allows the user to run programs continuously for long periods of time, without the user having to continuously watch for when a run is finishing.

Chapter 4 Spectral Diagnostics

Based on a great deal of experience in fitting SYNNEW spectra to the observed spectra of SNe Ia, I have developed a strategy for extracting information using selected spectral diagnostics. This strategy applies to SNe Ia that have a normal composition, such as that of the carbon deflagration hydrodynamical model W7 of Nomoto, Thieleman, and Yokoi (1984) The outermost layers are unburned carbon and oxygen. Deeper layers are rich in intermediate mass elements, primarily silicon and sulfur, with the deepest layers rich in iron peak elements.

Section 1 - Calcium H&K

The strongest feature in the optical spectra of SNe Ia is located near 3900 Angstroms and is caused by the blend of the Calcium H & K lines. In spectra taken near maximum, this feature usually allows the spectral fitter to determine the velocity at the photosphere and put a lower limit on the maximum velocity of the ejecta. In spectra taken more than two weeks after maximum, the Calcium H&K feature is useful in determining the minimum velocity of intermediate mass elements. In late time spectra, where Calcium H&K may still be optically thick, the wavelength of the sharp red edge of this feature correlates with the absolute luminosity (Fisher et al. 1995, Chapter 5 of this document). Unfortunately, good quality data showing this feature at late times are rather rare in the local set of SNe Ia and have not been obtained in the high-z SNe.

Section 2 - The sulfur tooth

The Type Ia spectra, near the maximum, usually have a nicely developed sulfur II blend between 5000 Angstroms and 6000 Angstroms. This feature often bears a resemblance to a tooth, so from this point on I will call this feature the sulfur tooth. Much information can be obtained from the sulfur tooth. The first step in this data mining procedure is to fit the flux minimums of the feature. This is accomplished by adjusting the minimum velocity of sulfur II and the photospheric velocity (see figure 5). Next the maximum velocity of sulfur II is determined by fitting the peak near 5400 Angstroms. This peak is very sensitive to the maximum velocity where SII has an appreciable optical depth (see figure 7). Either a maximum velocity of sulfur II must be set, or the scale height of sulfur II can be lowered until sulfur II is no longer forming above a certain velocity. Under good conditions the shape of the blue edge of the feature will dictate which of these is correct. Finally, the last piece of data that can be mined out of the sulfur tooth is the excitation temperature. The sulfur tooth remains largely the same over a wide range of excitation temperatures. This allows the feature to be fit with little regard to the excitation temperature. After the tooth has been fit, the excitation temperature can be fit using a sulfur II line just to the blue of the sulfur tooth, which is sensitive to the excitation temperature (see figure 6). An example of the observed variation in behavior for the sulfur tooth is shown in figure 8.

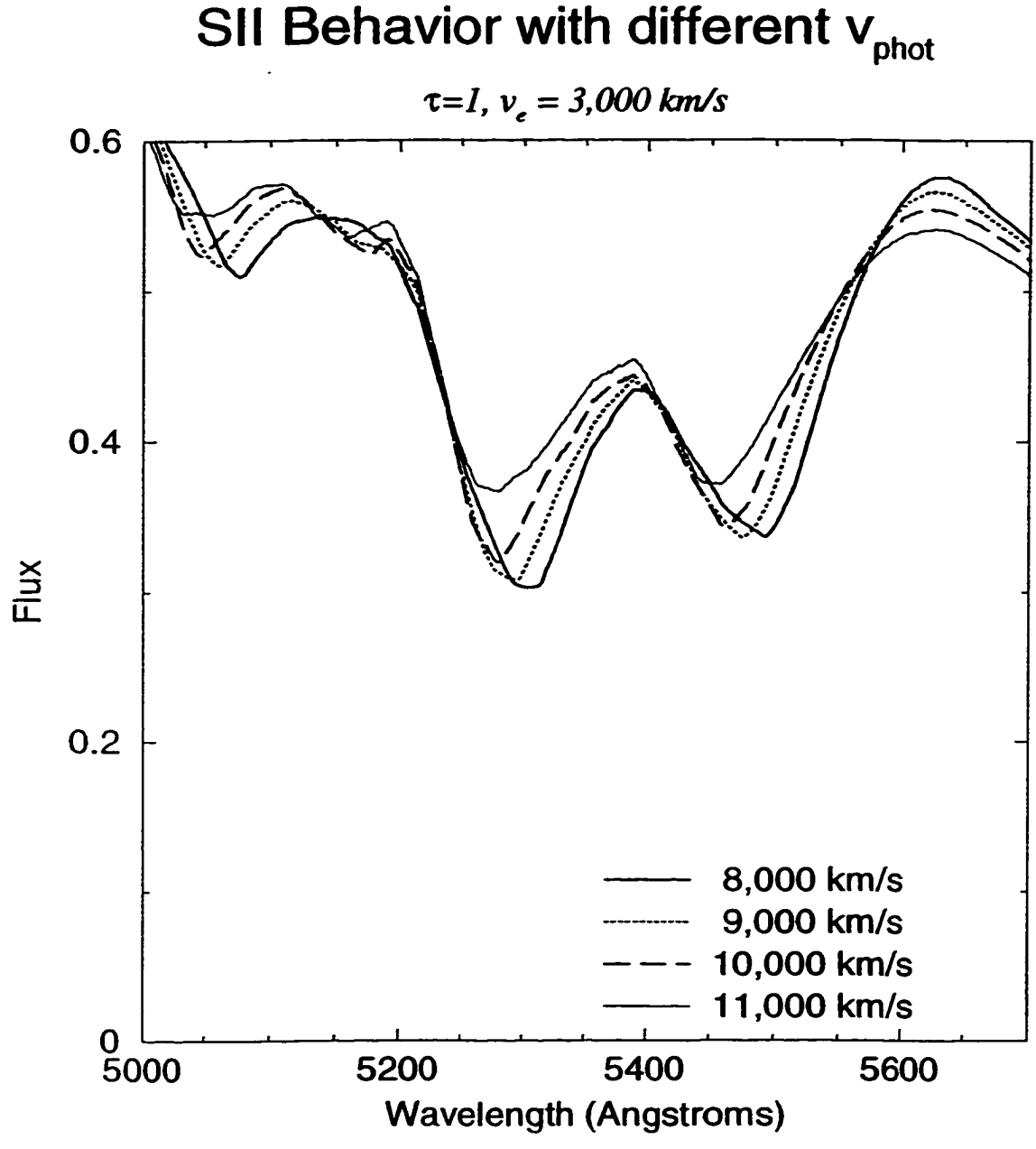

Figure 5. This figure shows that the minimums of the sulfur tooth are sensitive to the photospheric velocity.

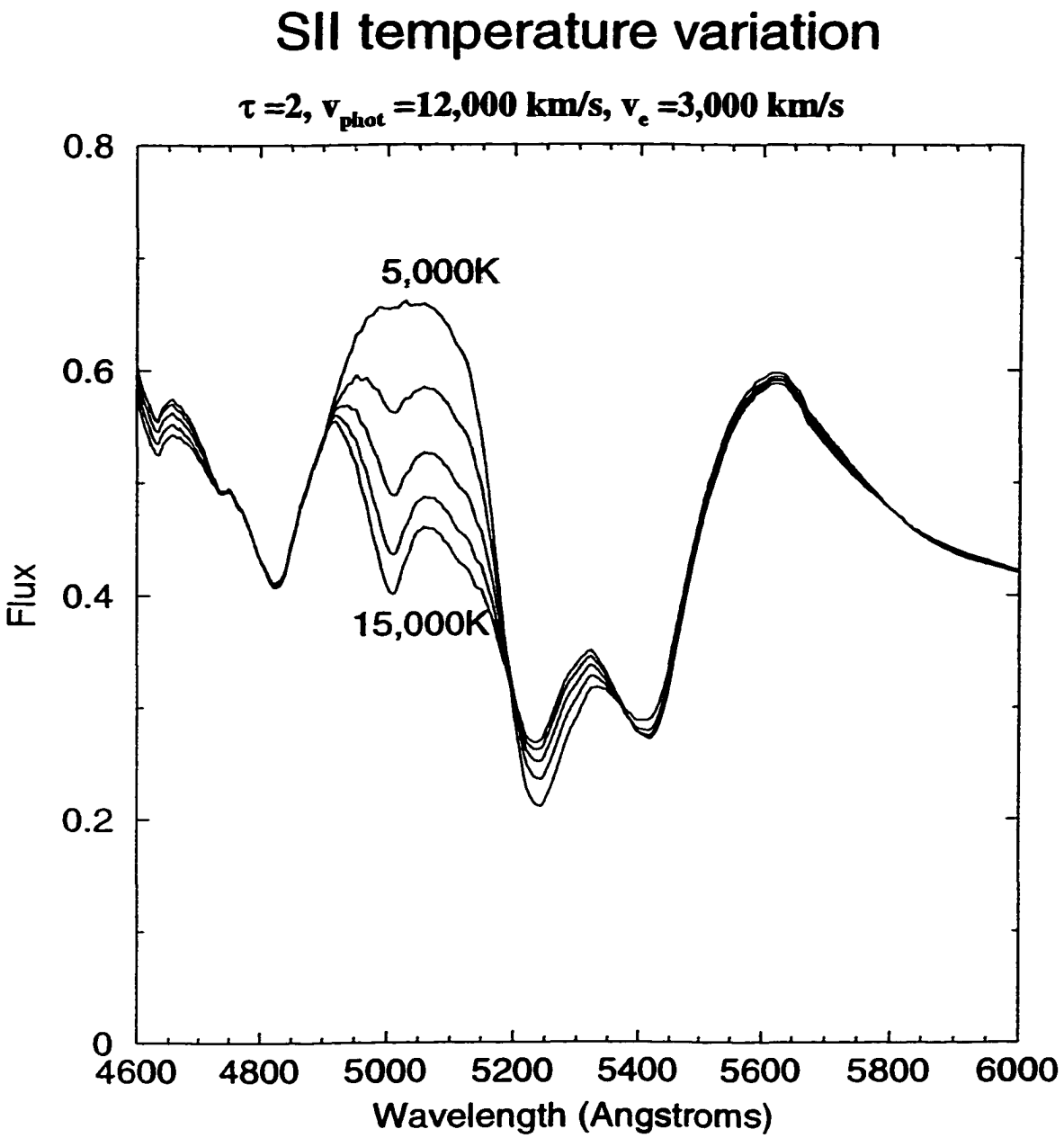

Figure 6. This figure demonstrates that the excitation temperature of SII can be constrained by the relative strength of the SII tooth and the SII feature near 5100 Angstroms.

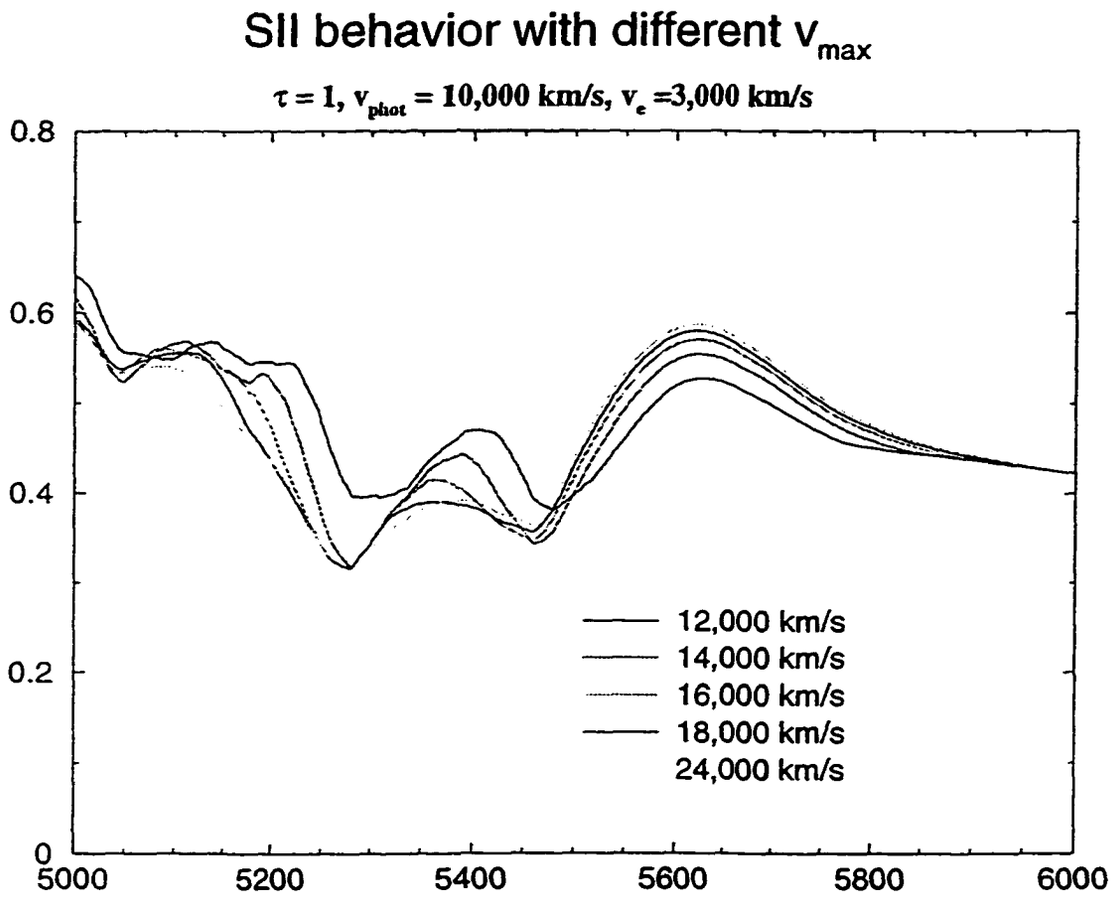

Figure 7. This figure shows that the shape of the maximum near 5400 Angstroms is sensitive to V_{max}(SII).

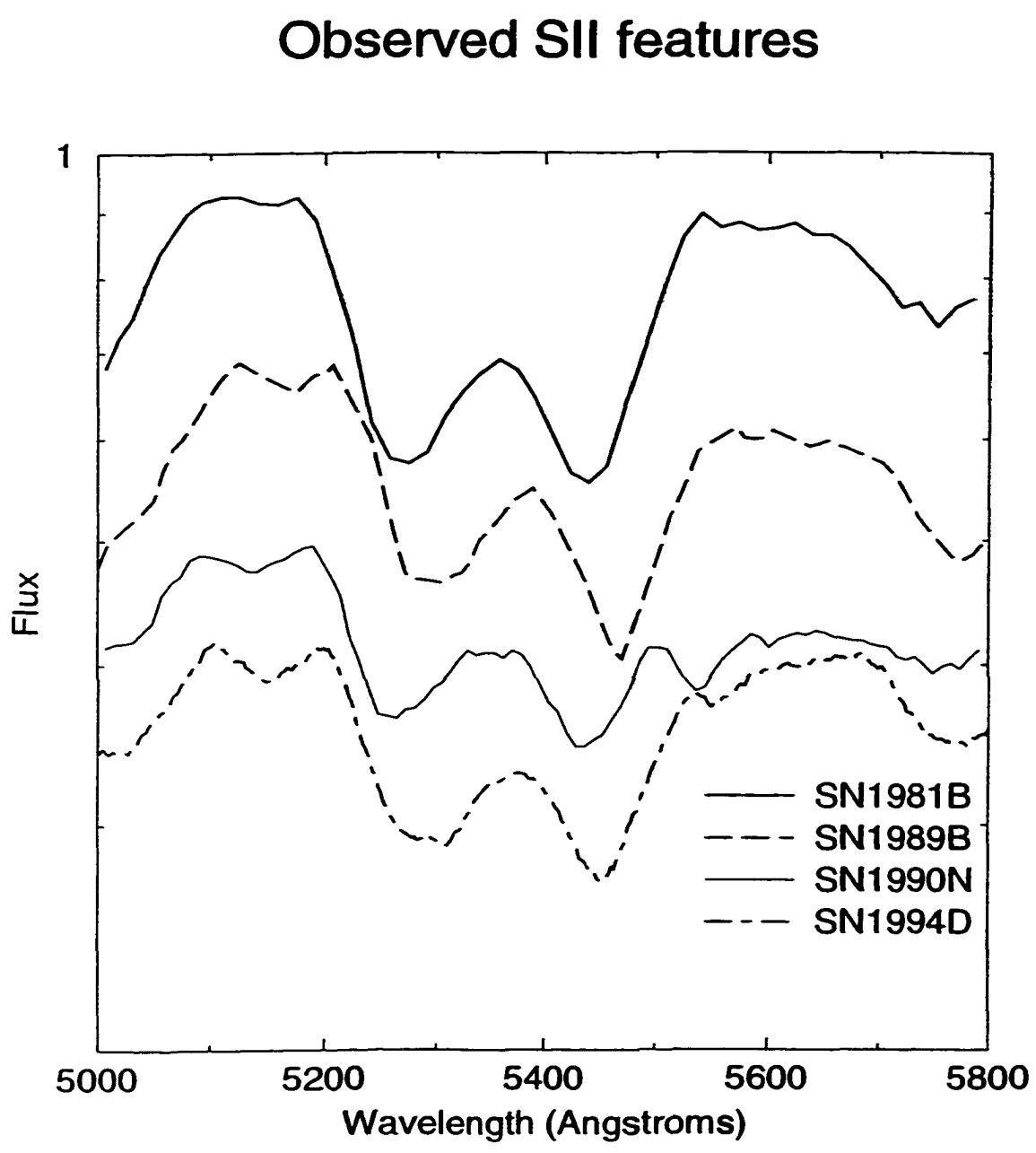

Figure 8. This figure shows the some of the variation of observed SII features.

Section 3 - Calcium Infrared Triplet

The calcium infrared triplet is responsible for the strong feature just to the red of 8000 Angstroms. This strong feature has several uses for the spectrum fitter. First, if an observed spectrum has both the calcium H&K and the calcium infrared triplet, then the relative strength of these features can help constrain the excitation temperature. If a spectrum does not have both features, the shape of the infrared triplet feature can, by itself, determine the excitation temperature. Figure 9 shows the behavior of the calcium infrared triplet at several excitation temperatures.

Another bit of information that the calcium infrared triplet provides relates to the detachment of the intermediate elements from the photosphere. When calcium becomes detached from the photosphere (i.e. when the photosphere has retreated into the iron-peak core), the calcium infrared triplet develops a knee on the red edge of the absorption trough. Since the calcium H&K lines may be strong enough to have a significant optical depth (even in a region where no calcium was synthesized), the calcium infrared triplet is arguably a better indicator of the location of the lower boundary of the intermediate mass element dominated region. Figure 10 shows this behavior by keeping the minimum velocity of the calcium constant while changing the photospheric velocity. Figure 11 shows a few examples of how the calcium infrared triplet appears in some observed spectra. Note that SN 1991bg is a spectroscopically peculiar SN Ia (Branch, Fisher, and Nugent 1993).

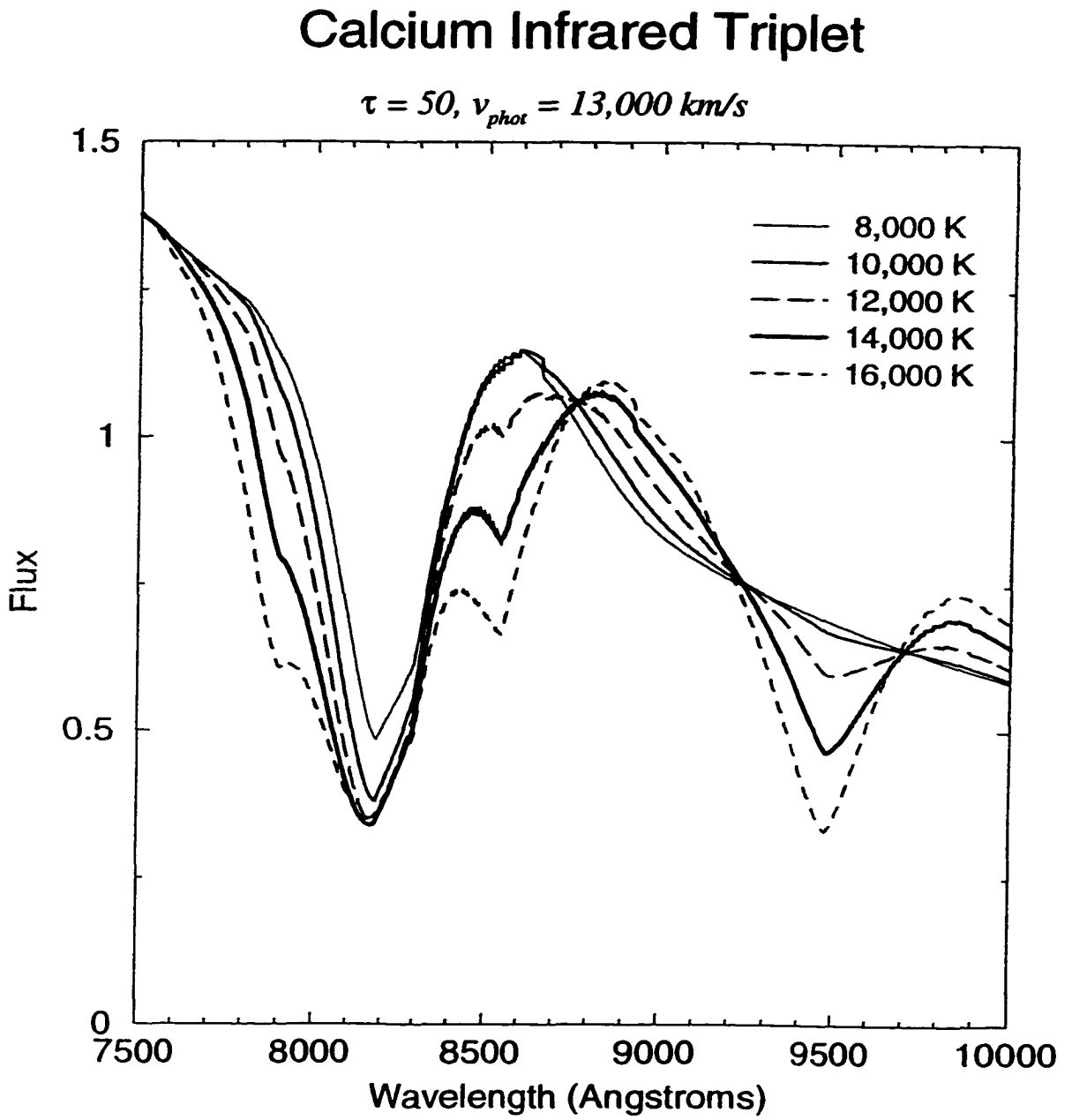

Figure 9. This figure shows the temperature dependancy of the Calcium Infrared Triplet (Ca IR3). Notice the auxialliary features around the Ca IR3 strengthen more than the the primary feature at 8200 Angstroms.

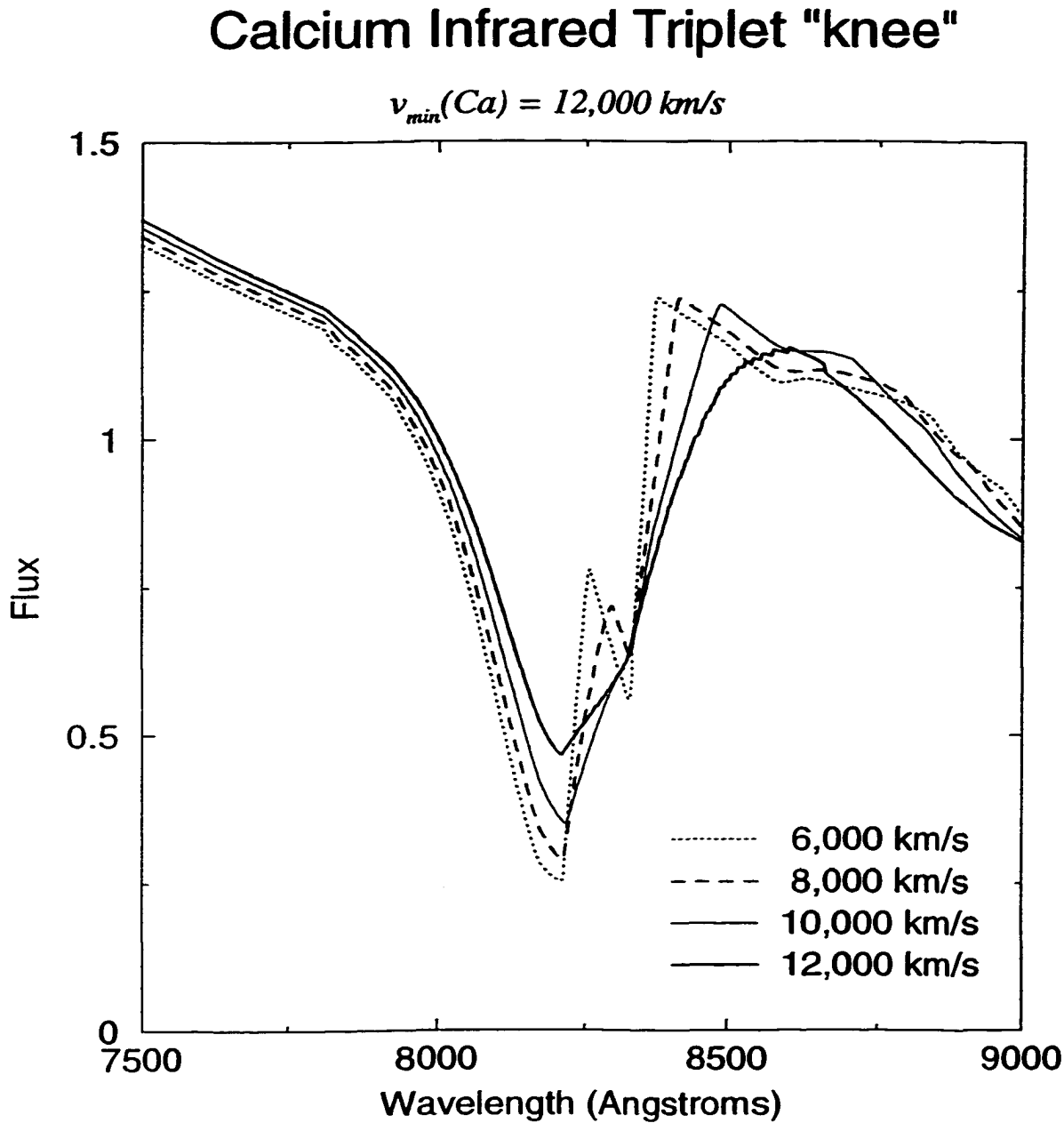

Figure 10. This figure shows the evolution of the Ca IR3 as the photosphere recedes beneath the calcium rich layer.

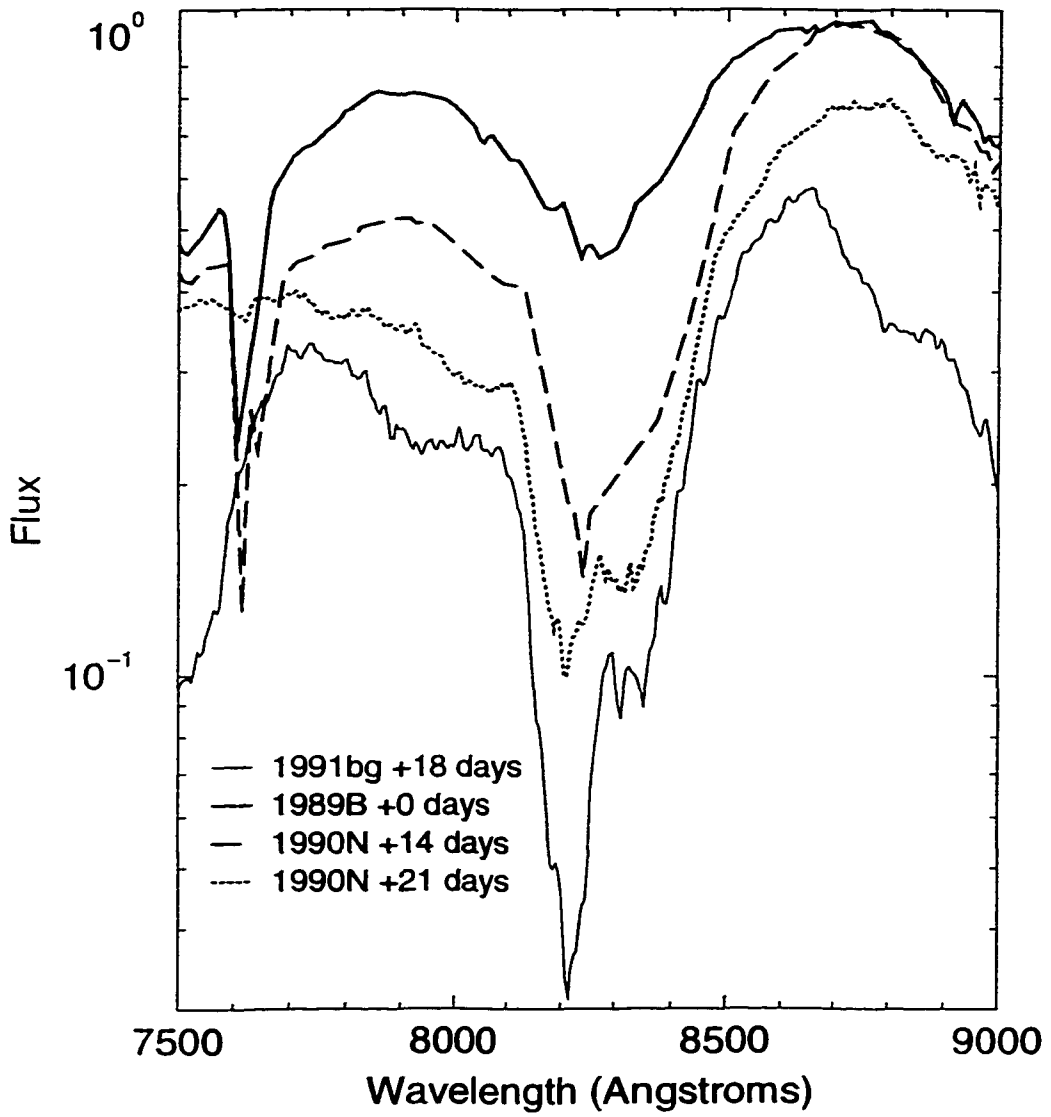

Figure 11. This figure shows the observed variation in Ca IR3 for several different SNe Ia.

Section 4 Silicon II and Carbon II

In near maximum light spectra, Silicon II plays a prominent role in several wavelength regions. The two most informative features are around 5700 Angstroms and 6100 Angstroms. Unfortunately, under certain conditions, a strong carbon II line can blend in with the 6100 Angstrom feature. If this is not identified in the spectrum, then several problems can arise. The first, and perhaps most serious problem, is that this can cause errors in the inferred velocity range of the intermediate mass elements. The second problem may be an artificially strong silicon II optical depth, producing unwanted lines elsewhere in the spectral fit, or if these lines are discouraged an artificially low excitation temperature would be found, resulting in a worse fit for the lines of the other species. In order to avoid these pitfalls, I recommend that spectrum fitters concentrate on fitting the 5700 Angstrom feature with silicon II, (provided that the SN is not so cool that Ti II lines affect this feature). Then I would encourage that it be taken as an assumption that the excitation temperature of silicon II be the same as sulfur II which has already been determined using the sulfur tooth. Then the user can fit carbon II to the remaining portions of the 6100 Angstrom feature. It should be stressed that this procedure is only a first step in the fitting process. The idea here is to avoid fits that are better than other fits with similar parameters (the best local fit), but are worse than a fit with a significantly different set of parameters (the best global fit).

If a series of near maximum-light spectra are available for the same supernova, there is a chance to use the temporal variation in this feature to help determine whether carbon or silicon is present.

Figure 12 shows that silicon moves to the red as the photosphere evolves toward the center of the supernova. When carbon happens to be in a high velocity shell, which is often the case in hydrodynamic models, it can affect the same wavelength region as the silicon II but, an unblended carbon feature moves toward the blue slightly as the photosphere declines. Attention should also be paid to the difference in the shapes of the features, silicon II appears smooth and rounded while a detached carbon II looks squared off and flat-topped. Unfortunately for the spectrum fitter, neither carbon nor silicon is often found to completely dominate this feature. This results in various structures of the 6100 Angstrom feature. Figure 13 shows examples of synthetic spectra, with a small amount of carbon II, interferring with a strong silicon II feature. The most important parameter in this interaction is determining the velocity difference between silicon and carbon. Notice in Figure 13 that if the velocity difference is greater than 6,000 km/s, the feature begins to look like a pure silicon feature with a slightly larger optical depth. Figure 14 shows some observational examples of the 6100 Angstrom region in near maximum light spectra.

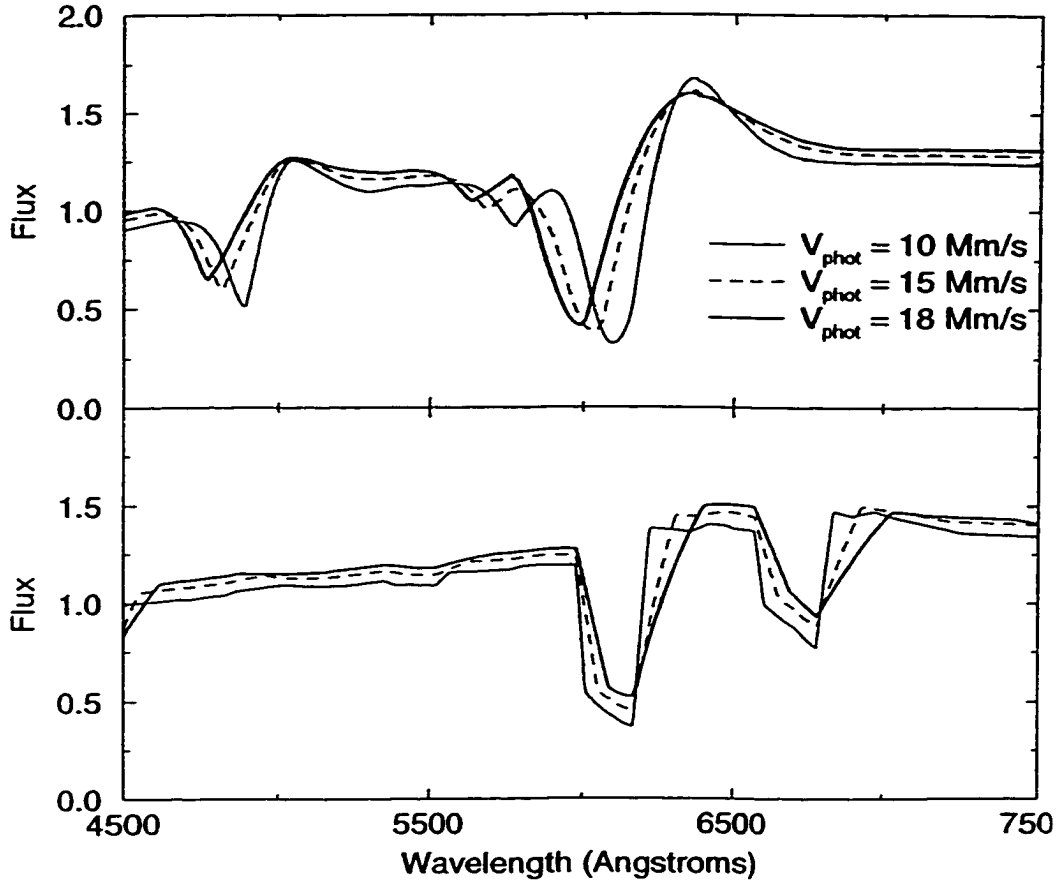

Figure 12. The top frame of this figure shows the behavior of Si II as the photosphere recedes to lower and lower velocities. The bottom frame of this figure shows how the behavior of a detached shell rich in carbon behaves in a similar situation. Notice that the silicon features move toward the red, while the carbon features remain mainly stationary.

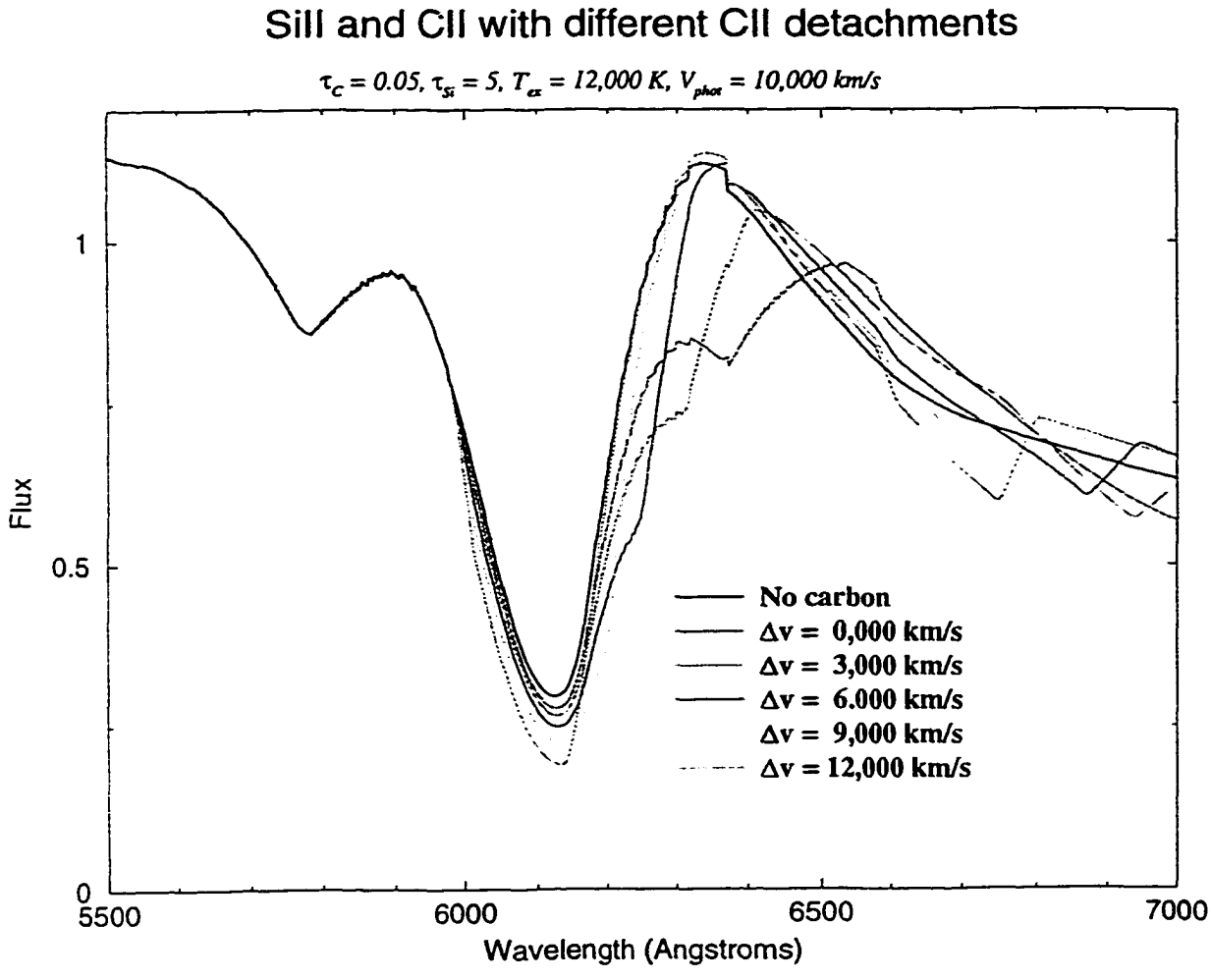

Figure 13. This figure shows the interaction of carbon and silicon features for different detachment velocities. Notice that if the difference between the photospheric velocity and the velocity of the carbon shell is in the range of 9,000 to 12,000 km/s that the feature looks very similar to an isolated Silicon feature.

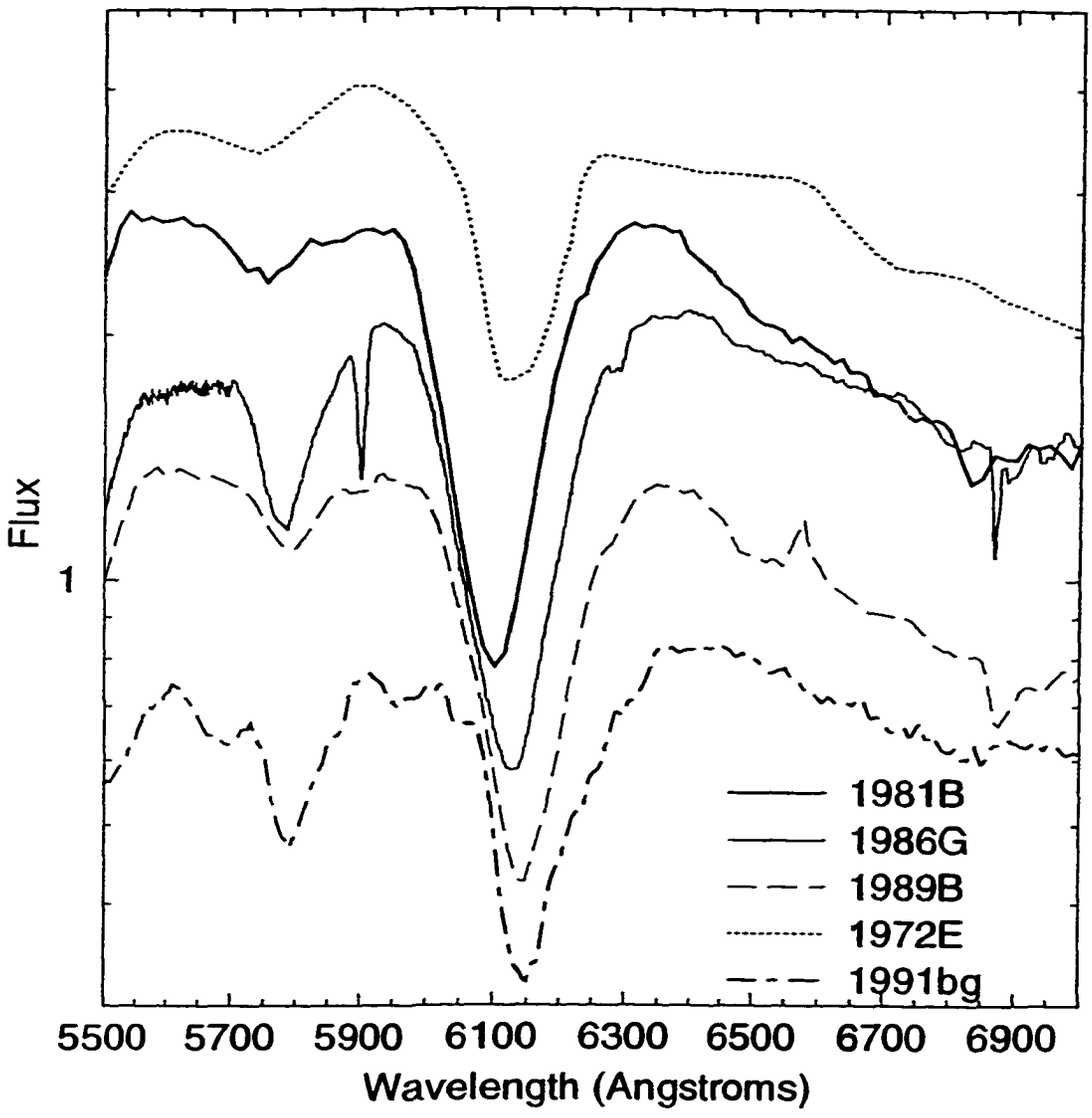

Figure 14. This figure shows the observed variation of the Silicon/Carbon feature near 6100 Angstroms. Note the flat top and steep red slope for 1972E, charicteristic of a Carbon dominated feature. Note the litte nicks in the red edge of this feature for the remaining SNe, this is probably carbon as well.

Section 5 - The "Hβ" Bump

As supernovae age, their spectra become more and more dominated by iron peak elements. In some spectra there appears to be a little bump at nearly the same wavelength as Hβ, thus the feature can be called the Hβ bump (see figure 15). Actually, this feature is caused by a gap in a series of strong transitions primarily arising from iron II. The shape of this feature is strongly dependent upon the maximum velocity of the iron peak core of the supernova. Figure 16 shows the behavior of this bump under several different v_{max}(Fe). Notice, that if the iron peak core is traveling with too high a velocity, the Hβ bump can disappear altogether. Also, in the extreme case, the central rise in this feature is also eliminated. Figure 17 shows how this feature appears in several observed supernovae.

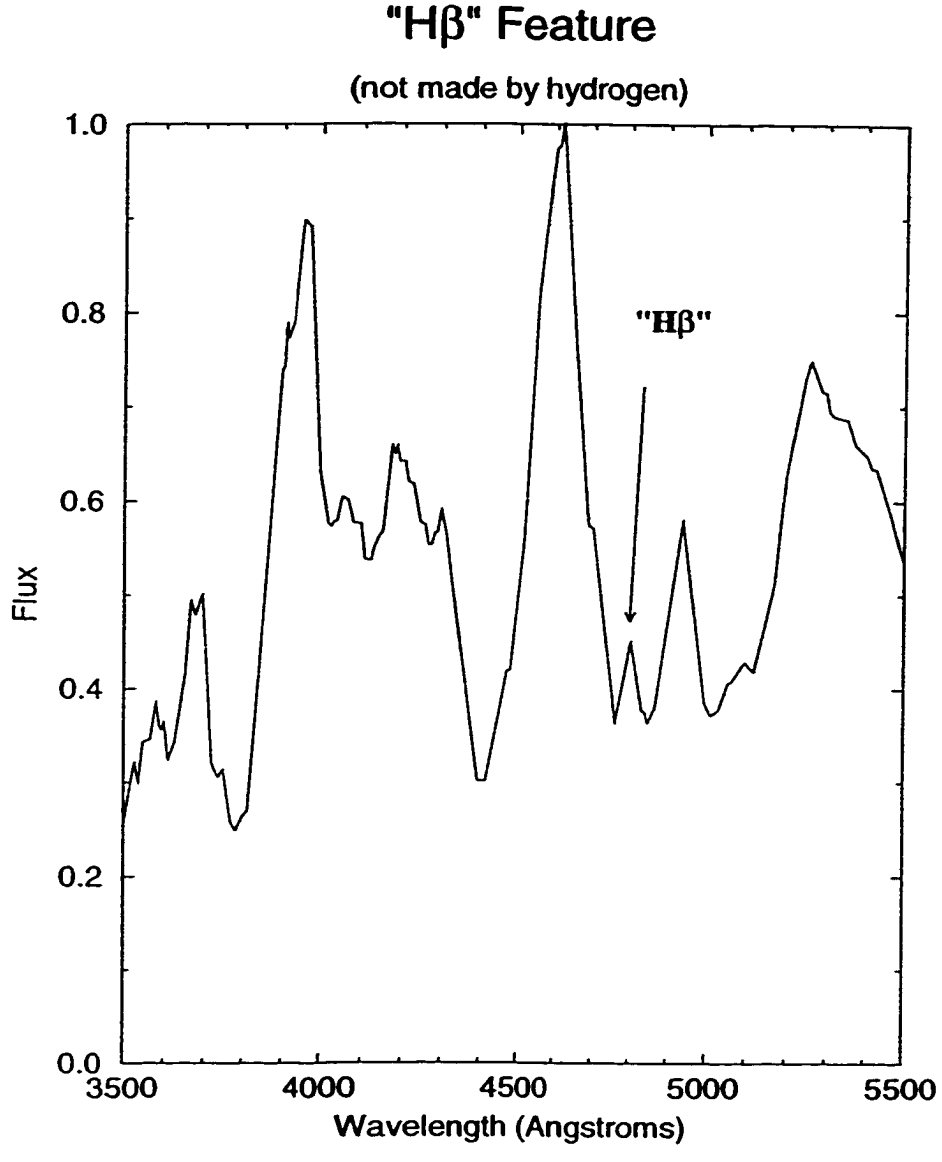

Figure 15. This feature shows the observed "Hβ" feature in SN1989B.

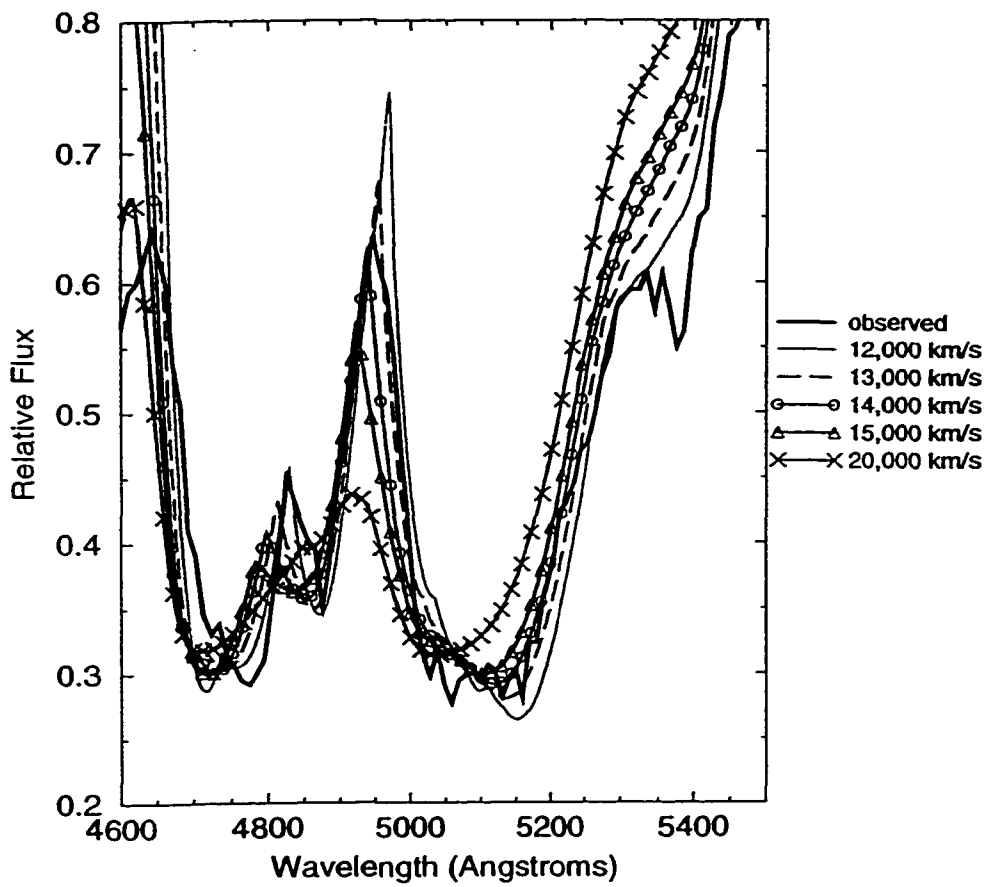

Figure 16. This figure shows the sensitivity of the Hβ feature to the maximum velocity of iron.

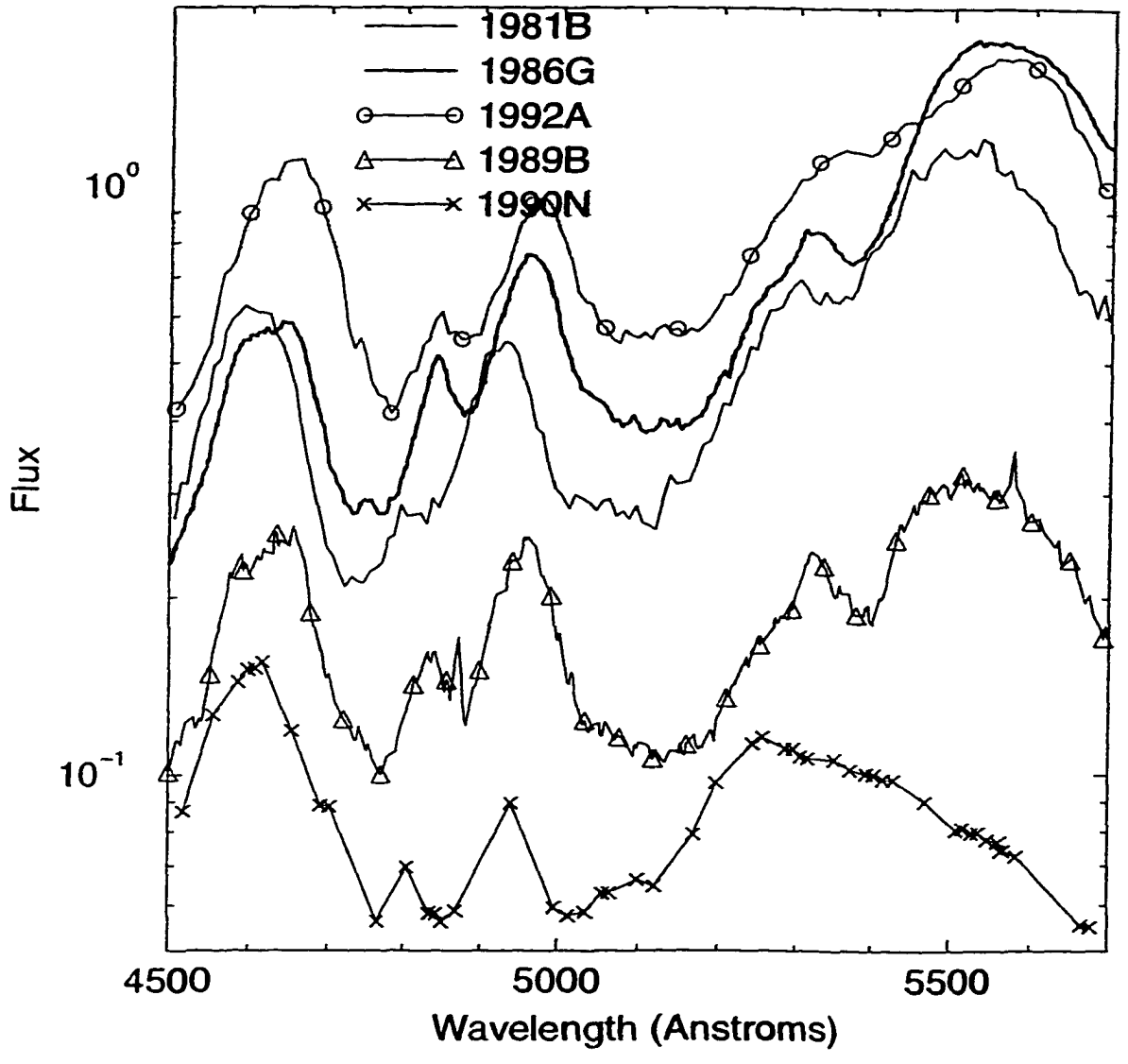

Figure 17. This figure shows the variation in the observed Hβ feature in several SNe Ia.

Chapter 5 -

THE MINIMUM EJECTION VELOCITY OF CALCIUM IN TYPE Ia SUPERNOVAE AND THE VALUE OF THE HUBBLE CONSTANT

Adam Fisher, David Branch, Peter Höflich, and Alexei Khokhlov

as published in The Astrophysical Journal Letters

ABSTRACT

Evidence is presented for a relationship between the visual absolute magnitude of Type Ia supernovae (SN Ia's) and their minimum ejection velocities of calcium, as indicated by the red edge of the Ca II H and K absorption blend, in moderately late-time spectra. Independent calibrations of the relation by means of (1) the Cepheid-based distance to NGC 5253, the parent galaxy of SN 1972E, and (2) light-curve calculations based on hydrodynamic models of SN Ia's, give low H_0 near 60 kps / Mpc.

1. INTRODUCTION

Type Ia supernovae (SN Ia's) are not strictly homogeneous in their observational properties. The current observational sample of SN Ia's is strongly peaked at "normal," both spectroscopically (Branch, Fisher, & Nugent 1993) and in terms of peak absolute magnitudes (Vaughan et al. 1995; Hamuy et al. 1995; Tammann & Sandage 1995), but even normal SN Ia's have some intrinsic spread in their spectroscopic and photometric properties (Branch & van den Bergh 1993; Phillips 1993; Branch et al. 1994; Hamuy et al. 1995; Riess, Press, & Kirshner 1995).

Diversity raises the issue of how best to use SN Ia's to determine the Hubble constant. In this Letter we present evidence for a relation between the visual absolute magnitudes of SN Ia's and

the minimum ejection velocity of calcium as indicated by the red edge of the Ca II H and K absorption blend in moderately late-time spectra. We determine the value of H_0 by calibrating the relation in two independent ways: (1) by means of the Cepheid-based distance to NGC 5253, the parent galaxy of the Type Ia SN 1972E (Saha et al. 1995), and (2) by means of light-curve calculations based on hydrodynamic models (Khokhlov, Müller, & Höflich 1993; Höflich 1995).

2. DATA

A spectrum of SN 1981B obtained by Beverley Wills 270 days after maximum light contained a blueshifted Ca II H and K absorption blend having sharp blue and red edges (Branch 1984). The red edge was particularly interesting because it indicated a sharp transition from the iron-peak elements in the inner layers of the ejecta to the intermediate-mass elements in the outer layers. Now that there is great interest in the physical differences among SN Ia's, it is interesting to see whether V_R(Ca) Varies among SN Ia's, and whether it is correlated with absolute magnitude. The Ca II H and K absorption profile of SN 1981B is displayed in Branch (1984); another good example, for SN 1992A, can be found in Ruiz-Lapuente et al. (1995); a third is presented in Figure 1. We have measured V_R(Ca) in the spectra of the 12 SN Ia's listed in Table I. The wavelength of the absorption red edge has been converted to V_R(Ca) by using the rest wavelength of the H line, 3968Å, and correcting for the heliocentric radial velocity of the parent galaxy.

The Ca II absorption feature in late-time SN Ia spectra is deep, which indicates that much of the luminosity originates from the iron-peak core of the ejecta, beneath the calcium, this is consistent with model predictions: only about 0.1 M_{sun} of ^{56}Ni is formed in regions of partial burning where calcium is produced. Therefore $V_R(Ca)$ provides a straightforward measure of the minimum velocity of ejected calcium, except perhaps for strongly subluminous SN Ia's with very low ^{56}Ni production (Höflich, Khokhlov, & Wheeler 1995). According to this interpretation $V_R(Ca)$ should be independent of phase after the photosphere has retreated beneath the calcium layer. This expectation is checked in Figure 2, where $V_R(Ca)$ is plotted against phase for six SN Ia's for which we have measurements at multiple phases. In the one SN Ia that is especially well observed for this purpose, SN 1989B (Wells et al. 1994), $V_R(Ca)$ does indeed appear to be constant, or nearly so, after about 50 days. In the other SN Ia's of Figure 2 the data are not inconsistent with $V_R(Ca)$ being constant after 50 days. Values of $V_R(Ca)$ are listed in Table 1. Where possible we have interpolated to a phase of 80 days.

Also given in Table 1 are visual absolute magnitudes from Vaughan et al. (1995). These are based on a mutually consistent set of distances, from the Tully-Fisher (TF) method (e.g. Pierce 1994) for late-type galaxies, and from the method of surface brightness fluctuations (SBF's; e.g. Tonry et al. 1990) for early-type galaxies, and they are consistent with $H_0 = 85$ kps/ Mpc. Following Phillips (1993), we adopt total extinction's of $A_V = 1.86$ for SN 1986G and 1.08 for SN 1989B. The other SN Ia's are corrected for foreground

extinction in the Galaxy but not for extinction in the supernovae parent galaxies, which is thought to be small (Vaughan et al. 1995).

3. ANALYSIS

Absolute visual magnitude, based on the TF and SBF distances, is plotted against V_R(Ca) in Figure 3a, which shows that there is a correlation between M_V and V_R(Ca) in the expected sense. Stronger explosions have faster V_R(Ca) values because their iron-peak cores occupy larger fractions of the ejected mass, and they are brighter because the eject more ^{56}Ni. The shape of the relation is also qualitatively consistent with expectation: in weak explosions M_V is sensitive to explosion strength, but in strong explosions M_V is less sensitive because gamma rays from ^{56}Ni near the surface tend to escape rather than to thermalize and contribute to the optical brightness (Khokhlov et al. 1993; Höflich et al. 1995; Höflich 1995). The uniquely peculiar SN 1991T (Filippenko et al. 1992a; Phillips et al. 1992b; Branch et al. 1993) is overluminous for its V_R(Ca) value.

In figure 3b, M_V is plotted against V_R(Ca) again, but now using different distance moduli. For SNs 1937C and 1972E, the Cepheid distances (Saha et al. 1994, 1995) are plotted. The Cepheid distance to NGC 5253 is a factor of 1.56 longer than the SBF distance, from Philips et al. (1992a), and the Cepheid distance to IC 4182 is a factor of 1.96 longer than the TF distance given by Pierce (1994). We refrained from using the TF distance to IC 4182 in Figure 3a because IC 4182 inclination of 30° is quite low for a TF distance determination. To make the other SN IA's of Figure 3b bright enough to be consistent with SNS 1972E and 1937C, their distances have

had to be increased. We have done this by matching the mean absolute magnitude of the seven spectroscopically normal SN IA's (Branch et al. 1993) -- SNs 1992A, 1989B, 1960F, 1981B, 1990N, 1989M, and 1994D -- to the Cepheid-based absolute magnitude of SN 1972E. We have not used the Cepheid-based absolute magnitude of SN 1937C in view of the fact that the apparent magnitude of SN 1937C is in dispute (Schaefer 1994; Pierce & Jacoby 1995). This procedure yields $H_0 = 57 \pm 4$ km s^{-1} Mpc^{-1} (1 σ fitting error). Note that an alernative procedure, matching the absolute magnitude of SN 1992A to that of SN 1972E which have the same V_R(Ca) would yield $H_0 = 45 \pm 7$ km s^{-1} Mpc^{-1} but this would make the SN Ia's having V_R(Ca) values like that of SN 1937C more luminous than SN 1937C, which is unsatisfactory, especially when we consider that according to Pierce & Jacoby (1995) SN 1937C may have been fainter than plotted here.

Figure 3c shows an independent way to calibrate the relation between M_V and V_R(Ca), based on the calculated absolute magnitudes for delayed detonation hydrodynamical models for SN Ia's as nuclear disruptions of carbon-oxygen white dwarfs near the Chandrasekhar mass (Khokhlov et al. 1993; Höflich 1995). Model parameters M_V, the minimum velocity of the calcium layer [V_{min}(Ca)], and the ejected mass of ^{56}Ni (M_V) are listed in Table 2. Note that in Figure 3c, the trend of the models is qualitatively like that of the real SN Ia's. The models do not quantitatively reproduce the positions of SNs 1986G and 1991bg, but as mentioned above, the interpretation of V_R(Ca) may not be straightforward for these subluminous events. The models do indicate, as mentioned above,

that the dependence of absolute magnitude on V_R(Ca) is mild for V_R(Ca) > 5000 kps. (The differences between the models presented by Höflich [1995] and the models of Khokhlov et al. [1993] can be traced to their different adopted values of the white dwarf central density at the onset of nuclear ignition.) Thus in Figure 3c the distance rescaling has been performed by matching the absolute magnitude of model M35, which has V_R(Ca) = 6904 kps, to the absolute magnitude of SN 1994D for which model M35 provides a reasonable fit to the light curves and spectra (Höflich 1995). This gives H_0 = 60 ± 4 kps/Mpc (1 σ fitting error) and a satisfactory overall match between models and real SN Ia's in Figure 3c, except for the spectroscopically peculiar SNs 1991bg, 1986G and 1991T.

4. DISCUSSION

Both methods of calibrating the relation between M_V and V_R(Ca) give $H_0 \cong 60$ km s^{-1} Mpc^{-1}, consistent with other determinations of H_0 using SN Ia's (Branch 1992; Müller & Höflich 1994; Saha et al. 1995; Höflich et al 1995; Hamuy et al. 1995; Riess et al. 1995). An important difference between using a relation between M_V and a spectroscopic observable, as we do here, and using a relation between M_V and a photometric observable (light-curve width or decay rate), is that spectroscopy indicates that 1972E was a typical SN Ia (Branch et al. 1994). Because the light curve of SN 1972E appears to have been unusually broad, like that of SN 1991T, and because SN 1991T appears to have been more luminous than normal SN Ia's, the photometric approach leads to the assignment of dimmer absolute magnitudes to normal SN Ia's other than SN 1972E, and a value of H_0 that is somewhat higher (Hamuy

et al. 1995; Riess et al. 1995) than the value indicated by our spectroscopic approach. Another difference is that V_R(Ca) is more straightforward to measure and interpret than a light-curve decline rate.

It should be mentioned that the blueshift of the minimum of the Ca II absorption feature at maximum light correlates with light-curve decay rate (Wells et al. 1994) and also with absolute magnitude. The physical interpretation of that spectroscopic observable is complicated, however, and establishing its numerical value for a particular model would require detailed spectrum calculations.

We are grateful to Eddie Baron, Peter Nugent, Thomas Vaughan, and Craig Wheeler for discussions, to Bob Kirshner, Alex Filipenko, and Lisa Wells for providing data in digital form, and to referee Mark Phillips for constructive suggestions. This work has been supported by NSF grant AST 9115061.

FIGURES

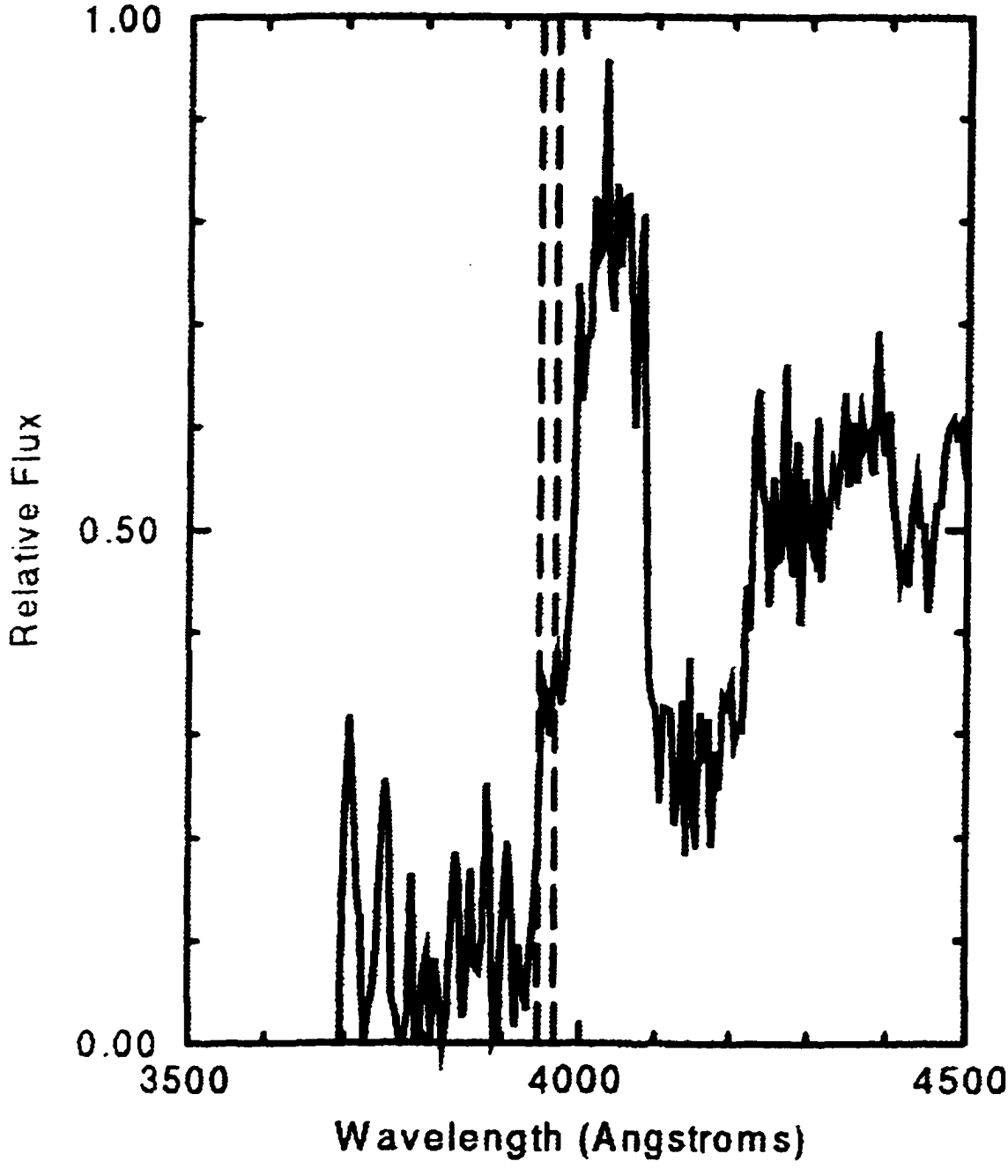

FIG 1. -- Spectrum of SN 1991bg (Filippenko et al. 1992b) near the Ca II H and K blend. Vertical line on the right denotes the rest wavelength of the H line. Line on the left passes through the red edge of the absorption and yields $V_R(Ca) = 1600 \pm 20$ km s^{-1}.

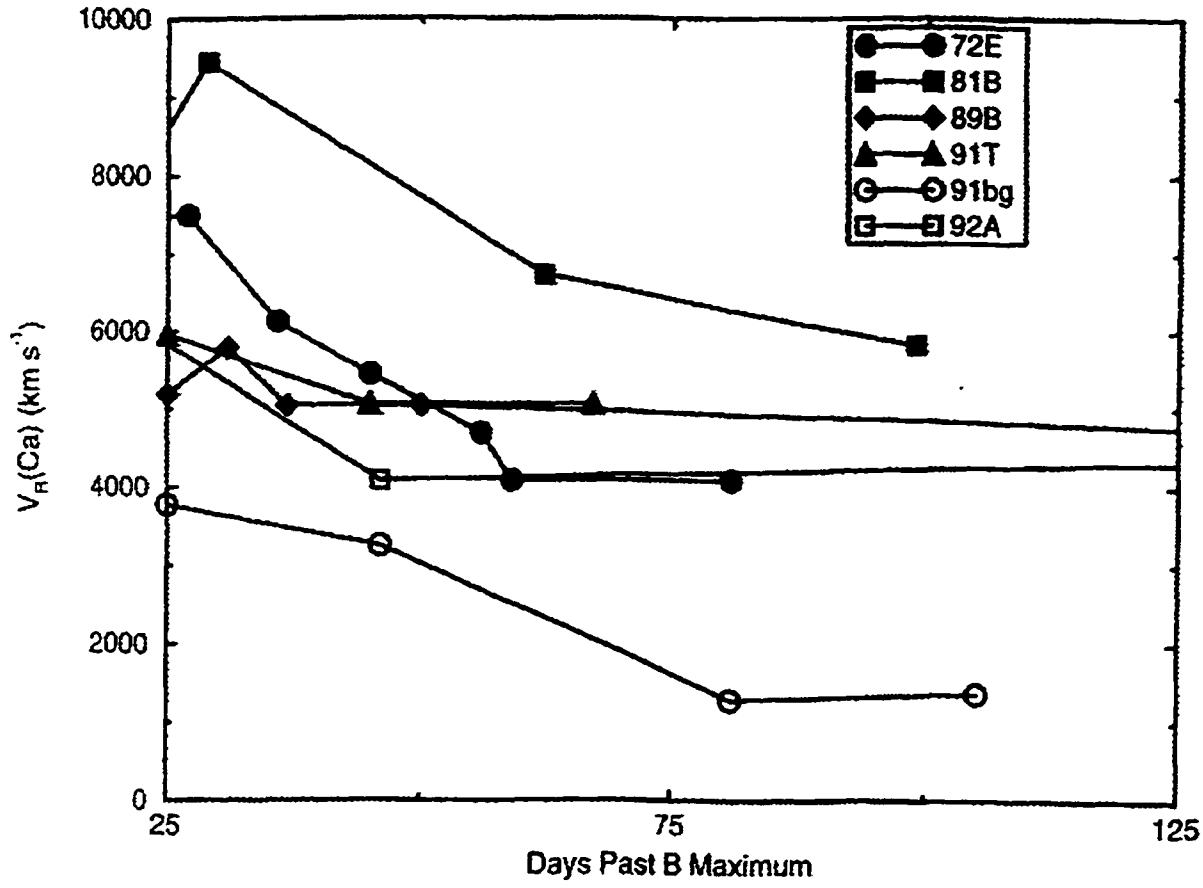

FIG 2. -- V_R(Ca) is plotted against phase for six SN Ia's: 1972E (Kirshner et al. 1973; Branch & Tull 1979), 1981B (Branch et al. 1983), 1991T (Filippenko et al. 1992a; Phillips et al. 1992b), 1989B (Wells et al. 1994), 1991bg (Filippenko et al. 1992b; Leibundgut et al. 1993), and 1992A (Kirshner et al. 1993).

FIG 3. (Following Page) -- M_V is plotted against V_R(Ca). (a) M_V values based on the Tully-Fisher method (squares) and surface brightness fluctuations (circles), on a scale of H_o = 85 km s^{-1} Mpc^{-1}. Filled symbols denote spectroscopically normal SN Ia's, and open symbols denote spectroscopically peculiar SN Ia's. (b) M_V values of SNs 1937C and 1972E based on Cepheids (filled symbols) and based on rescaling H_o from 85 to 57 km s^{-1} Mpc^{-1}(open symbols). (c) Filled symbols denote hydrodynamical models (squares, Khokhlov et al. 1993; circles, Höflich 1995), and M_V values of the SN Ia's are based on rescaling H_o from 85 to 60 km s^{-1} Mpc^{-1}.

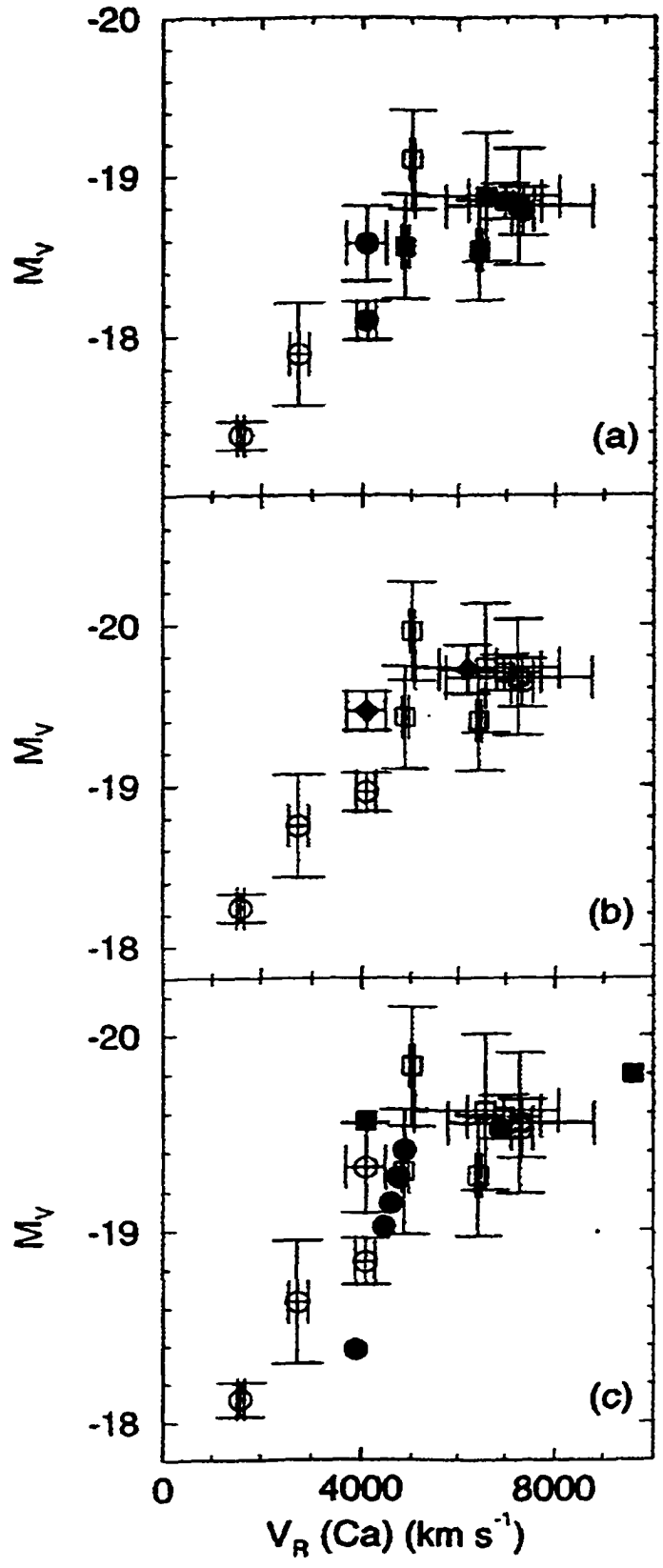
-20
-19
-18
M_V
(a)
-20
-19
-18
M_V
(b)
-20
-19
-18
M_V
(c)
0
4000
8000
V_R (Ca) (km s^{-1})

TABLES

TABLE 1

SUPERNOVA PARAMETERS

SN	Galaxy	M_V	Distance Technique	V_R(Ca) (km s^{-1})	Phase (days)	Reference
1937C	IC 4182	-19.72 ± 0.15	Cepheid	6200 ± 600	72	1
1960F	NGC 4496	-18.87 ± 0.40	T-F	6580 ± 1500	64	2
1972E	NGC 5253	-18.53 ± 0.23	SBF	4075 ± 400	81	3
		-19.46 ± 0.12	Cepheid			
1981B	NGC 4536	-18.54 ± 0.31	T-F	6450 ± 50	62, 99	4
1986G	NGC 5128	-17.89 ± 0.32	SBF	2725 ± 200	56	5
1989B	NGC 3627	-18.56 ± 0.32	T-F	4900 ± 75	50, 154	6
1989M	NGC 4579	-18.81 ± 0.36	T-F	7300 ± 1500	270	7
1990N	NGC 4639	-18.84 ± 0.11	T-F	6950 ± 750	310	7
1991T	NGC 4527	-19.10 ± 0.31	T-F	5050 ± 50	67	8
1991bg	NGC 4374	-17.38 ± 0.09	SBF	1600 ± 70	81	9
1992A	NGC 1380	-18.10 ± 0.12	SBF	4080 ± 200	46	10
1994D	NGC 4526	-18.78 ± 0.15	SBF	7325 ± 225	77	11

REFERENCES.—(1) Minkowski 1939; (2) J. L. Greenstein, unpublished; (3) Kirshner et al. 1973; (4) Branch et al. 1983; (5) Phillips et al. 1987; (6) Wells et al. 1994; (7) Ruiz-Lapuente et al. 1995; (8) Phillips et al. 1992b; (9) Leibundgut et al. 1993; (10) Kirshner et al. 1993; (11) Gomez & Lopez 1994.

TABLE 2

MODEL PARAMETERS

Model	M_V	V_{min}(Ca) (km s^{-1})	M_{Ni} ($M_\odot$)
N21	−19.80	9600	0.83
N32	−19.56	4100	0.56
M35	−19.52	6904	0.67
M36	−19.41	4875	0.60
M37	−19.27	4758	0.51
M38	−19.14	4597	0.43
M39	−19.02	4471	0.34
M312	−18.38	3875	0.20

REFERENCES

Branch, D. 1984, in Ann. N. Y. Acad. Sci., no. 422, Eleventh Symposium on Relativistic Astrophysics, ed. D. S. Evans, 186

--------. 1982, ApJ, 392, 35

Branch, D., Fisher, A., Herczeg, T. J., Miller, D.L., and Nugent, P. 1994, ApJ, 421, L87

Branch, D., Fisher, A., and Nugent, P., 1993, AJ, 106, 2383

Branch, D., Lacy, C. H., McCall, M.L., Sutherland, P.G., Uomoto, A., Wheeler, J.C., and Willis, B.J. 1983, ApJ, 270, 123

Branch, D., and Tull, R.G. 1979, AJ, 84, 1837

Branch, D., and van den Bergh, S. 1993, AJ, 105, 2231

Filippenko, A. V., et al. 1992a, ApJ, 384, L15

---------. 1992b, AJ, 104, 1543

Gomez, G., & Lopez, R. 1994, private communication

Hamuy, M. et al. 1995, AJ, 109, 1

Höflich, P. 1995, ApJ, 443, 89

Höflich, P., Khokhlov, A.M., & Wheeler, J.C. 1995, ApJ, 444, 831

Khokhlov, A., Müller, E., Höflich, P. 1993, A&A, 270, 223

Kirshner, R.P., et al. 1993, ApJ, 415, 589

Kirshner, R.P., Oke, J.B., Penston, M.V., and Searle, L. 1973, ApJ, 185, 303

Leibundgut, B., et al. 1993, AJ, 105, 301

Minkowski, R. 1939, ApJ, 89, 156

Müller, E., and Höflich, P. 1994, A&A, 281, 51

Phillips, M.M. 1993, ApJ, 413, L105

Phillips, M.M., et al. 1987, PASP, 99, 592

Phillips, M.M., Jacoby, G.H., Walker, A.R., Tonry, J.L, and Ciardullo, R. 1992a, BAAS, 24, 749

Phillips, M.M., et al. 1992b, AJ, 103, 1632

Pierce, M.J. 1994, ApJ 430, 53

Pierce, M., and Jacoby, G. 1995, preprint

Riess, A.G. Press, W.H., and Kirshner, R.P. 1995, ApJ, 438, L17

Ruiz-Lapuente, P., Kirshner, R.P., Phillips, M.M., Challis, P.M., Schmidt, B.P., Filippenko, A.V., and Wheeler, J.C. 1995, ApJ, 439, 60

Saha, A., Labhardt, L., Schwengeler, H., Macchetto, F.D., Panagia, N., Sandage, A., and Tammann, G.A. 1994, ApJ, 425, 14

Saha, A., Sandage, A., Labhardt, L., Schwengeler, H., Tammann, G.A., Panagia, N., Macchetto, F.D. 1995, ApJ, 438, 8
Schaefer, B.E. 1994, ApJ, 426, 493
Tammann, G.A., and Sandage, A. 1995, ApJ, in press
Tonry, J.L., et al. 1990, AJ, 100, 1414
Vaughan, T., Branch, D., Miller, D.L., and Perlmutter, S. 1995, ApJ, 439, 558
Wells, L.A., et al. 1994, AJ, 108, 2233

Chapter 6

EVIDENCE FOR A HIGH-VELOCITY CARBON-RICH LAYER IN THE TYPE Ia SN 1990N

Adam Fisher, David Branch, Peter Nugent, and E. Baron

published in the Astrophysical Journal Letters.

ABSTRACT

We use a parameterized spectrum-synthesis code to make a direct analysis of a high quality spectrum of the Type Ia SN 1990N that was obtained by Leibundgut et al. 14 days before the time of optical maximum. We suggest that the absorption feature observed near 6400Å, which has been attributted to blueshifted λ6355 of Si II, actually was produced by blueshifted λ6580 of CII, in a high-velocity (v > 26,000 kps) carbon-rich region. Implications for SN Ia explosion models are briefly discussed.

1. INTRODUCTION

Rapid progress is being made toward achieving the ability to carry out physically self-consistent NLTE modeling of the spectra of Type Ia supernovae (Höflich 1995; Höflich et al. 1997; Nugent et al. 1995a, 1995b, 1997; Baron et al. 1996b). Such detailed calculations are essential for making quantitative abundance determinations from spectra and for testing particular hydrodynamical models of supernovae against observation. However, given the computaional complexity, it is not feasible to calculate detailed synthetic spectra for large numbers of parameterized atmosphere models.

This paper is the first of a series in which our goal is to extract information from observed supernova spectra in a much more direct way, using a comparatively simple, parameterized, spectrum-synthesis code, SYNOW. Because SYNOW does not solve rate equations t obtain atomic level populations and does not do continuum transfer, it cannot be used for quantitative abundance determinations. The virtue of SYNOW is its speed, which enables us to calculate a very large number of spectra, with a very large line list, for comparison with each observed spectrum. Therefore, we can use SYNOW interactively, in an empirical spirit, to establish line-identifications and the intervals of ejection velocity within which the presence of particular ions can be detected. In this kind of "direct" spectral analysis, the essential role of SYNOW is to take line blending into account. The composition and velocity constraints that we obtain using SYNOW can provide guidance to those who compute hydrodynamical explosion models and to those who carry out the much more computationally intensive NLTE spectrum modeling.

In this Letter we concentrate on the high quality spectrum of the Type Ia SN 1990N that was obtained 15 days before maximum light by Leibundgut et al. (1991). This spectrum showed important differences from spectra of SN 1990N at later phases (Leibundgut et al. 1991; Phillips et al. 1992; Jeffery et al. 1992; Mazzali et al. 1993), which were those of a normal SN Ia (Branch, Fisher, & Nugent 1993). Leibundugt et al., Jeffery et al., and Mazzli et al. inferred, from the -14 day spectrum, the presence of calcium, silicon, iron, and cobalt moving at velocities up to ~ 25,000 kps, and stressed that

these elements are not present at such high velocities in the standard (unmixed) carbon-deflagration model W7 (Nomoto, Thielemann, & Yokoi 1984; Thielemann, Nomoto, & Yokoi 1986). This then motivated several discussions of alternative explosion models for SN 1990N (Shigeyama et al. 1992; Yamaoka et al. 1992).

In §2, we briefly describe SYNOW, and the differences between it and other parameterized spectrum-synthesis codes that been used to interpret this spectrum of SN 1990N. Our analysis of the spectrum is presented in §3, and the implications of our results for SN Ia explosion models are discussed in §4.

2. SPECTRUM CALCULATIONS

SYNOW is an improved an efficient version of the supernova spectrum-synthesis code that has been used in the past by Branch and collaborators (e.g. Branch et al. 1983, 1985; Filippeno et al. 1992). Line formation is treated in the Sobolev approximation. An extensive general discussion of Sobolev line formation in supernova spectra has been given by Jeffery & Branch (1990), and further details of SYNOW will be given elsewhere (Fisher, Branch & Baron 1997). Line formation occurs outside a sharp spherical photosphere that emits a blackbody continuum at temperature T_{bb} parameter; its value is chosen simply to give a reasonable slope of the underlying continuum. The ejection velocity of matter at the photsphere is v_{phot}, and outside the photosphere the ejection velocity is proportional to radius, so velocity serves as the radial coordinate. In the Sobolev approximation we must specify, for each line, the radial dependence of the optical depth and the source function; for an isolated

(unblended) line these two functions would determine the line profile in the flux spectrum. For each ion, the optical depth of a reference line, at some specified velocity is a fitting parameter, and the strengths of the other lines of that ion, relative to the reference line, are determined by oscillator strengths and the approximation of a Boltzmann distribution of the lower level populations at an exciation temperature T_{exc}, which is independent of velocity. The source function is treated in the approximation of pure resonance scattering. The effects of multiple scattering (line blending) are properly taken into account (within the limitaions of the Sobolev approximation; see Baron, Hauschildt, & Mezzacappa 1996a for strictures on the use of the Sobolev approximation in *detailed* calculations). We use the 42 million line list of Kurucz (1993).

For a synthetic-spectrum calculation, we must specify values of T_{bb}, V_{phot}, T_{exc}, a reference-line optical depth for each ion whose lines are being used, and the radial dependence of the optical depths. A maximum velocity V_{max} of the line-forming region also can be introduced.

Parameterized spectrum-synthesis studies of SN 1990N have been carried out by Jeffery et al. (1992) and Mazzali et al. on approximate radiative-equilibrium temperature distributions. Jeffery et al. carried out full LTE calculations, including a Planckian rather than a resonance-scattering line source function. They used an exponential density distribution, and the list of 0.55 million lines of Kurucz. Mazzali et al. used a Monte Carlo code, taking the effects of departures from LTE on line optical depths into account in a very approximate way (i.e., without solving rate equations). They used a

resonance scattering line source function, the density distribution of model W7, and a line list derived from those of Abbott (1982) Kurucz & Peytremann (1975).

The most significant differences between our conclusions and those of Jeffery et al. (1992) and Mazzali et al. (1993) will turn out to have less to do with the treatment of the radiative transfer than with the composition structures that are considered. For $v > 14{,}900$ kps, Jeffery et al. used a uniform composition that was determined by trial and error spectrum fitting. Mazzali et al. used a single composition (for all velocities) that was obtained by homogenizing the composition of model W7 above the model velocity of 8000 kps.

3. ANALYSIS OF THE -14 DAY SPECTRUM OF SN 1990N

We have calculated a very large number of synthetic spectra for comparison with the -14 day spectrum of SN 1990N (as well as a large number for comparison with spectra at later epochs that will be presented elsewhere). For the spectra shown in this paper, T_{exc} = 9000 K, T_{bb} =12,000 K, and v_{phot} = 19,000 kps. The radial dependence of the line optical depths is Exp (-v / v_e), with v_e = 2900 kps.

Figure 1a shows a "conventional" interpretation of the optical part of the -14 day spectrum. Only lines of Ca II, Fe III, S II, Mg II, and Si II are used, and these contribute significant features in the synthetic spectrum as indicated in the figure. We regard the presence of the Ca II, Fe III, and S II features in the observed spectrum to by unambiguous, and the presence of Mg II to be probable. (it should be noted that the sharp decline in the observed

spectrum redward of ~8070Å may be spurious [Jeffery et al. 1992].) The height of the emission peak to the blue of the Ca II H and K absorption feature is sensitive to the maximum velocity. If v_{max} is too high, the blue edge of the synthetic Ca II H and K absorption extend to such short wavelengths that the synthetic flux peak near 3500-3600 Å becomes too suppressed. We adopted v_{max} = 45,000 kps. Jeffery et al. (1992) adopted 40,000 kps for the same reason. Like Jeffery et al. (1992) and Mazzali et al. (1993), we encountered difficulty in fitting the unusual, flat bottomed absorption observed near 6040 Å with λ6355 of Si II. The contrast between the synthetic emission peak and the synthetic absorption trough is too strong, and the bottom of the synthetic absorption is not flat enough. The profile of the observed feature is more like one formed in a high-velocity shell that is detached from the photosphere (see Fig. 6 of Jeffery & Branch 1990). If Type Ia SNs are exploding carbon-oxygen white dwarfs, the element that is most likely to be confined to a high-velocity shell is carbon (see section 4). And, it happens that CII has a strong line that is suitably located to account for the 6040 Å feature - λ6580 of C II is about 10,000 kps to the red of λ6355 of Si II. In Figure 1b, which shows an unconventional interpretation of the -14 day spectrum, lines of Si II have been removed and lines of C II have been introduced instead. Now the 6040 Å feature is produced by CII λ6580, forming in a detached shell that has a minimum velocity of 26,000 kps. The C II line optical depths are taken to be independent of velocity, and the blue edge of the absorption requires C II up to 35,000 kps. A close-up of the region near the 6040 Å feature is shown in Figure 2. Because C II clearly provides a better

fit than Si II, and because the confinement of carbon to a high velocity shell is physically plausible, we think that the 6040Å feature actually was produced by C II rather than by Si II. Elsewhere (Fisher et al. 1997) we will consider the extent to which C II generally appears in premaximum spectra of Type Ia SNs. There is no doubt that the absorption observed near 6100 Å at maximum light is produced mainly by Si II, in SN 1990N and in other Type Ia SNs. Therefore, in premaximum spectra a weakening CII line may be blended with a strengthening Si II line. A consequence of this could be that the maximum detected velocities of silicon that have been inferred from the blue edges of the "Si II" absorption features in premaximum SN Ia spectra (e.g. SN 1994D, Pata et al. 1996; SN 1992A, Kirshner et al. 1993) have been overestimated.

It is clear from Figures 1a and 1b that the ions that produce the conspicuous features in the optical spectrum cannot account for the observed ultraviolet deficiency. In Figure 1c, we have introduced Fe II, Cr II, and Mn II, whose numerous lines, along with those of Mg II, do approximately account for the ultraviolet without spoiling the fit in the optical. The issue of whether freshly synthesized, high-velocity iron-peak elements are required to account for the spectrum at wavelengths shorter than about 3500Å is an important one, as far as hydrodynamical models are concerned. Jeffery et al. (1992) found that in an LTE analysis the ultraviolet part of the SN 1990N -14 day spectrum could not be fitted with just primordial (stellar progenitor) iron-peak elements, while Wheeler, Swartz, & Harkness (1993) argue, also on the basis of LTE, that primordial abundances probably *are* responsible.

To summarize our conclusions about the composition structure of the outer layers of SN 1990N from its -14 day spectrum; a carbon-rich region extended from ~26,000 kps to at least 35,000 kps. The only other ion detected above 26,000 kps is Ca II, which must not extend beyond ~45,000 kps. This high-velocity calcium probably is primordial. Between the velocity at the photosphere, 19,000 kps, and the bottom of the carbon-rich zone at 26,000 kps, lines of Ca II, Fe III, SII, and probably Mg II are detected. Because noticeable S II lines, in particular, are unlikely to be produced by primordial sulphur, it is likely that freshly synthesized intermediate-mass elements are present in this velocity range. This is to be expected from SN Ia explosion models generally; those that have an unburned C-O shell on the outside have a region just beneath it in which carbon-burning took place and which is rich in oxygen and freshly synthesized elements of intermediate mass.

A detailed NLTE analysis of the -14 day spectrum of SN 1990N now should be carried out to test our C II identification and to determine whether freshly synthesized iron-peak elements are needed to account for the optical Fe III lines and the ultraviolet deficiency.

4. IMPLICATIONS FOR EXPLOSION MODELS

The composition that we infer for SN 1990N is not consistent with published "helium-ignitor" models, in which an off-center ignition in an accumulated helium layer leads to a second detonation deep inside underlying C-O (Livne 1990; Wooseley & Weaver 1994b; Livne & Arnet 1995; Höflich & Khokhlov 1996). These models eject little

carbon. Detailed NLTE calculations for some of the helium-ignitor models confirm that they also fail to account for the spectra of Type Ia SNs near maximum light (Höflich et al. 1997; Nugent et al. 1997)

Recent work on flame propagation in C-O white dwarfs (Arnett & Livne 1994a, 1994b; Khokhlov 1995; Bychkov & Liberman 1995a, 1995b; Niemeyer & Hillebrandt 1995a, 1995b; Garcia-Senz & Woosley 1995; Khokhlov, Oran & Wheeler 1997) make it increasingly clear that three-dimensional calculations will be required in order to calculate the composion structure of "carbon-ignitors", in which the first nuclear ignition is of carbon, deep inside the C-O. The presence of a high-velocity carbon-rich layer in SN 1990N would provide an important constraint on such modeling. Because detailed three dimensional composion predictions are not yet available, here we briefly discuss the extent to which the compositions of the one-dimensional models of carbon-ginitors in their published forms (i.e., without invoking radial composition mixing) are or are not consistent with the composition structure that we have inferred for the outermost layers of SN 1990N.

Published late-detonation models (Nomoto et al. 1984; Woosley & Weaver 1986; Yamaoka et al. 1992), in which the deflagration turns into a detonation relatively near the surface of the ejecta, also produce little carbon. Detonation of sub-Chandrasekhar CO white dwarfs (Shigeyama et al. 1992; Khokhlov et al. 1993) do have high-velocity carbon, but their light curves probably would be too fast for normal Type Ia SNs, and especially for SN 1990N, whose light curve was on the slow side.

Höflich & Khokhlov (1996) consider the light curves of many kinds of SN Ia models and conclude that the ones that provide acceptable fits to the light curves of SN 1990N are the pulsating-delayed detonation models of PDD3 and PDD1a, in which a pulsation of the white dwarf, driven by a weak central DET2ENV2 and DET2ENV4 in which sub-Chandrasekhar mass C-O white dwarfs detonate inside extended low-density C-O envelopes. In their published forms (Khokhlov et al. 1993) PDD3, DET2ENV2, DET2ENV4 have little but unburned C-O down to v ~ 10,000 kps, which cannot account for the spectra of SN 1990N. PDD1a and some other PDD models have unburned C-O only down to ~16,000 kmps, and it might be possible to construct PDD models higher minimum velocities of unburned C-O (P. Höflich 1996, private communication).

The deflagration model W7 has a carbon-oxygen zone that extends down to ~15,000 kps. Whether a deflagration model with the bottom of the C-O zone speed up to 26,000 kps could be engineered by suitably parameterizing the velocity of the burning front is not clear, because the deflagration might turn into a late detonation.

The published models that do have a high-velocity C-O zone are delayed detonations (Khokhlov et al. 1993; Woosley & Weaver 1994a; Höflich 1995), in which the deflagration-detonation transition occurs deeper inside the ejecta than it does in late detontions. The composition of a delayed detonation model is plotted against velocity in Figure 17 of Nomoto et al. (1994) and that of model DD4 of Woosley & Weaver is displayed in Figure 4 of Kirsher et al. (1993). Both models have a carbon-rich zone above ~25,000 kps, atop a

region of oxygen and synthesized intermediate-mass elemnts. Synthesized iron-peak elements extend only up to ~15,000 ks. Delayed detonations appear to be the most promising one-dimensional models for SN 1990N, but it is important to test our C II identification by means of NLTE calculations and to determine whether synthesized iron-peak elements are need at v > 15,000 kps in SN 1990N.

We are grateful to Ken Nomoto and to an anonymous Texan referee for helpful comments. This work has been supported by NSF grants AST 94-17102 and 94-17242.

FIGURES

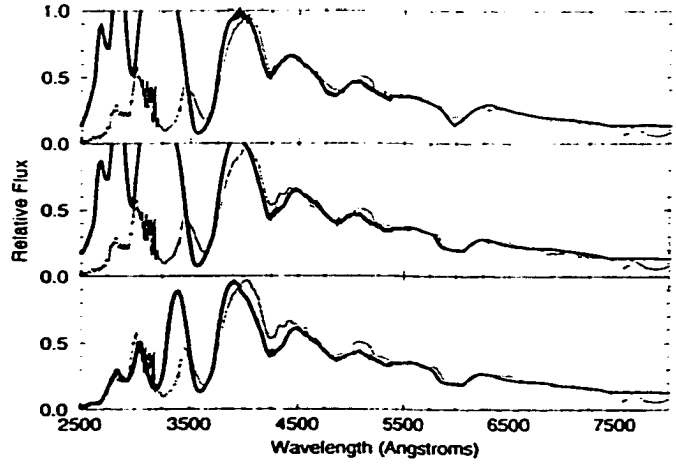

FIG. 1.—The −14 day spectrum of SN 1990N (Leibundgut et al. 1991) is compared to three synthetic spectra. The top panel contains lines of Ca II, S II, Fe III, Mg II; the middle panel is like the top but with C II lines included and Si II lines omitted; the bottom panel is like the middle but with lines of Fe II, Cr II, and Mn II also included.

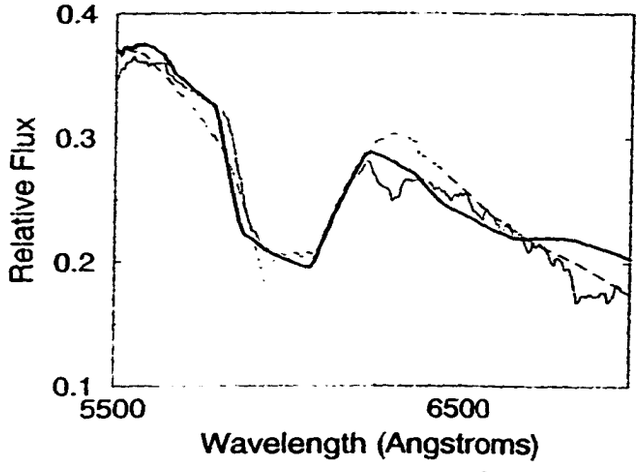

FIG. 2.—Enlarged view of the region near the 6040 Å absorption feature. The dashed line is from the top panel of Fig. 1 (with Si II), and the thick solid line is from the middle panel of Fig. 1 (with C II).

REFERENCES

Abbot, D.C. 1982, ApJ, 259, 282

Arnett, W.D. , & Livne, E. 1994a, ApJ, 427, 315

-------.1994b, ApJ, 427,330

Baron, E., Hauschildt, P.H., & Mezzacappa, A. 1996a, MNRAS, 278, 763

Baron, E., Hauschildt, P.H., Nugent, P., & Branch D. 1996b, MNRAS, 283

Branch, D., Doggett, J.B., Nomoto, K., & Thielemann, F.-K. 1985 ApJ, 294, 619

Branch, D., Fisher, A., & Nugent, P. 1993, AJ, 106, 2383

Branch, D., Lacy, C..H., McCall, M.L., Sutherland, P.G., Uomoto, A., Wheeler, J.C., & Willis, B.J. 1983 ApJ, 270, 123

Bychkov, V.V, & Liberman, M.A. 1995a, A&A, 304 440

---------. 1995b, ApJ, 451,711

Filippenko, A.V., et al. 1992, AJ, 104,1543

Fisher, A., Branch, D., & Baron, E. 1997, in preparation

Garcia-Senz, D., & Woosley, S.E. 1995, ApJ, 454, 895

Höflich, P. 1995, ApJ, 443, 89

Höflich, P. , & Khoklov, A. 1996, ApJ, 457, 500

Höflich, P. , Khoklov, A., Wheeler, J.C., Nomoto, K., & Thielemann, F.-K. 1997, in Thermonuclear Supernovae, ed. P. Ruiz-Lapuente, R. Canal, & J. Isern (Dordrecht: Kluwer), 659

Jeffery, D.J., & Branch, D. 1990 in Jerusalem Winter School for Theoretical Physics, Vol. 7 Supernovae, ed. J.C. Wheeler, T.Piran, & S. Weinberg (Singapore: World Scientific), 90

Jeffery, D.J., Liebundgut, B., Kirshner, R.P., Benetti, S., Branch, D., & Sonneborn, G. 992, ApJ, 397, 304

Khokhlov, A. 1995, ApJ, 449, 695

Khokhlov, A., Müller, E., & Höflich, P. 1993m A&A, 270, 223

Khokhlov, A. M., Oran, E.S., & Wheeler, J.C. 1997 in Thermonuclear Supernovae, ed. P. Ruiz-Lapuente, R. Canal, & J. Isern (Dordrecht: Kluwer), 475

Kirshner, R.P., et al. 1993, ApJ, 415, 589

Kurucz, R.L. 1991, in Stellar Atmospheres: Beyond Classical Models, ed L. Crivellari, I. Hubeny, & D.G. Hummer (Dordrecht: Kluwer), 441

Kurucz, R.L. 1993, CD ROM, Atomic Data for Opacity Calculations

Kurucz, R.L. & Peytremann, E. 1975, Smithsonian Ap. Obs. Spec. Rep. 362
Liebundgut, B., Kirshner, R.P., Filippenko, A.V., Shields, J.C., Foltz, C.B., Phillips, M.M., & Sonnebom, G. 191, ApJ, 371, L23
Livne, E. 1990, ApJ, 354, L53
Livne, E., & Arnett, W.D. 1995, ApJ 452 769
Mazzali, P.A., Lucy, L. Danziger, I.J., Gouiffes, C., Cappelarro, E., & Turrato, M. 1993, A&A, 269, 423
Niemeyer, J.C., & Hillebrandt, W. 1995a, ApJ, 452, 769
--------. 1995b, ApJ, 452, 779
Nomoto, K., Thielemann, F.-K., & Yokoi, K. 1984, ApJ, 286, 644
Nomoto, K., Yamaoka, H., Shigeyamma, T., Kumagai, S., & Tsujimoto, T. 1994, in Supernovae, ed. S.A. Bludman, R. Mochkovitch, & J. Zinn-Justin (Amsterdam: North-Holand), 199
Nugent, P., Baron, E., Hauschildt, P.H., & Branch, D. 1995a, ApJ, 441, L33
--------. 1997, ApJ, submitted
Patat, F., et al. 1996, MNRAS, 278, 111
Phillips, M.M., et al. 1992, AJ, 103, 1632
Shigeyama, T., Nomoto, K., Yamaoka, H.m & Thielemann, F.-K. 1992, ApJ, 386, L13
Thielemann, F.-K., Nomoto, K., & Yokoi, K. 1986, A&A, 158 17
Wheeler, J.C., Swartz, D.A., & Harkness, R.P. 1993, Phys. Rep., 227 113
Woosley, S.E., & Weaver, T.A. 1986, in Radiation Hydrodynamics in Stars and Compact Objects, ed. D. Mihalas & K.-H. Winkler (Berlin: Springer), 91
---------. 1994a, in Supernovae, ed. S.A. Bludman, R. Mochkovitch, & J. Zinn-Justin (Amsterdam: North-Holland), 63
---------. 1994b, ApJ, 423, 371
Yamaoka, H., Nomoto, K., Shigeyama, T., & Theilemann, F.-K. 1992, ApJ, 393

Chapter 7 -

On the spectrum and nature of the peculiar Type Ia supernova 1991T

Adam Fisher, David Branch, Kazuhito Hatano and E. Baron

published in Monthly Notices of the Royal Astronomical Society

ABSTRACT

A parametrized supernova synthetic-spectrum code is used to study line identifications in the photospheric-phase spectra of the peculiar Type Ia SN 1991T, and the extract some constraints on the composition structure of the ejected matter. The inferred composition structure is not like that of any hydrodynamical model for Type Ia supernovae. Evidence that SN 1991T was over-luminous for a SN Ia is presented. and it is suggested that this peculiar event probably was a substantial super-Chandrasekhar explosion that resulted from the merger of two white dwarfs.

1. INTRODUCTION

SN 1991T was a well observed and spectroscopically peculiar Type Ia supernova (Filippenko et al. 1992; Phillips et al. 1992; Ruiz-Lapuente et al. 1992; Branch, Fisher & Nugent 1993). Before and around the time of maximum light its optical spectrum showed strong lines of Fe III rather than the usual SN Ia lines of singly ionized elements of intermediate mass, and although the deep red Si II absorption that is characteristic of SNe Ia finally did develop after maximum light it never reached its usual strength.

In this paper we report the results of a study of photospheric-phase spectra of SN 1991T using the parameterized supernova spectrum-synthesis code SYNOW (Fisher et al. 1997, Fisher 1999). In Section 2, previous studies of the optical spectra of SN 1991T are briefly summarized. Our method of 'direct' spectral analysis is described in Section 3, and results are presented in Section 4. In Section 5 we discuss evidence that SN 1991T was too luminous to be a Chandrasekhar-mass explosion, and suggest that it probably was a substantially super-Chandrasekhar explosion resulting from the merger of two white dwarfs. A general discussion appears in Section 6.

2. PREVIOUS STUDIES OF SN 1991T SPECTRA

Filippenko et al. (1992) presented optical spectra obtained from -12 to +47 days. [Throughout this paper, epochs are in days with respect to the date of maximum light, 1991 April 28 (Phillips et al 1992; Lira et al. 1998). Filippenko et al. (1992) used April 26.] They showed that although the pre-maximum optical spectra did not resemble those of any other supernova, beginning near maximum light the usual SN Ia lines of intermediate-mass elements slowly developed, and months after explosion the iron-dominated spectrum appeared almost identical to that of a typical SN Ia. They identified the two strong features in the pre-maximum optical spectrum with the Fe III λ4404 and λ5129 multiplets, and concluded that the composition of the outer layers was dominated by iron-group elements. Given their inferred composition structure of a thin layer of intermediate-mass elements sandwiched between inner and out regions dominated by

iron-peak elements, they favored a double-detonation model (the nearly complete incineration of a mildly sub-Chandrasekhar-mass white dwarf by detonation waves propagating inward and outward from the base of an accumulated helium layer) for the origin of SN 1991T. They noted that it was odd, then, that in their +6 day spectrum an absorption near 7550Å that is ordinarily attributed to OI λ7773 seemed to be present at is usual strength.

Ruiz-Lapuente et al. (1992) presented optical spectra obtained on seven consecutive nights from -13 to -7 days. They too identified the Fe III lines, as well as lines of Ni III, and they too concluded that the outer layers had undergone complete burning to iron-peak elements. They supported that conclusion by presenting synthetic spectra based on approximate NLTE calculations, for the time-dependent nickel-cobalt-iron composition that results from the radioactive decay of initially pure ^{56}Ni. As they noted, though, the lines in their synthetic spectra tended to be stronger than the observed lines. Their spectra did not extend late enough in time for them to encounter the oxygen line. They did, however, discuss another puzzle. Their spectra showed no evidence for the high velocities of the outer layers that would follow from complete burning to iron-peak elements. They suggested that the line-forming layers had been decellerated upon encountering a low-density carbon-oxygen envelope associated with a merger to two white dwarfs.

Phillips et al. (1992) presented optical spectra obtained from -13 to +66 days. From the appearance of the spectra the concluded that the abundances of silicon, sulfur, and calcium in the outer layers

were unusually low, but they did not specify what was present in their place.

Jeffery et al. (1992) carried out parameterized synthetic-spectrum calculations, based on the Sobolev approximation, an approximate radiative-equilibrium temperature distribution, and full LTE including a Planckian rather than a resonance scattering source function. They modified the composition structure of the carbon deflagration model W7 (Nomoto, Thielemann & Yokoi 1984; Thielemann, Nomoto & Yokoi 1986), by trial and error, to get reasonable fits to observed optical (and some IUE near-ultraviolet) spectra obtained at -9, -3 and +10 days. The adopted composition (displayed in their fig. 7 was complex, and not simply dominated in the outer layers by iron-peak elements. It was like that of model W7 for ejection velocities less than 8500 kps; heavily modified between 8500 and 14,400 kps in favor of iron-peak elements at the expense of intermediate-mass elements; heavily modified between 14,400 and 21,000 kps in favor of both intermediate-mass and iron-peak elements at the expense of carbon and primarily carbon and oxygen above 21,000 kps. Noting that somewhat weaker Fe III lines might have gone unrecognized in previous studies of other SNe Ia, they suggested that although the composition structure was unusual, the explosion history of SN 1991T probably was not fundamentally different from that of a normal SN Ia.

Mazzali, Danziger & Turatto (1995) also carried out parameterized spectrum calculations, using a Monte Carlo code and a resonance scattering source function. They were restricted to

using a homogeneous composition above the photosphere at each of the eight epochs considered. For each epoch they used a combination of a mixed W7 composition and the time-dependent ^{56}Ni-decay composition. They concluded that an unusually high temperature was partly responsible for the weakness of the lines of singly ionized intermediate-mass elements, but also that iron-peak elements dominated the composition above 13,000 kps. They favored a 'late-detonation' (Yamaoka et al. 1992) explosion mechanism in a Chandraskhar-mass white dwarf for the origin of SN 1991T. (Mazzali et al. 1995 referred to it as a 'delayed detonation', but by custom that term is used to refer to a class of models that, unlike the late detonations do not synthesize ^{56}Ni in the outer layers; e.g., Khokhlov, Müller & Höflich 1993).

Nugent et al. (1995 calculated detailed NLTE spectra using the PHOENIX code (Hauschildt & Baron 1999, and references therein), for a fixed composition (W7 mixed above 8000 kps, with titanium enhanced by a factor of 10) and a series of temperatures. They found that their series of synthetic spectra gave a good account of many of the spectral differences among SNe Ia, from the peculiar, cool, 'weak' SN 1991bg, through the normal SNe Ia, to the peculiar, warm 'strong' SN 1991T. A high temperature can enhance the FeIII and Si III lines and weaken the lines of singly ionized elements. Still, the temperature differences among SNe Ia are presumably caused by differences in the amounts of ejected ^{56}Ni and differences in the composition structures are certainly to be expected.

Meikle et al. (1996) displayed and discussed an infrared spectrum obtained at the time of maximum light. They considered

the possibility that a P Cygni-like feature having an emission peak near 10,800Å and an absorption near 10,500Å could be attributed to either HeI λ10830 or MgII λ10926, but found difficulties with both identifications.

3. SPECTRUM SYNTHESIS PROCEDURE

In this paper we use the fast, parameterized, supernova spectrum-synthesis code SYNOW to make a 'direct' analysis (Fisher et al. 1997) of spectra of SN 1991T. The goal is to study line identification and determine intervals of ejection velocity within which the presence of lines of various ions are detected, without initially adopting any particular composition structure. The composition and velocity constraints that we obtain with SYNOW can then provide guidance to those who carry out computationally intensive NLTE spectrum modeling. The SYNOW code was described briefly by Fisher et al.(1997) and in detail by Fisher (1999). In our work on SN 1991T we have made extensive use of the paper by Hatano et al. (1999), which presented plots of LTE Sobolev line optical depths versus temperature for six different compositions that might be expected to be encountered in supernovae, and which presented SYNOW optical spectra for 45 individual ions that can be regarded as candidates for producing identifiable spectral features in supernova spectra.

Fisher et al. (1997) concentrated on a high-quality spectrum of the normal Type Ia SN 1990N that was obtained by Leibundgut et al.(1991) at -14 days. Fisher et al. suggested that at this very early phase an absorption feature observed near 6040Å, which had

previously been attributed to moderately blueshifted Si II λ6355, actually was produced by highly blueshifted (v > 26,000 kps) C II λ6580, indicating the presence of an outer high-velocity carbon-rich layer in SN 1990N. In this paper we suggest that SN 1991T also contained an outer carbon-rich layer, but extending to lower velocity than SN 1990N.

We have studied spectra of SN 1991T at seven epochs ranging from -13 days to +59 days. For comparison with each observed spectrum, we have calculated a large number of synthetic spectra with various values of the fitting parameters. These include: T_{bb} , the temperature of the underlying blackbody continuum; T_{exc} , the excitation temperature; v_{phot} , the velocity of matter at the photosphere; and v_{max} , the maximum ejection velocity. For each ion that is introduced, the optical depth of a reference line is also a fitting parameter, with the optical depths of the other lines of the ion calculated assuming Boltzmann excitation at T_{exc} . In addition, we can introduce restrictions on the velocity interval within which an ion is present; when the minimum velocity assigned to an ion is greater than the velocity at the photosphere, the line is said to be detached from the photosphere. The radial dependence of the line optical depths is taken to be exponential with e-folding velocity v_e = 3000 kps (with one exception to be discussed in Section 4.2) and the line source function is taken to be that of resonant scattering in the Schuster-Schwarzchild approximation. The most interesting fitting parameters are v_{phot} ,which as expected decreases with time, and the individual ion velocity restrictions, which constrain the composition structure.

4. SPECTRUM SYNTHESIS RESULTS

In this section we present comparisons of synthetic spectra with observed spectra for four of the seven epochs we studied, to illustrate how we reach our conclusions about the composition structure of the ejecta. The pre-maximum and post-maximum spectra are discussed separately, because the former were so peculiar, while the latter became more increasingly normal.

4.1 Pre-maximum

In the pre-maximum spectra only two features have obvious identifications: two strong features produced by the FeIII λ4404 and λ5129 multiplets. Fig. 1 compares a -13 day observed spectrum to a synthetic spectrum that has v_{phot} = 15,000 kps and T_{ex} = 13,000 K. The optical depth of the FeIII reference line and the velocity at the photosphere have been chosen such that the λ5129 multiplet gives a reasonable fit to the strong P Cygni feature near 5000Å. Similarly, the optical depth of the reference line of Ni III has been chosen to give a reasonable fit to the weaker absorption near 5300Å; then in the synthetic spectrum, Ni III also is responsible for the weak absorption near 4700Å. We consider the presence of Ni III lines in the observed spectrum to be probable.

The diagnostic value of a spectral feature is not simply proportional to its strength. A weak feature in the pre-maximum spectra that is of special interest to is the broad, shallow absorption near 6300Å, which definitely is a real feature because it can be seen in almost all of the spectra obtained earlier than -6 days by Filippenko et al. (1992), Phillips et al. (1992) and Ruiz-Lapuente et al.

(1992) this feature was not mentioned in the previous discussions of the SN 1991T spectra. As shown in Fig 1, CII λ6580 can account for this feature, and in spite of searching for a plausible alternative with the help of the plots of Hatano et al. (1999), we have none to offer.

Fig. 2 compares a -4 days observed spectrum to a synthetic spectrum that has v_{phot} = 10,000 kps and T_{exe} = 13,000 K. The two strong Fe III features are fitted reasonably well, and Ni III and Ni II probably account for some of the other observed features. Additional ions of iron-peak elements would need to be introduced to account for the observed flux deficiency and λ < 3000 Å. The narrow absorption near 4400Å is well fitted by the Si III λ4560 multiplet, which is the strongest optical multiplet of Si III and was identified in SN 1991T by Jeffery et al. (1992). Note that at this phase, there is a weak absorption near 6200Å, rather than the 6300Å absorption of earlier phases. In general, supernova absorption features shift redward as the photosphere recedes with respect to the matter, or they remain unshifted if the line has become detached. A blueward shift of an absorption is generally a sign that a new line is beginning to make a significant contribution In this case the new line is very likely Si II λ6355, which in normal Sne Ia is very strong at this phase. (in the synthetic spectrum, lines of Ni II and Fe III also are affecting this feature.)

From the pre-maximum spectra we infer that iron, silicon, and probably nickel were present above 10,000 kps, with iron being detected up to 20,000 kps. If the nickel identifications are correct, the freshly synthesized iron-peak elements were present in these outer layers. Carbon seems to have been present down to at least

15,000 kps. Between -13 and -4 days, the red absorption feature apparently transformed from mainly C II forming above about 15,000 kps to mainly Si II forming above 10,000 kps. A very careful study of a good series of spectra obtained within this time interval might better determine the minimum velocity at which C II was present. If the C II line became detached before the Si II line made its appearance, the observed absorption minimum would have remain constant at the detachment velocity until the development of the Si II line started to cause a shift to the blue.

4.2 Post-Maximum

Fig. 3 shows a +6 days observed spectrum. By this time the spectrum had begun to look much less peculiar. The synthetic spectrum has v_{phot} = 9,500 kps and T_{exc} = 10,000 K. The synthetic feature near 5000Å is now a blend of Fe III and Fe II lines. The observed S II and Si II features are weaker and narrower than in normal SNe Ia. In the synthetic spectrum of the top panel, a maximum velocity of 12,000 kps for S II lines has been introduced to fit the absorptions near 5300 and 5500Å, and a maximum velocity of 15,000 kps has been used to fit the Si II absorption near 6200Å. The lower panel shows how the fit degrades when these maximum velocities are not used.

The observed spectrum that appears in Figs 4 and 5 was obtained by W.P.S. Meikle et al. (unpublished) at +59 days. The synthetic spectra have v_{phot} = 4000 kps and T_{exc} = 10,000 K. The upper panel of Fig. 4 shows that resonance scattering by permitted lines of just three ions (Fe II, Ca II, and Na I) can give a reasonable

account of most of the features in the observed spectrum, although the height of the synthetic peaks in the blue indicates that the synthetic spectrum is underblanketed. In the synthetic spectrum Na I and Ca II are detached at 9000 kps, and an abrupt decrease in the Fe II line optical depths, by a factor of 10, has been introduced at 10,000 kps. This is inferred to be a measure of the maximum velocity of the iron-peak core. The structure of the synthetic spectrum near 5000Å is quite sensitive to the velocity of the Fe II line optical depth discontinuity (Fisher 1999).

The major shortcoming in the upper panel of Fig. 4 is that the broad minimum observed near 7000Å is not reproduced by the synthetic spectrum. The weak synthetic absorptions in the vicinity are from Fe II. It should be noted that Mazzali et al. (1995) attributed this absorption in a +25 days spectrum to Fe II lines, but at that epoch their other synthetic absorptions, produced by Fe II, appeared to be much too strong. We, too, find that the 7000Å feature cannot be attributed to Fe II without making other Fe II features much too strong.

A possible Identification for the absorption near 7000Å is [O II] λ7320,7330 (Fisher 1999; Hatano et al. 1999). For a forbidden transition the natural first approximation to the source function would be the Planck function evaluated at the local electron temperature, but instead of introducing a whole new fitting function involving the radial dependence of the electron temperature, we have simply retained the resonance scattering source function. In the lower panel of Fig. 4 the [O II] feature is calculated with a line optical depth that is detached at 10,000 kps, where τ =0.5, and has a shallow radial

gradient (v_e = 20,000 kps) such that τ = 0.24 at the maximum [O II] velocity of 25,000 kps. The upper panel of Fig. 5, which is like the upper panel of Fig. 4 but with the [O II] feature included in the synthetic spectrum, looks better than the upper panel of Fig. 4. The lower panel of Fig. 5 shows how the fit degrades when Na I is not detached, the discontinuity in the Fe II line optical depths is not introduced, and the upper and lower velocity limits of [O II] are dropped.

From a spectroscopic point of view the [O II] identification is attractive and plausible. Moreover, Kirshner et al. (1993) discussed the velocity interval in which the O I λ7773 line could be detected in the early spectra of a small sample of well observed SNe Ia. For SN 1991T they estimated that the O I line had a significant optical depth from at least as low as 9000 kps to at least as high as 19,000 kps, which is not inconsistent with what we are using for [O II]. However, the mass and associated kinetic energy of the oxygen that would be required to produce a significant [O II] line optical depth, at such high velocities and at this fairly late phase, appear to be high. For this feature, with its very low transition probability, just producing a uniform line optical depth of 0.2 requires

$$M = 0.26\ v_{25}^{3}\ t_{77}^{2}\ f_O^{-1}\ M_{sun} \qquad \mathrm{E_K} = 10^{51}\ v_{25}^{5}\ t_{77}^{2}\ f_O^{-1}\ \mathrm{erg}$$

where v_{25} is the maximum velocity in units of 25,000 kps, t_{77} is the time since explosion in units of 77 days (allowing for a rise time to maximum of 18 days), and f_O is the fraction of all oxygen that is in

the lower level of the transition. It is possible that essentially all of the oxygen is singely ionized at this phase, but f_O must be significantly less than unity, because the lower level of the transition is 3.3 eV above the ground level of singely ionized oxygen. (The ground level of the transition is, at least, the metastable lowest level of the doublets, the true ground level of singely ionized oxygen being a quartet.)

We have no plausible alternative to offer for the 7000 Å minimum. If it is not an absorption feature at all, then the continuum must be at a level that is considerably lower than we have adopted to obtain the fits shown in the top panels of Figs 4 and 5. In that case the minimum would be a consequence of a lack of opacity at the relevant wavelength, as has been suggested for flux minima in infrared spectra of SN 1991T (Spyromilio, Pinto & Eastman 1994) and other SNe Ia (Wheeler et al. 1998). We suspect that the [O II] identification is correct, but in view of the mass and energy problem the maximum [O II] velocity may need to be somewhat lower than the 25,000 kps that we have used.

4.3 Summary of the inferred composition structure

Our line identifications in the spectra of SN 1991T are, for the most part, the same as those of Jeffery et al. (1992) and Mazzali et al. (1995), e.g. Fe III and Fe II, Ni III, Ca II, S II, Si III and Si II, and Na I. In addition, though, we identify C II λ6580 in the -13 days spectrum and, somewhat more tentatively, [O II] λλ7320,7330 in the +59 days spectrum.

In Fisher et al. (1997) we presented evidence for the presence of C II in SN 1990N at v > 26,000 kps. It is thought that when SNe Ia are arranged in a sequence from powerful events like SN 1991T to weak ones like SN 1991bg SN 1990N belongs on the power side (e.g. Phillips et al. 1992; Nugent et al. 1995). One might then expect events that are weaker than SN 1990N to have unburned carbon extending down to velocities lower than 26,000 kps, and our SYNOW studies of other SNe Ia suggest that this generally is the case (Fisher 1999). Similarly, one might expect events like SN 1991T that are thought to be stronger than SN 1990N to have a minimum velocity of carbon that is higher than 26,000 kps. However, in SN 1991T we find evidence for C II moving at least as slow as about 15,000 kps. At the same time, we find evidence that the iron-peak core of SN 1991T extended out to velocities at least as high as in SN 1990N and other SNe Ia. Independently, Mazzali et al. (1998) lists outer velocities of the iron core for 14 SNe Ia inferred from nebular-phase spectra, and they find that SN 1991T has the highest velocity in their sample. Thus SN 1991T seems to have had both slower unburned carbon and a faster iron-peak core than SN 1990N, with its intermediate-mass elements being confined to an unusually narrow velocity interval.

Fig. 6 plots the velocity at the photosphere adopted for our synthetic spectrum fits, as a function of time. The pause in the velocity decrease, around 10,000 kps, presumably reflects an increase in the density or the opacity near the outer edge of the iron-peak core. It should be noted, however, that such a pause is not evident in fig. 17 of Mazzali et al. (1995). Their adopted values of the

velocity at the photosphere are higher than ours before maximum light, lower than ours after maximum light, and they decrease smoothly with time.

Our combined constraints on the composition structure are shown in Fig. 7. The inferred structure is not like that of any hydrodynamical model that has been published. A speculation about the cause of the peculiar composition structure of SN 1991T will be offered in Section 6, after the implication for the high luminosity of SN 199T is considered in the next section.

5. THE LUMINOSITY OF SN 1991T

NGC 4527, the parent galaxy of SN 1991T, is in the southern extension of the Virgo cluster complex. According to the Nearby Galaxies Catalogue (Tully 1988) it is a member of the same small group of galaxies (group 11-4 in Tully's notation) as NGC 4536 and 4496, the parent galaxies of the normal Type Ia SNe 1981B and 1960F. The three galaxies have similar heliocentric radial velocities of 1730, 1866 and 1736 kps, respectively, and they are the three brightest galaxies in the group. On the sky, NGC 4527 is 1.9 degrees from NGC 4496 and only 0.6 degrees from NGC 4536. Peletier & Wilner (1991) found nearly identical Tully-Fisher distances for NGC 4527 and 4536. Independently, Pierce (1994) obtained nearly identical Tully-Fisher distance moduli for all three of these galaxies. Tully (1988), Peletier & Wilner (1991) and Tully, Shaya & Pierce (1992) all agreed that this galaxy group is on the near side of the Virgo cluster complex. Since then, Saha et al. (1996a) have determined a Cepheid-based determination of the distance to NGC

4527 is μ= 31.10 ± 0.13 for NGC 4536, and similarly Saha et al. (1996b) obtain μ = 31.03 ± 0.14 for NGC 4496. Pending a direct Cepheid-based determination of the distance to NGC 4527, which is to be attempted (A. Saha 1998, personal communication), we assume here that the distance modulus to NGC 4527 is μ = 31.07 ± 0.13 (D= 16.4 ± 1.0 Mpc). Much of what follows depends critically on this assumption.

The magnitudes and luminosities of SNe 1960F, 1981B and 1991T are compared in Table 1. The B and V peak apparent magnitudes are from Saha et al. (1996b), Schaefer (1995a) and Lira et al. (1998), respectively. The observed B and V magnitudes of SNe 1960F and 1991T were similar, while those of SN 1981B were about 0.5-0.6 mag fainter.

The extinction of these three events by dust in our Galaxy should be negligible (Burstein & Heiles 1982), but there are reasons to think that SN 1991T was significantly extinguished by dust in its parent galaxy. (1)In projection, at least, the event occurred near a spiral arm of low surface brightness in NGC 4527, an Sb galaxy that is very dusty and has a high inclination of 74 degrees. For a good photograph that shows the location of SN 1991T in NGC 457, see fig. 1 of Schmidt et al (1994). (2) Photometric and spectroscopic observations of SN 1991T at an age of 2-3 yr have been interpreted by Schmidt et al. in terms of a light echo caused by dust in NGC 4527. (3) Interstellar lines of Ca II (Meyer & Roth 1991) and Na I (Smith & Wheeler 1991; Filippenko et al 1992; Ruiz-Lapuente et al. 1992), at the redshift of NGC 4527, were detected in the spectra of SN 1991T. Values of the color excess that have been estimated on

the basis of the strength of the Na I lines include E(B-V) = 0.34 by Ruiz-Lapuente et al. (1992) and 0.13-0.23 by Filippenko et al. (1992). Although these estimates are recognized to be uncertain, some significant amount of extinction is to be expected. (4) Mazzali et al. (1995) and Nugent et al (1995) concluded from its spectral features that SN 1991T was hotter than normal SNe Ia, yet some of the broad-band colors of SN 1991T were observed to be redder than those of normal SNe Ia. Phillips et al. (1992) estimated E(B-V) =0.10 ± 0.05 (M. Phillips 1995, personal communication), and we assume that the extinction of SN 1960F was negligible (Saha et al 1996b; Schaefer 1996). It may be worth noting that these estimates are in accord with the galaxy 'dustiness' categories of van den Bergh & Pierce (1990), who put NGC 4496 in category 1 ('some dust visible' and NGC 4536 in category 2 ('dust easily visible) and NGC 4527 in category 3 ('galaxy appears very dusty'); only 12 of the 230 galaxies in their sample were assigned to the very dusty category. With our adopted extinction estimates, the extinction-free apparent (B^O and V^O) and absolute ($M_B{}^O$and $M_V{}^O$) magnitudes of the normal SNe 1960F and 1981B become similar while SN 1991T becomes brighter than SNe 1960F and 1981B by 0.7-0.8 mag (see Table 1).

For the bolometric correction, M_{bol}-M_V, of normal SNe Ia such as 1981B and 1960F, we adopt 0.1 ± 0.1 (Höflich 1995, Mazzali et al. 1995; Nugent et al. 1995; Branch, Nugent & Fisher 1997). Even before being corrected for extinction, SN 1991T had a larger fraction of its energy in the near-ultraviolet than do normal SNe Ia (Nugent et al. 1995; Shaefer 1995b; Branch et al. 1997); therefore a smaller fraction of its total flux was emitted in the B and V bands, and its

M_{bol}-M_V was more negative than that of normal SNe Ia. For SN 1991T we adopt M_{bol}-M_V = -0.10 ± 0.1 (not inconsistent with 0.0 ± 0.10 of Mazzali et al. 1995). The bolometric absolute magnitude of SN 1991T then exceeds that of SN 1981B by a factor between 1.7 and 3.4, with the best estimate being a factor of 2.4 (see Table 1).

The peak luminosity of a Type Ia supernova can be written (Arnett 1982; Branch 1992)

$$L = \alpha \, R(t_r) \, M_{Ni}$$

where R, the instantaneous radioactivity luminosity per unit nickel mass at the time of maximum light, is a known function of the rise time t_r , M_{Ni} is the mass of the ejected ^{56}Ni, and α is dimensionless and of order unity. For normal SNe Ia, such as SN 1981B, characteristic values of M_{Ni} = 0.6 M_{sun}, t_r= 18 days, and α =1.2 (e.g. Höflich & Khokhlov 1996; Branch et al. 1997) give L = 2.03 x 10^{43} erg/s. This corresponds to a bolometric absolute magnitude M_{bol} = -19.57, a little brighter than but not inconsistent with, the value implied by the Cepheid distance and the adopted extinction.

At first glance one might think that sufficient overluminosity of SN 1991T with respect to SN 1981B could be achieved with a Chandrasekhar mass, just by allowing the nickel mass to approach the Chandrasekhar mass in SN 1991T (i.e. 1.4/0.6 = 2.33, and we have estimated that SN 199T was more luminous than SN 1981B by a factor of 2.4). However, there are severe problems with this simple picture, in which nearly all of the ejected mass of SN 1991T is initially in the form of ^{56}Ni. (1)Spectral lines formed by elements other than nickel, cobalt and iron show that the initial composition of SN 1991T

was not just ^{56}Ni. (2) No hydrodynamical models of Chandrasekhar-mass explosions produce just ^{56}Ni. Even the pure detonation model of Khokhlov et al. (1993) produce only 0.92 M_{sun} of ^{56}Ni, with the rest of the mass being in the form of other iron-peak isotopes. (3) A rapid expansion of the ejecta caused by the high kinetic energy per gram, together with the prompt escape of gamma-rays emitted by ^{56}Ni in the outer layers, would make the light curve too fast, and with gamma-rays escaping the value of α would be low. For example, for the detonation model of Khokhlov et al (1993), Höflich & Khokhlov (1996) calculated α = 0.76 (in their notation it is Q). (5) the optical and gamma-ray luminosities depend on distance in the same way. From the optical brightness of SN 1991T and the lack of detection of gamma-rays by Lichti et al. (1994) and Leising et al (1995), the latter authors conclude that 'some way of producing optically brighter but gamma-ray fainter supernovae (compared to SN Ia models in the literature) is required to explain SN 1991T'. A Chandraskhar-mass explosion that contained nearly a Chandrasekhar mass of ^{56}Ni would have a low ratio of optical to gamma-ray luminosity.

If SN 1991T is at the same distance as SN 1981B and 1960F, as we assume here, then it is unlikely that its luminosity can be explained in terms of a Chandrasekhar mass ejection.

6. DISCUSSION

If the luminosity of SN 1991T was too high to be explained in terms of a Chandrasekhar mass ejection, the only recourse would seem to be to appeal to the explosion of a super-Chandrasekhar product of

the merger of two white dwarfs. The question of whether mergers of white dwarfs actually can produce explosions is not yet settled (e.g. Mochkovitch, Guerreo & Segretain 1997). An attractive recent suggestion was that of Iben (1997), who noted that because tidal torques will spin up the pre-merger white dwarfs to rotate in near synchronism with the orbital motion, huge shear forces will arise at the onset of the merger. If both white dwarfs ignite prior to or during the merger, owing to shear and tidal heating, or if the ignition of one of the white dwarfs then provokes the ignition of the other, this might be a way to get not only a super-Chandrasekhar mass ejection, but even a super Chandrasekhar mass of ^{56}Ni if such should prove to be required. Getting a super-Chandrasekhar mass of ^{56}Ni out of a thermonuclear explosion was difficult to envisage before Iben's suggestion. It must be noted, though, that in the first calculations of tidal heating during a merger, it failed by a narrow margin to cause carbon to ignite (Iben, Tutokov & Fedorova 1998).

It is interesting that on the basis of their population-synthesis studies, Tutukov & Yungelson (1994) predict that for 'young' mergers, those that occur within 300 Myr of star formation, the average combined mass is substantially super-Chandraskehar typically about $2.1M_{sun}$(see their fig. 4). Recall that SN 1991T appears to have occurred near a spiral arm. Preliminary indications are that the several other events resembling SN 1991T that have been discovered in recent years also tend to be associated with star forming regions and/or to be significantly extinguished by dust (A. V. Filipenko 1998, personal communication; P. Garnavich 1998,

personal communication). SN 991T-type events may be from a younger population than most Sne Ia.

It also is interesting the Ruiz-Lapuente et al. (1992) discuss the possible detection of a narrow circumstellar line of O I λ8446 in their earliest spectrum of SN 1991T. Searching for narrow circumstellar lines of hydrogen, helium, carbon, or oxygen is one the best ways to probe the composition of the donor star in the binary progenitor system of SN Ia (Branch et al. 1995). No signs of circumstellar interaction, and no clear detections of narrow circumstellar lines of hydrogen or helium, have been found in any SN Ia.

On the basis of a light-curve study that was based on a constant-opacity approximation, Cappellaro et al (1997) discussed the possibility that SN 1991T was super-Chandrasekhar, even for their adopted 'short' distance of 13.5 Mpc.

In a very general sense, the composition structure expected of a merger explosion might resemble the composition structure that has been inferred for SN 1991T (cf. Ruiz-Lapuente et al. 1992). An unusually strong explosion produces a high-mass, high-velocity iron-peak core surrounded by an unusually small mass of intermediate-mass elements; this encounters a surrounding low-density mass of carbon and oxygen which decelerates the intermediate-mass elements and forces them into a narrow velocity interval.

The proposition that SN 1991T was the result of a super-Chandrasekhar merger may also be consistent with the findings of Höflich & Khokhlov cited as best fitting the light curve having a peak $M_V \sim -19.4$, which is not luminous enough for SN

1991T. Khokhlov et al. (1993) constructed super-Chandrasekhar models in which the underlying explosion was the detonation of 1.2 M_{sun}, inside low-density carbon-oxygen envelopes of 0.2, 0.4 and 0.6 M_{sun}. In these models the minimum velocity of unburned carbon was less than 10,000 kps, a value which is lower than we infer from the spectra. The detonation of Chandrasekhar mass inside the carbon-oxygen envelopes would give a brighter light curve and a higher minimum velocity of unburned carbon.

None of this explains the presence of iron-peak elements at higher velocity than the intermediate-mass elements, or the possible coexistence in velocity space of iron-peak elements and unburned carbon. Eventually, only multidimensional hydrodynamical studies of the merger process can tell us whether this is possible.

It should be noted that Liu, Jeffery &Schultz (1997b) used a steady-state model of ionization and thermal structure to calculate early nebular-phase spectra for comparison with observed spectra obtained hundreds of days after the explosion. Although they favored a sub-Chandrasekhar mass ejection for SN 1991T, the mass was higher than they favored for normal SNe Ia (Liu, Jeffery and Schultz 1997a). Spyromilio et al (1992) argued on the basis of a nebular-phase spectrum that SN 1991T ejected an exceptionally high mass of ^{56}Ni, around 1 M_{sun}.

The argument that SN 1991T was super-Chandrasekhar depends, of course, on our assumption that SN 1991T is at the same distance as SNe 1981B and 1960F. A Cepheid based determination of the distance to NGC 4527, though perhaps not easy for such a dusty, inclined galaxy, is vital to check on this assumption.

TABLES

Table 1. Luminosities of three Type Ia supernovae

	SN 1960F	SN 1981B	SN1991T
galaxy	NGC 4496	NGC 4536	NGC 4527
B	11.60 ± 0.10	12.04 ± 0.04	11.70 ± 0.02
V	11.51 ± 0.15	11.98 ± 0.04	11.51 ± 0.02
E(B-V)	0.00 ± 0.00	0.10 ± 0.05	0.20 ± 0.10
B^0	11.60 ± 0.10	11.63 ± 0.20	10.88 ± 0.41
V^0	11.51 ± 0.15	11.67 ± 0.16	10.89 ± 0.31
M^0_B	-19.43 ± 0.14	-19.47 ± 0.24	-20.19 ± 0.43
M^0_V	-19.56 ± 0.20	-19.43 ± 0.21	-20.18 ± 0.34
$M_{bol} - M_V$	0.10 ± 0.10	0.10 ± 0.10	0.10 ± 0.10
M_{bol}	-19.46 ± 0.22	-19.33 ± 0.23	-20.28 ± 0.35
$L/ 10^{43}$ erg s^{-1}	1.85 ± 0.43	1.63 ± 0.38	3.93 ± 1.54

FIGURES

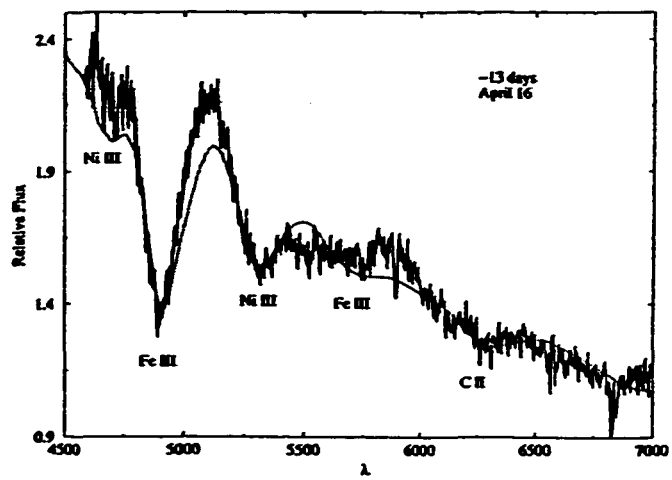

Figure 1. A spectrum of SN 1991T obtained at −13 d (Phillips et al. 1992) is compared to a synthetic spectrum that has $v_{phot} = 15000$ km s^{-1} and $T_{exc} = 13000$ K. Ions responsible for features in the synthetic spectrum are marked. The x-axis is wavelength in Å. The y-axis is F_λ.

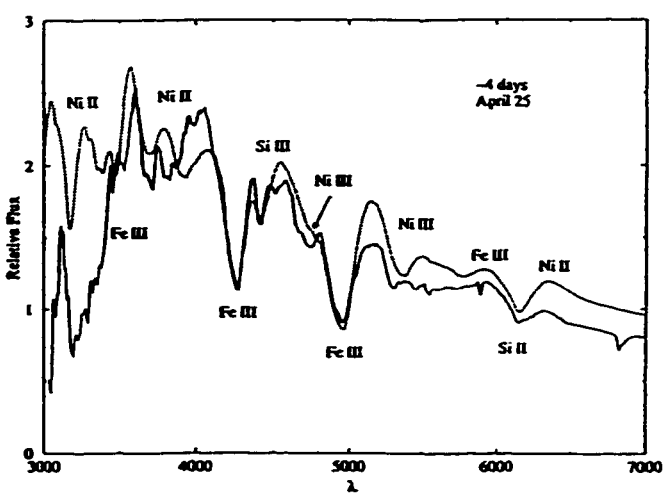

Figure 2. A spectrum of SN 1991T obtained at −4 d (Phillips et al. 1992) is compared to a synthetic spectrum that has $v_{phot} = 10000$ km s^{-1} and $T_{exc} = 13000$ K. Ions responsible for features in the synthetic spectrum are marked. The x-axis is wavelength in Å. The y-axis is F_λ.

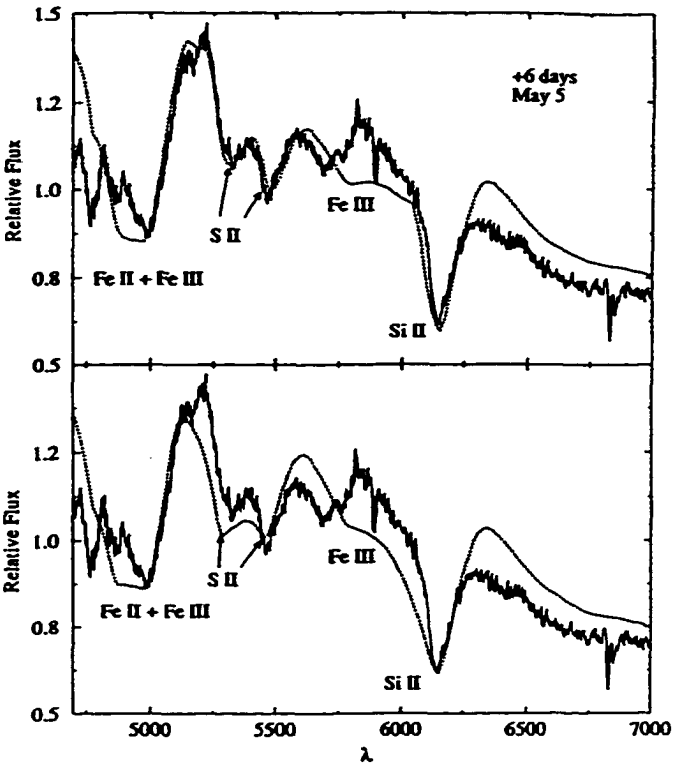

Figure 3. A spectrum of SN 1991T obtained at +6 d (M. M. Phillips et al., unpublished) is compared to synthetic spectra that have $v_{phot} = 9500$ km s^{-1} and $T_{exc} = 10\,000$ K. Ions responsible for features in the synthetic spectrum are marked. In the upper panel, maximum velocities of 12 000 and 15 000 km s^{-1} have been imposed on S II and Si II, respectively. In the lower panel, these limits have been removed. The x-axis is wavelength in Å. The y-axis is F_λ.

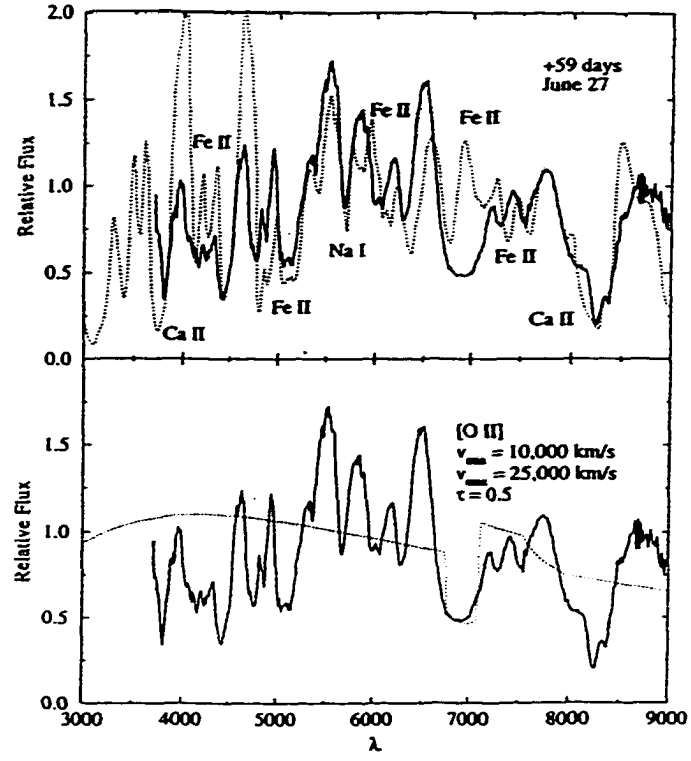

Figure 4. A spectrum of SN 1991T obtained at +59 d (W. P. S. Meikle et al., unpublished) is compared to synthetic spectra that have $v_{photo} = 4000$ km s^{-1} and $T_{exc} = 10\,000$ K. In the synthetic spectrum of the upper panel, one feature is produced by Na I (detached at 9000 km s^{-1}), two features are produced by Ca II, and all others are produced by Fe II (which has an abrupt factor of 10 decrease in its optical depths at 10 000 km s^{-1}). In the synthetic spectrum of the lower panel, the one feature is produced by [O III]. The x-axis is wavelength in Å. The y-axis is F_λ.

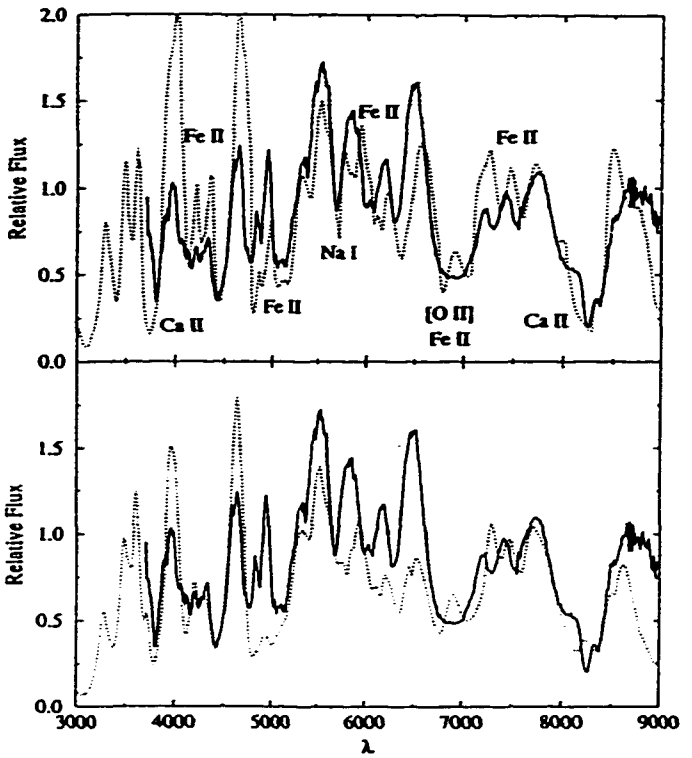

Figure 5. A spectrum of SN 1991T obtained at +59 d (W. P. S. Meikle et al., unpublished) is compared to synthetic spectra that have $v_{phot} = 4000\ \mathrm{km\ s^{-1}}$ and $T_{exc} = 10\,000$ K. The synthetic spectrum of the upper panel is like the one in the upper panel of Fig. 4, but now [O II] is included. In the synthetic spectrum of the lower panel, the detachment of Na I and Ca II, the Fe II optical depth discontinuity, and the velocity limits on [O II] have been removed. The x-axis is wavelength in Å. The y-axis is F_λ.

ACKNOWLEDGMENTS

We are grateful to an anonymous referee for comments that helped us to improve the paper. This work has been supported by NSF grants AST 9417102, 9417242, and 973140 and NASA grant NAG 5-3505.

REFERENCES

Arnett W.D., 1982, ApJ, 253, 785
Branch D., 1992, ApJ, 392, 35
Branch D., Fisher A., Nugent P., 1993, AJ, 106, 2383
Branch D., Livio M., Yungleson L.R., Boffie F.R., Baron E., 1995, PASP, 107, 1019
Burstein D., Heiles C., 1982, AJ, 87, 1165
Cappelaro E., Mazzali P.A., Benetti, S., Danziger, I.J., Turatto, M., Della Valle M., Patat F., 1997, A&A, 328, 203
Filippenko A.V. et al., 1992, ApJ, 384, L15
Fisher A., 1999, PhD thesis, Univ. of Oklahoma
Fisher A., Branch D., Nugent P., Baron E., 1997, ApJ, 481, L89
Hatano K., Branch D., Fisher A., Baron E., 1999, ApJS, in press
Höflich P., 1995, ApJ, 443, 89

Höflich P., Khokhlov A., 1996, ApJ, 457, 500
Iben I., Jr.,1997 in Ruiz-Lapunete P., Canal R., Isern J., eds, Thermonuclear Supernovae. Kluwer, Dordrecht, p. 111
Iben I., Jr., Tutukov A. V., Fedorova, A. V., 198, ApJ, 503, 344
Jeffery D.J., Leibundgut B., Kirshner R.P., Benetti S., Branch D., Sonneborn G., 1992, ApJ, 397, 304
Khoklov A., Müller E., Höflich P., 1993, A&A, 270, 223
Kirshner R.P. et al., 1993, ApJ, 415, 589
Leibundgut B., Kirshner R.P. Filippenko A. V., Shields J.C., Foltz C.B., Phillips M.M., Sonneborn G., 1991, ApJ, 371, L23
Leising M.D. et al., 1995, ApJ, 450
Lichti G.G., et al. 1994, A&A, 292, 569
Lira P. et al., 1998, AJ, 115, 234
Liu W., Jeffery D.J., Schultz D.R., 1997a, ApJ, 483, L107
Liu W., Jeffery D.J., Schultz D.R., 1997b, ApJ, 486, L35

Mazzali P.A., Danziger I.J., Turatto M. 1995, A&A, 297, 509
Mazzali P.A., Cappellaro E., Danziger I.J., Turatto M., Benetti S., 1998. ApJ, 499, L49
Meikle W.P.S. et al., 1996 MNRAS, 281, 263
Meyer D.M., Roth K.C., 1991, ApJ, 383, L41
Mochkovich R., Guerrero J. Segretain L., 1997, in Ruiz-Lapuente P., Canal R., Isern J. , eds, Thermonuclear Supernovae. ed. Kluwer, Dordrecht, p. 187
Nomoto K., Thielemann F.-K., Yokoi K., 1984, ApJ, 286, 644
Nugent P., Phillips M., Baron E., Branch D., Hauschildt P., 1995, ApJ 455, L147
Peletier R.F., Willner C.P., 1991, ApJ, 382, 382
Phillips M.M. et al., 1992, AJ, 103, 1632
Pierce M.J., 1994, ApJ, 430, 53
Ruiz-Lapuente P. et al., 1992, ApJ, 387, L33
Saha A., Sandage A., Labhardt L., Tammann G. A., Macchetto F.D., Panagia N., 1996a, ApJ, 466, 55
Saha A., Sandage A., Labhardt L., Tammann G. A., Macchetto F.D., Panagia N., 1996b, ApJS, 107, 693
Schaefer B.E., 1995a, ApJ, 449, L9
Schaefer B.E., 1995b, ApJ, 450, L5
Schaefer B.E., 1996, ApJ, 460, L19
Schmidt B.P., et al., 1994, ApJ, 434, L19
Smith V., Wheeler J.C., 1001, IAU Circ., 5256
Spyromilio J., Pinto, P.A., Eastman, R.G., 994, MNRAS, 266, L17
Thielemann F.-K., Nomoto K., Yokoi K., 1986, A&A, 158, 17
Tully R.B., 1988, Nearby Galaxies Catalogue, Cambridge Univ. Press, Cambridge.
Tully R.B., Shaya E.J., Pierce M.J. 1992, ApJS, 80, 479
Tutukov A.V., Yungelson L.R., 1994, MNRAS, 268, 871
van den Bergh S., Pierce M.H., 1990, ApJ, 364, 444
Wheeler J.C., Höflich P., Harkness R.P., Spyromilio J., 1998, ApJ, 496, 908
Yamaoka H., Nomoto K., Shigeyama T., Thielemann F.-K., 1992, ApJ, 393, L55

Chapter 8-- Conclusions.

The work presented here mainly shows that it is possible to extract information from supernova spectra using the SYNNEW program. SYNNEW is currently being used and refined by several graduate and undergraduate students. Future areas of study using SYNNEW or SYNNEW derivatives, include studying the effects of aspherical explosions and non-uniform compositions (blobs and whatnot). Other avenues also exist, such as the study of type Ic supernovae, later phases of type Ia supernovae, and near maximum light spectra not presented here. SYNNEW can provide us with valuable information about individual supernova and supernova in general. It is the hope of the author that SYNNEW will be used in arguments concerning the nature of supernova and the universe they populate for many years to come.

REFERENCES

Arnett W.D., 1982, ApJ,253,785
Branch D. 1992, ApJ, 392,35
Branch D., Fisher A., Nugent P. 1993, AJ 106, 2383
Branch D., Livio M., Yungleson L. R., Boffi F.R., Baron E., 1995 PASP 107, 1019
Branch D., Nugent P. Fisher A., 1997, in Ruiz-Lapuente P., Canal R., Isern J. eds, Thermonuclear Supernovae, Kluwer, Dordrecht, p. 715
Burstein D., Heiles C., 1982, ApJS, 54, 33
Cappelarro E., Mazzali P. A., Benetti S., Danziger, I.J. Turatto, M. Della Valle M., Patat F., 1997, A&A, 328, 203
Filippenko A. V. et al., 1992, ApJ, 384, L15
Fisher A., 1999 PhD thesis. Univ. Oklahoma
Fisher A., Branch D., Nugent P. Baron E., 1997, ApJ 481, L89
Haton K., Branch D., Fisher A., Baron E., 1999, APJS, in press
Haushildt P., Baron E., 1999, J. Comp and APplied Math., in press
Höflich P., 1995, ApJ, 443, 89
Höflich P., Khokhlov A., 1996, ApJ, 457, 500
Iben I., Jr., 1997 in Ruiz-Lapuente. P, Canal R., Isern J., eds, Thermonuclear Supernovae. Kluwer, Dordrecht, p. 111
Jeffery D. J., Leibundgut B., Kirshner R.P., Benetti S., Branch D., Sonneborn G., 1992, ApJ, 397, 304
Khokhlov A., Müller E., Höflich P., 1993, A&A, 270, 223
Kirshner R. P. et al., 1993, ApJ 415, 589
Leibundgut B., Kirshner R. P., Filippenko A. V. Shields J.C., Foltz C. B., Phillips M. M., Sonnebom G., 1991, ApJ 371, L23
Leising M. D. et al., 1995 ApJ, 450, 805
Lichti G. G., et al., 1994, A&A, 292, 569
Lira P. et al., 1998, AJ , 115, 234
Liu W., Jeffery D.J., Schultz D. R. 1997a, ApJ, 483, L107
Liu W., Jeffery D.J., Schultz D. R. 1997b, ApJ, 486, L35
Mazzali P. A., Danziger I.J., Turatto M., 1995, MNRAS, 297, 509
Mazzali P. A., Cappelaro E. Danziger I. J., Turatto M., Benetti S., 1998, ApJ, 499,L49
Meikle W. P. S. et al., 1996, MNRAS,281, 263,
Meyer D. M., Roth K.C., 1991, ApJ, 383, L41
Mochkovich R., Guerrero J., Segretain L., 1997 in Ruiz-Lapuente P., Canal R., Isern J. eds, Thermonuclear Supernovae. ed Kluwer, Dordrecht, p. 187
Nomoto K., Thielemann F.-K., Yokoi K., 1984, ApJ, 286, 644
Nugent P., Phillips M., Baron E., Branch D., Hauschildt P., 1995, ApJ 455, L147.
Peletier R.F., Willner C. P., 1991, ApJ, 382, 382
Phillips M. M. et al., 1992, AJ, 103, 1632
Pierce M. J., 1994, ApJ, 430, 53
Ruiz-Lapuente P. et al., 1992, ApJ, 387, L33

Saha A., Sandage A., Labhardt L., Tammann G. A., Macchetto F. D., Panagia N., 1996a, ApJ, 466,55
Saha A., Sandage A., Labhardt L., Tammann G. A., Macchetto F. D., Panagia N., 1996b, ApJS, 107, 693
Schaefer B. E., 1995a, ApJ, 449, L9
Schaefer B. E., 1995b, ApJ, 450, L5
Schaefer B. E., 1996, ApJ, 460, L19
Schmidt B. P. et al., 1994, ApJ, 434, L19
Smith V., Wheeler J.C., 1991, IAU Circ., 5256
Spyromillio, J., Meikle, W.P.S., ALlen D.A., Graham J.R., 1992, MNRAS, 258, 53p
Thielemann, F.-k., Nomoto K., Yokoi K., 1986, A&A, 158, 17
Tully R. B., 1988, Nearby Galaxies Catalogue. Cambridge Univ. Press, Cambridge
Tully R.B., Shaya E. J., Pierce M.J., 1992, ApJS, 80, 479
Tutukov A. V., Yungelson L.R., 1994, MNRAS, 268, 871
van den Bergh S., Pierce M.J., 1990, ApJ, 364, 444
Wheeler, J.C., Höflich P., Harkness, R. P., Spyromilio J., 1998, ApJ, 496, 908
Yamaoka H., Nomoto K., Shigeyamma T., Thielemann F.-K., 1992, ApJ 393, L55

Appendix 1. The SYNNEW code

SECTION 1 SYNNEW

```
      PROGRAM synnew

      PARAMETER (nradstep=350,nwavestep=1024)
      REAL elamx(92,0:5),gfx(92,0:5),chix(92,0:5),taux(92,0:5,nradstep)
      REAL vphot,vmax
      REAL tbb
      REAL ea,eb
      REAL taumin,zeta
      REAL elam(nwavestep)
      REAL t(nwavestep,nradstep) ,s(nwavestep,nradstep)
      REAL td(nwavestep,nradstep),sd(nwavestep,nradstep)
      REAL filparm(50,5) ,stspec
      INTEGER blueline,thisline,ifile
      INTEGER used,usedold,numref
      REAL black(10000),xplot(10000)
      REAL CTHETA(nradstep,21)
      INTEGER grid,jrlim,nlam,ffilenum,sfilenum,last,i,j
      INTEGER an(50),ai(50)
      LOGICAL flambda

      COMMON /param/ elamx,gfx,chix,taux,vphot,vmax,tbb,ea,eb
     a   ,taumin ,zeta,grid,jrlim,nlam,flambda,an,ai,numref,stspec
      COMMON /radial/ t,td,s,sd

c     READ IN INITIAL PHYSICAL PARAMETERS
      CALL INITIALIZE()
      blueline=1
      usedold=0
      used=0
C     SETUP TO READ PROPER LINE,FILE

      CALL BB(ea,eb,nlam,black,xplot,tbb)
      CALL THETA(ctheta,grid,jrlim)

      sfilenum=int(log(ea/900.0)/log(1.001)/256.0)+1
      ffilenum=int(log(eb/900.0)/log(1.001)/256.0)+1
      IF (sfilenum.lt.2) THEN
       PRINT *,'EA TOO SMALL',ea
       stop
      ENDIF
```

```
      IF (ffilenum.gt.12) THEN
       PRINT *,'EB TOO BIG',eb
       stop
      ENDIF
      last=0
      DO i=1,nlam
       IF  (xplot(i).lt.stspec)  last=i
      ENDDO
C     READ IN NEXT BIN AND INITIALIZED OPTICAL DEPTHS
      DO ifile=sfilenum,ffilenum
       CALL FILE(taux,gfx,chix,an,ai,ifile,filparm,numref)
       PRINT *,'ON FILE ',ifile,' of ',ffilenum
       CALL GETBIN(elam,t,usedold,used,ifile,filparm)
       IF (ifile.eq.sfilenum) THEN
        DO i=1,used-1
         if (elam(i).lt.ea) then
          blueline=i+1
          thisline=i+1
          DO j=1,jrlim
           t(i,j)=0.0
           td(i,j)=0.0
          ENDDO
         ENDIF
        ENDDO
       ENDIF
       DO thisline=usedold+1,used
         if (elam(thisline).gt.eb) goto 555

c          PRINT *,elam(thisline),t(thisline,grid+1)
c        CALCULATE SOURCE FUNCTIONS FOR THIS LINE
         CALL SOURCE(elam,thisline,blueline,ctheta,black)

c        CALCULATE SPECTRUM
         IF (elam(thisline).gt.stspec) THEN
          CALL SPECTRUM (elam,thisline,blueline,xplot,black
     a     ,jrlim,grid,last,vmax,vphot,flambda,nlam,zeta,ea,eb)
         ENDIF

        ENDDO
        IF (used.gt.(nwavestep-257)) THEN

         PRINT *,'SHUFFLE',thisline,blueline,used,usedold

         DO is=blueline,used
           DO j=grid+1,jrlim
```

```
            t(is-blueline+1,j) = t(is,j)
            t(is,j)=0.0
            td(is-blueline+1,j)= td(is,j)
            s(is-blueline+1,j) = s(is,j)
            sd(is-blueline+1,j)= sd(is,j)
           ENDDO
           elam(is-blueline+1)=elam(is)
           elam(is)=1.1*eb
           t(is,4)=0.0
          ENDDO
          DO is=used-blueline+2,blueline
           DO j=grid+1,jrlim
            t(is,j)=0.0
           ENDDO
          ENDDO
          used=used-blueline+1
          thisline=thisline-blueline+1
           blueline=1
         ENDIF
         usedold=used
        ENDDO
C     CALCULATE LAST BIT OF SPECTRUM.
 555   PRINT *,'ALMOST DONE'

      DO i=thisline,1024
       elam(i)=eb*10.0
      ENDDO
      CALL SPECTRUM (elam,thisline,blueline,xplot,black,jrlim,
     a grid,last,vmax,vphot,flambda,nlam,zeta,ea,eb)

C                    END OF MAIN PROGRAM
      END
```

Section 2- INITIALIZE

```
      SUBROUTINE INITIALIZE()
      PARAMETER (nradstep=350)
c      IMPLICIT none
      REAL hc,k
      REAL elamx(92,0:5),gfx(92,0:5),chix(92,0:5),taux(92,0:5,nradstep)
      REAL vphot,vmax,tauxold
      REAL tbb
      REAL ea,eb,wk,pwrlawin,xsto
      REAL taumin,zeta,rmax,wzone
      INTEGER grid,jrlim,nlam,numref,i,j
      LOGICAL flambda,pwrlaw
```

```
      REAL alam,agf,aelow,stspec
      INTEGER anum,aion,ii,ij,ik
      INTEGER ai(50),an(50),begin,stop
      REAL  tau1(50),vmine(50),vmaxe(50),ve(50),temp(50)
      COMMON /param/ elamx,gfx,chix,taux,vphot,vmax,tbb,ea,eb
     a   ,taumin ,zeta,grid,jrlim,nlam,flambda,an,ai,numref,stspec
      NAMELIST  /parms/ ve ,
     A              vphot, tbb, vmax, numref, ai, an,
     B              ea, eb, taumin, grid,
     C              tau1,flambda,nlam,vmine,vmaxe,
     D              zeta,temp,
     E              stspec,pwrlaw,pwrlawin
      hc=12400.
      k=8.6167e-5
      PRINT *,'INITIALIZING'
c     READ IN REFERENCE LINE PARAMETERS
C     INSERT PATH NAME FOR REF.DAT
      OPEN(UNIT=1,FILE='$SYNPATHNAME$/ref.dat',STATUS='old')

 1    READ (1, 3, END=2)  alam, agf, anum, aion, aelow

 3    FORMAT  (F12.4, 1X, F6.3, 1X, I2, 2X, I1, 1X, F12.8)

      elamx(anum,aion) =  alam*10.0
      gfx(anum,aion)   =  agf*log(10.)
      chix(anum,aion)  =  aelow
      GOTO 1

C     READ IN PHYSICAL PARAMETERS

 2    OPEN  (UNIT=5, FILE= 'in.dat', STATUS='OLD')

      READ (5,parms)

      CLOSE (5)
      IF (pwrlaw) PRINT *,'POWER LAW OVERIDES ve'
      DO anum=1,92
       DO aion=0,5
        taux(anum,aion,1)=0.0
       ENDDO
      ENDDO
      rmax    =  vmax/vphot
      tbb=tbb*k/hc
      jrlim=INT(rmax*real(grid)+.5)
C     NOW WE SET UP RADIAL PROFILES
```

```
      DO j=1,numref
        vmine(j)=1000.*vmine(j)
        vmaxe(j)=1000.*vmaxe(j)
        ve(j)=1000.*ve(j)
        IF (vmine(j).le.vphot*1.001) THEN
         begin=grid+1
         wzone=.5
         vmine(j)=vphot
        ELSE
         begin=INT(1.5+REAL(grid)*(vmine(j)/vphot))
         wzone= .5*(1.0-(1.0 - (vmine(j)/vphot)**(-2))**.5)
         begin=MIN(begin,jrlim)
        ENDIF
        stop=INT(1.5+REAL(grid)*(vmaxe(j)/vphot))
        stop =MIN(stop,jrlim)
C  NOW WE SET UP THE optical depth profiles.
C  REMEMBER that we have to anticorrect for stimulated emmission.
        IF (elamx(an(j),ai(j)).lt.1000.) THEN
         PRINT *,'NEED ref.dat line for',an(j),ai(j)
         STOP
        ENDIF
        wk=(exp(1./tbb/elamx(an(j),ai(j)))-1.)/wzone/zeta/zeta+1.
        wk=1.-1./wk
        tauxold=taux(an(j),ai(j),1)
        taux(an(j),ai(j),1)=tau1(j)/wk
        taux(an(j),ai(j),2)=temp(j)*1000.*k
        DO i=begin,stop
         IF (pwrlaw) THEN
          xsto=max(1.0,vphot/vmine(j))
          taux(an(j),ai(j),i)=taux(an(j),ai(j),1)
     a      *(xsto*real(i-1)/REAL(grid))**(-pwrlawin)
         ELSE

          taux(an(j),ai(j),i)=taux(an(j),ai(j),1)
     a      *exp((vmine(j)-vphot*real(i-1)/REAL(grid))/ve(j))
         ENDIF
        ENDDO
        taux(an(j),ai(j),1)=tauxold+taux(an(j),ai(j),1)
      ENDDO
C this part close packs the species in use
        ii=1
        DO ij=1,numref
         IF (tau1(ij).gt.0.0001*taumin) THEN
          DO ik=1,ii-1
           IF (ai(ik).eq.ai(ij).and.an(ik).eq.an(ij)) GOTO 200
```

```
      ENDDO
      ai(ii)=ai(ij)
      an(ii)=an(ij)
      tau1(ij)=0.0
      ii=ii+1
      ENDIF
200   ENDDO
     numref=ii-1

    PRINT *, 'INITIALIZATION COMPLETE FOR ',numref,' SPECIES'
    RETURN
    END
```

Section 3 - BB

```
      SUBROUTINE BB(ea,eb,nlam,black,xplot,tbb)

      IMPLICIT none
      REAL ea,eb,black(10000),xplot(10000),tbb
      INTEGER i,nlam
      DO i=1,nlam
        xplot(i)=ea*(eb/ea)**(REAL(i-1)/REAL(nlam-1))
        black(i)=(ea/xplot(i))**3*
     a       (exp(1./tbb/ea)-1.)/(exp(1./tbb/xplot(i))-1.)
      ENDDO
      RETURN
      END
```

Section 4- THETA

```
      SUBROUTINE theta(ctheta,grid,jrlim)
      PARAMETER (nradstep=350)
      REAL ctheta(nradstep,21),crit,pi
      INTEGER jrlim,grid,rad,step
      pi=ACOS(-1.)
      rad=grid+1
      DO step=1,10
       crit=.5*pi
       ctheta(rad,21)=.5
       ctheta(rad,step)=1.
       ctheta(rad,step+10)=0.05-0.1*REAL(step)
      ENDDO
      DO rad=grid+2,jrlim
       crit=SQRT(1.-(REAL(grid)/REAL(rad-1))**2)
       ctheta(rad,21)=.5*(1.-SQRT(1.-(REAL(grid)/real(rad-1))**2))
```

```
        DO step=1,10
          ctheta(rad,step)=crit+(1.-crit)*(2*REAL(step)-1.)/20.
          ctheta(rad,step+10)=-1.+(1.+crit)*(2*REAL(step)-1.)/20.
        ENDDO
      ENDDO
      RETURN
      END

Section 5 - FILE
      SUBROUTINE FILE(taux,gfx,chix,an,ai,i,filparm,numref)
      PARAMETER (nradstep=350)
      REAL taux(92,0:5,nradstep),gfx(92,0:5),chix(92,0:5),tex
      INTEGER an(50),ai(50),i
      REAL filparm(50,5)
       isto4=0
       DO j=1,numref
        filparm(j,5)=0.0
       ENDDO
       OPEN (unit=13
     &   ,file='linelist.info'
     &    ,status='old')

       DO j=1,numref
        filparm(j,1)=0.0
        filparm(j,2)=0.0
        filparm(j,3)=0.0
        filparm(j,4)=0.0
        filparm(j,5)=0.0
       ENDDO

 1      READ (13,*,end=2) isto1,isto2,isto3,xsto1,xsto2
     &  ,xsto3,xsto4,isto4
       IF (isto3.eq.i) THEN
        DO j=1,numref
         IF (isto1.eq.an(j).and.isto2.eq.ai(j)) THEN
          tex=taux(an(j),ai(j),2)
          filparm(j,1)=xsto1*log(10.0)-gfx(isto1,isto2)
          filparm(j,2)=(-xsto1+xsto2)*log(10.0)
          filparm(j,3)=
     &        (chix(an(j),ai(j))-xsto4*1.240E-4)/tex
          filparm(j,4)=-1.240E-4*(xsto3-xsto4)/tex
          filparm(j,5)=REAL(isto4)
          GOTO 1
         ENDIF
        ENDDO
```

```
c        ELSE
c         if (isto3.gt.i) goto 2
         ENDIF
         GOTO 1
 2       CONTINUE
         CLOSE (13)
         RETURN
         END
```

Section 6 - GETBIN

```
      SUBROUTINE GETBIN(wavelength,t,usedold,used,i,filparm)
      PARAMETER (nradstep=350)
      REAL wavelength(1024),t(1024,nradstep),wk
      REAL elamx(92,0:5),gfx(92,0:5),chix(92,0:5),taux(92,0:5,nradstep)
      REAL vphot,vmax
      REAL tbb
      REAL ea,eb
      REAL taumin,zeta
      REAL chi,gfl
      INTEGER used,usedold,i
      INTEGER an(50),ai(50),numref,isto1,isto2,isto3,isto4,isto5
      REAL filparm(50,5),stspec
      INTEGER num,ion
      INTEGER grid,jrlim,nlam,rad,j
      LOGICAL flambda
      CHARACTER*80 filename
      INTEGER*4 IWL,IEL,IGF
      INTEGER*4 IIII
        COMMON /param/ elamx,gfx,chix,taux,vphot,vmax,tbb,ea,eb
     a   ,taumin,zeta,grid,jrlim,nlam,flambda,an,ai,numref,stspec
      isto4=int(i/10)
      isto5=i-isto4*10+48
      isto4=isto4+48
      DO j=1,numref
       if ((filparm(j,5)+.01).lt.1.0) goto 2

       isto1=int(an(j)/10)
       isto2=an(j)-10*isto1+48
       isto1=isto1+48
       isto3=ai(j)+48
       filename='$SYNPATHNAME$/linelist/'//
     &   char(isto1)//char(isto2)//char(isto3)//char(isto4)
     &   //char(isto5)
        OPEN (unit=2,file=filename,access='direct',recl=4,
     &   form='unformatted')
```

```
      num=an(j)
      ion=ai(j)
      DO k=1,int(filparm(j,5)+.01)
       READ (2,rec=k) IIII
       IWL=IBITS(IIII,24,8)
       IGF=IBITS(IIII,12,12)
       IEL=IBITS(IIII,0,12)
       chi=filparm(j,3)+filparm(j,4)*
     &      REAL(IEL)/4095.
       gfl=filparm(j,1)+filparm(j,2)*
     &      REAL(IGF)/4095.
C  gfl  is the natural log of (gf/gfx)
C  chi  is the (elo-elox)/k/tex

        wavelength(IWL+usedold+1)=900.*1.001**real(256*(i-1)+IWL)
       wk=exp(gfl+chi)*wavelength(IWL+usedold+1)/elamx(num,ion)
       IF (wk.gt.1.0e-5) THEN
C        print *,wavelength(IWL+usedold+1),gfl,chi,igf,iel,filparm(j,1),
C     &  filparm(j,2),wk

         DO rad=grid+1,jrlim
           t(iwl+usedold+1,rad)=t(iwl+usedold+1,rad)
     &          +wk*taux(num,ion,rad)
         ENDDO
       ENDIF
 22   ENDDO
     CLOSE(2)
  2  ENDDO
     ii=usedold

     DO ik=usedold+1,usedold+256
      IF (wavelength(ik).lt.ea) GOTO 4
      DO j=grid+1,jrlim
       IF (t(ik,j).gt.taumin) THEN
          t(ik,4)=1.0
          GOTO 3
       ENDIF
      ENDDO

 3    IF (t(ik,4).gt.0.5) THEN
      ii=ii+1
      IF (ii.ne.ik) THEN
       wavelength(ii)=wavelength(ik)
       wavelength(ik)=0.0
       t(ii,4)=1.0
```

```
          t(ik,4)=0.0
          DO ij=grid+1,jrlim
           t(ii,ij)=t(ik,ij)
           t(ik,ij)=0.0
          ENDDO
         ENDIF
        ENDIF
 4     ENDDO
       used=ii
       RETURN
       END
```

Section 7 - SOURCE

```
       SUBROUTINE SOURCE (elam,thisline,blueline,ctheta,black)
C   THIS SUBROUTINE CALCULATES THE MEAN INTENSITY ariving at a point
C   in the atmosphere.
C   IT THEN CALCULATES THE SOURCE FUNCTION AND OPTICAL DEPTH OF
THIS C   LINE AT THAT POINT.
       PARAMETER (nradstep=350,nwavestep=1024)
       REAL elam(nwavestep)
       REAL t(nwavestep,nradstep),s(nwavestep,nradstep)
       REAL td(nwavestep,nradstep),sd(nwavestep,nradstep)
       INTEGER thisline,blueline,rad,line,lline
       REAL ctheta(nradstep,21),sp,so
       REAL dr,rm
       REAL elamx(92,0:5),gfx(92,0:5),chix(92,0:5),taux(92,0:5,nradstep)
       REAL vphot,vmax
       REAL tbb
       REAL ea,eb
       REAL taumin,zeta,black(10000),wk,wk2,u
       LOGICAL flambda
       INTEGER grid,jrlim,nlam,krm,klam,iwk,step
       REAL in,drm,factor,tav,sav,stspec
       INTEGER an(50),ai(50),numref

       COMMON /param/ elamx,gfx,chix,taux,vphot,vmax,tbb,ea,eb
      a   ,taumin,zeta,grid,jrlim,nlam,flambda,an,ai,numref,stspec
       COMMON /radial/ t,td,s,sd
       IF (thisline.lt.blueline) THEN
         IWK=thisline+nwavestep
       ELSE
         IWK=thisline
       ENDIF
```

```
      factor=(exp(1./tbb/ea)-1.)*(ea/elam(thisline))*3
C  CALCULATE J FOR FIRST GRID LOCATION.
C  ASSUME THAT THE PHOTOSPHERE CONTRIBUTES .5 of the blackbody
C  SO WE ONLY HAVE TO WORRY ABOUT THE OUTSIDE STUFF.
      rad=grid+1
      IF ((t(thisline,rad)+t(thisline,rad+1)+t(thisline,rad-1))
     a     .gt.taumin) THEN
        klam=INT(log(elam(thisline)/ea)/log(eb/ea)*(nlam-1))+1
        sp=.5*black(klam)*zeta*zeta
        so= 0.0
        wk=REAL(rad-1)/REAL(grid)
        IF (blueline.lt.IWK)  THEN
         DO  step=11,20
          in=0.0
          DO line=blueline,IWK-1
           lline=MOD(line-1,nwavestep)+1
           dr=(elam(thisline)-elam(lline))/elam(thisline)*3.0e5/vphot
           rm=SQRT(wk*wk+dr*dr-2.*dr*wk*ctheta(rad,step))
           IF (rm.lt.vmax/vphot) THEN
            krm=INT(rm*REAL(grid))+1
            drm=rm*REAL(grid)-REAL(krm-1)
            tav=t(lline,krm)+drm*td(lline,krm)
            sav=s(lline,krm)+drm*sd(lline,krm)
            in=in*exp(-tav)+sav*(1.-exp(-tav))
     a         *(elam(lline)/elam(thisline))**3
           ENDIF
          ENDDO
          so=so+in
         ENDDO
         so=so/10.*.5
        ENDIF

C  NOW CALCULATE S,T FOR FIRST GRID LOCATION
        s(thisline,rad)=so+sp
        t(thisline,rad)=t(thisline,rad)
     a              *(1.-1./(factor/s(thisline,rad)+1.))
       ELSE
        t(thisline,rad)=0.0
        s(thisline,rad)=0.0
       ENDIF

C  NOW CALCULATE J FOR THE REST OF THE GRID LOCATIONS
      DO rad=grid+2,jrlim
       IF (t(thisline,rad)+t(thisline,rad+1).gt.taumin) THEN
        sp= 0.0
```

```
      so= 0.0
      in= 0.0
      DO step=1,10
       wk=REAL(rad-1)/REAL(grid)
C  wk is the radius we are at
C  u is cos theta for this ray
       u=ctheta(rad,step)
       wk2=wk*u-SQRT(wk*wk*(u*u-1.)+1.)
       klam=INT(log(elam(thisline)*(1.-vphot*wk2/3.0e5)/ea)/
     a        log(eb/ea)*REAL(nlam-1))+1
       klam=MAX(klam,1)
       in=black(klam)*(1.-vphot*wk2/3.0e5)**3*zeta*zeta
       IF (blueline.lt.IWK) THEN
        DO line=blueline,IWK-1
         lline=MOD(line-1,nwavestep)+1
         dr=(elam(thisline)-elam(lline))/elam(thisline)
     a          *3.0e5/vphot
         rm=SQRT(wk*wk+dr*dr-2.*dr*wk*u)
         IF (rm.gt.1.and.u*dr.lt.wk) THEN
          krm=INT(rm*REAL(grid))+1
          drm=rm*REAL(grid)-REAL(krm-1)
          tav=t(lline,krm)+drm*td(lline,krm)
          sav=s(lline,krm)+drm*sd(lline,krm)
          in=in*exp(-tav)+sav*(1.-exp(-tav))
     a          *(elam(lline)/elam(thisline))**3
         ENDIF
        ENDDO
       ENDIF
       sp=sp+in
      ENDDO
c NOW WE TAKE THE AVERAGE RAY AND MULTIPLY IT BY THE FRACTION
c  OF SOLID ANGLE WHICH THE PHOTOSPHERE SUBTENDS
      sp=sp/10.*ctheta(rad,21)
C NOW WE MUST DO THE INTERACTION TERM FOR LINES AWAY FROM
C THE PHOTOSPHERE
      IF (blueline.lt.IWK) THEN
       DO step=11,20
        in=0.0
        DO line=blueline,IWK-1
         lline=MOD(line-1,nwavestep)+1
         dr=(elam(thisline)-elam(lline))/elam(thisline)
     a          *3.0e5/vphot
         rm=SQRT(wk*wk+dr*dr-2.*dr*wk*ctheta(rad,step))
         IF (rm.lt.vmax/vphot) THEN
          krm=INT(rm*REAL(grid))+1
```

```
            drm=rm*REAL(grid)-REAL(krm-1)
            tav=t(lline,krm)+drm*td(lline,krm)
            sav=s(lline,krm)+drm*sd(lline,krm)
            in=in*exp(-tav)+sav*(1.-exp(-tav))
     a         *(elam(lline)/elam(thisline))**3
           ENDIF
          ENDDO
          so=so+in
         ENDDO
         so=so/10.*(1.-ctheta(rad,21))
        ENDIF
        s(thisline,rad)=so+sp
        t(thisline,rad)=t(thisline,rad)
     a            *(1.-1./(factor/s(thisline,rad)+1.))
       ELSE
        s(thisline,rad)=0.0
        t(thisline,rad)=0.0
       ENDIF
        sd(thisline,rad-1)=s(thisline,rad)-s(thisline,rad-1)
        td(thisline,rad-1)=t(thisline,rad)-t(thisline,rad-1)

       ENDDO


       RETURN

       END
Section 8 - SPECTRUM
      SUBROUTINE SPECTRUM(elam,thisline,blueline,xplot,black,
     a jrlim,grid,last,vmax,vphot,flambda,nlam,zeta,ea,eb)
      PARAMETER (nradstep=350,nwavestep=1024
     &  ,acc=2.,iacc=2)
      REAL elam(nwavestep),xplot(10000),black(10000)
      INTEGER thisline,blueline,jrlim,grid,IWK,last,nlam,jp,klam
      REAL s(nwavestep,nradstep),sd(nwavestep,nradstep),tot,in,p,xp
      REAL t(nwavestep,nradstep),td(nwavestep,nradstep),vmax,vphot
      REAL ea,eb,zeta,z,wk,rm,tav,sav,drm
      INTEGER lline,krm,ii
      LOGICAL flambda
      COMMON /radial/ t,td,s,sd
      IWK=thisline
    1 IF (elam(thisline)/xplot(last+1).gt.1.+vmax/3.0e5) THEN
C      NOW WE CAN CALCULATE THE SPECTRUM A LITTLE
       last=last+1
       tot=0.
```

```
      DO jp=iacc,jrlim*iacc
       in=0.
       p=REAL(jp-acc)/REAL(grid)/acc
       IF (p.lt.1.) THEN
        xp=(1.-vphot/3.0e5*SQRT(1.-p*p))
        klam=INT(LOG(xplot(last)/xp/ea)/LOG(eb/ea)
     &  *(REAL(nlam)-1.))+1
        klam=MIN(klam,nlam)
        in=black(klam)*zeta*zeta/xp/xp/xp
       ENDIF
       IF (blueline.lt.IWK) THEN
        DO lline=blueline,IWK
c         lline=MOD(line-1,nwavestep)+1
C    FOR EACH LINE LOCATE IT IN Z
          z=(elam(lline)-xplot(last))/xplot(last)*3.0e5/vphot
          IF (z.gt.0.0.or.p.gt.1.) THEN
            rm=SQRT(z*z+p*p)
            IF (rm.gt.1.and.rm.lt.vmax/vphot) THEN
             krm=INT(rm*REAL(grid))+1
             drm=rm*REAL(grid)-REAL(krm-1)
             tav=t(lline,krm)+drm*td(lline,krm)
             sav=s(lline,krm)+drm*sd(lline,krm)
             in=in*exp(-tav)+sav*(1.-exp(-tav))
    a          *(elam(lline)/xplot(last))**3
            ENDIF
          ENDIF
        ENDDO
       ENDIF
       tot=tot+in*p
       in=0.
      ENDDO
      IF (flambda) tot=tot*(ea/xplot(last))**2
      WRITE (11,*) xplot(last),tot*2.
    a        /acc/REAL(grid),black(last)
c      CALL FLUSH(11)
      wk=2.0*SQRT(vmax*vmax-vphot*vphot)/3.0e5
      wk=xplot(last)*(1.-wk)/(1.+wk)
      DO ii=blueline,IWK-1
       IF (elam(ii).lt.wk) THEN
        blueline=ii+1
       ENDIF
      ENDDO

      IF (last.eq.nlam) STOP
      GOTO 1
```

```
ENDIF
RETURN
END
```

Appendix 2. Flow charts and variable lists.

Section 1 - SYNNEW (and global variables)

an(i)	atomic number of species i
ai(i)	ionization stage of species i (0 for neutral, 1 for singly ionized, etc.)
black	the Plank function divided by the Plank function at ea for each wavelength in xplot
blueline	the bluest wavelength bin that can interact with the current line
ctheta	for each radial zone the first twenty entry are the cosines of 10 angles that intersect the photosphere, 10 that don't and the last element contains the dilution factor.
ea	the minimum wavelength considered
eb	the maximum wavelength considered
elam(i)	the wavelength of the wavelength bin i
ffilenum	final linelist file number
fileparm(i,j)	compression parameters for species i for this wavelength region
fileparm(i,1)	natural log of the ratio of the largest gf in this file over the reference gf
fileparm(i,2)	the spacing between binned values in natural log of gf
fileparm(i,3)	the natural log of the Boltzman factor for the highest lower energy level
fileparm(i,4)	the spacing between binned values in natural log of Boltzman factors
fileparm(i,5)	the number of transitions
flambda	.true. if the output spectrum is per unit wavelength .false. if the output spectrum is per unit frequency
grid	number of radial zones per photospheric radius
i	dummy looping variable
ifile	the current wavelength file
j	dummy looping variable
jrlim	the last radial zone
last	the last wavelength bin where spectrum was calculated

nlam	the number of wavelengths where the output spectrum is calculated
nradstep	the maximum number of radial zones the code is prepared for
numref	the number of active species in the calculation
nwavestep	the number of wavelength steps included in memory
used	the last wavelength bin that has been filled
usedold	the bluest bin that can still affect the spectrum calculations
taumin	the minimum optical depth considered (usually set at 0.01)
tbb	temperature of the underlying continuum
t(i,j)	the optical depth at l(i)and r(j)
td(i,j)	the derivative of t(i,j)
thisline	the current wavelength bin
s(i,j)	the source function at l(i)and r(j)
sd(i,j)	the derivative of s(i,j)
sfilenum	starting linelist file number
stspec	the minimum wavelength of the output spectrum
vmax	the maximum velocity included in the calculation
vphot	the photospheric velocity
xplot	contains the wavelengths where the Plank function has been calculated.
zeta	the dilution factor at the photosphere

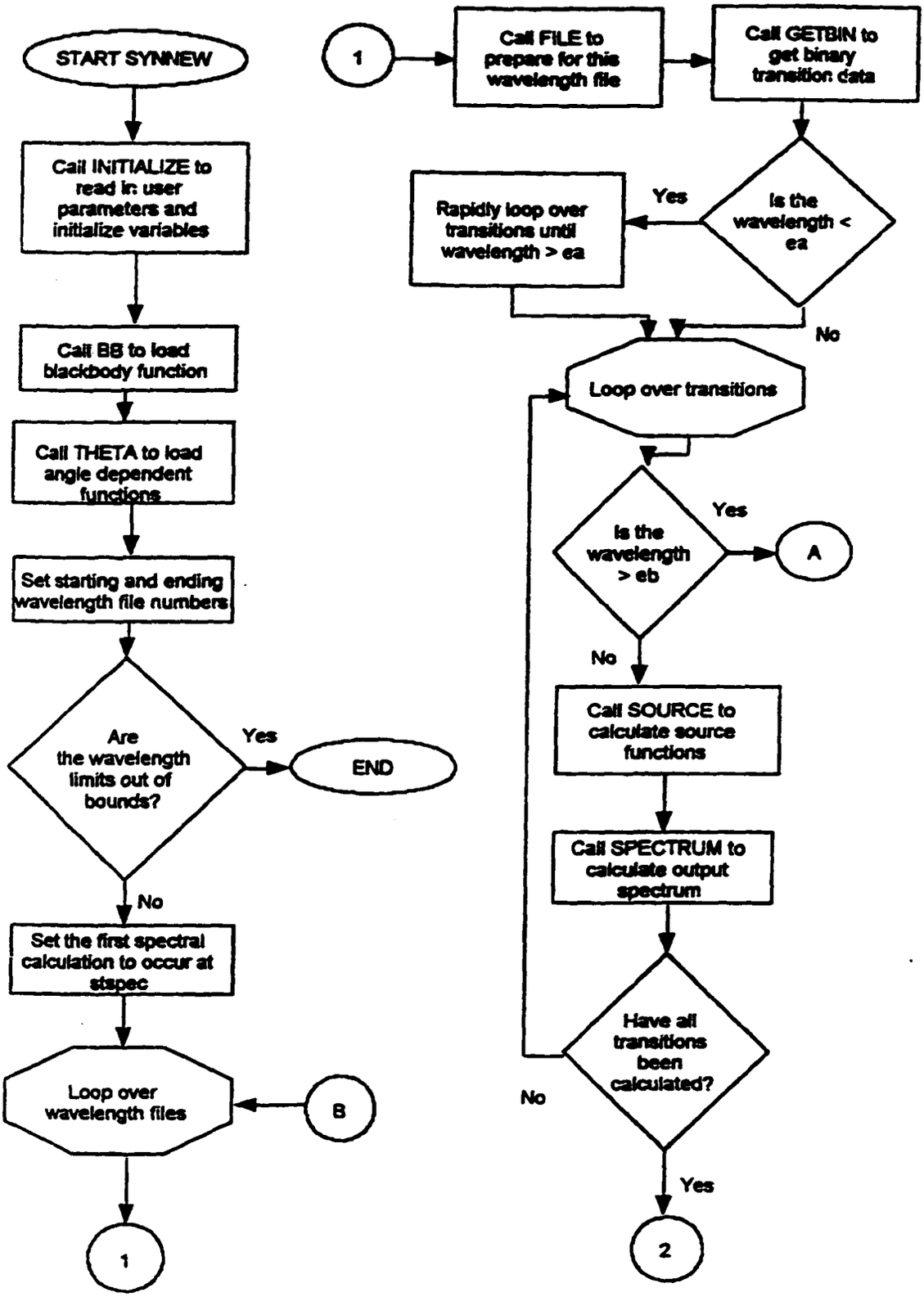
START SYNNEW
Call INITIALIZE to read in user parameters and initialize variables
Call BB to load blackbody function
Call THETA to load angle dependent functions
Set starting and ending wavelength file numbers
Are the wavelength limits out of bounds?
Yes
END
No
Set the first spectral calculation to occur at stspec
Loop over wavelength files
B
1
1
Call FILE to prepare for this wavelength file
Call GETBIN to get binary transition data
Is the wavelength < ea
Yes
Rapidly loop over transitions until wavelength > ea
No
Loop over transitions
Is the wavelength > eb
Yes
A
No
Call SOURCE to calculate source functions
Call SPECTRUM to calculate output spectrum
Have all transitions been calculated?
No
Yes
2

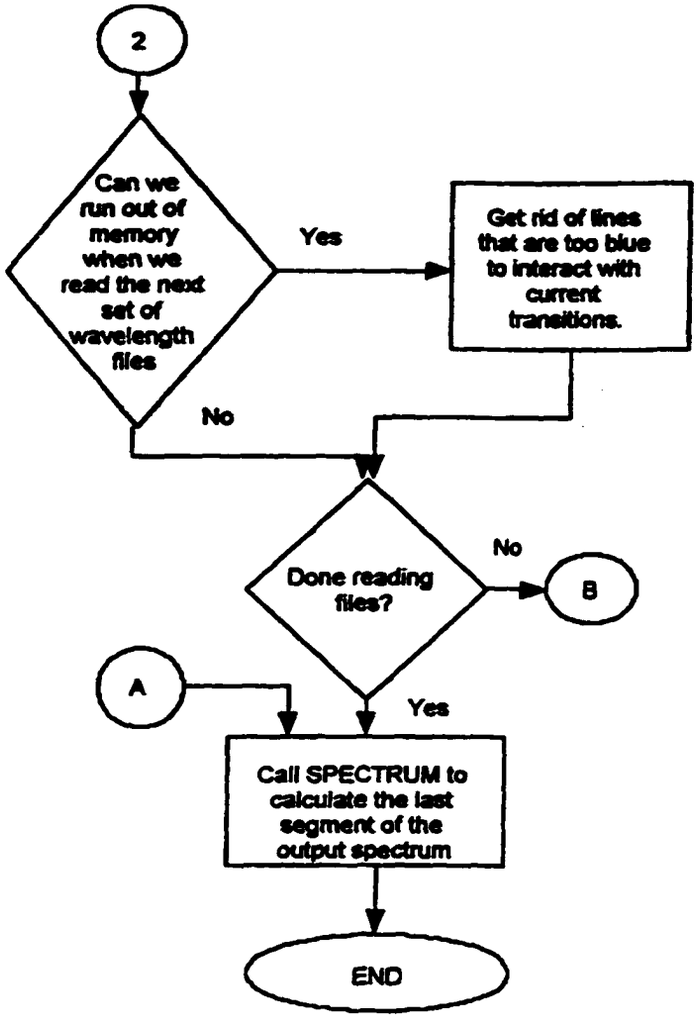
2
Can we run out of memory when we read the next set of wavelength files
Yes
Get rid of lines that are too blue to interact with current transitions.
No
Done reading files?
No
B
A
Yes
Call SPECTRUM to calculate the last segment of the output spectrum
END

Section 2 INITIALIZE

aelow	reference line lower level energy
agf	reference line log(gf),read from ref.dat
aion	ionization stage of reference line
alam	reference line wavelength in nanometers, read from ref.dat
anum	atomic number of reference line
begin	radial zone to begin setting optical depths for this species
chix(i,j)	the lower level energy of the reference line for element i with ionization j
elamx(i,j)	the wavelength of the reference line for element i with ionization j
gfx(i,j)	the ln(gf) value for the reference line for element i with ionization j
hc	Plank's constant time the speed of light in eV Angstroms
i,j,ii,jj,ik	dummy variables
k	Boltzman's constant
pwrlaw	.true. if the optical depth profile is a power law.
pwrlawin	the index of the power law optical depth profile
rmax	maximum radius of the calculation
stop	radial zone to stop setting optical depths for this species
tau1(i)	the optical depth of the reference line i
taux(i,j,k)	the optical depth of the reference line with anum=i, aion=j, and r(k)
temp(i)	the excitation temperature of the species i
ve(i)	the scale height of the optical depth of the species i
vmax(i)	the maximum velocity of the species i
vmine(i)	the minimum velocity of the species i
wk	dummy variable
wzone	the dilution factor for this radial zone

xsto	dummy variable

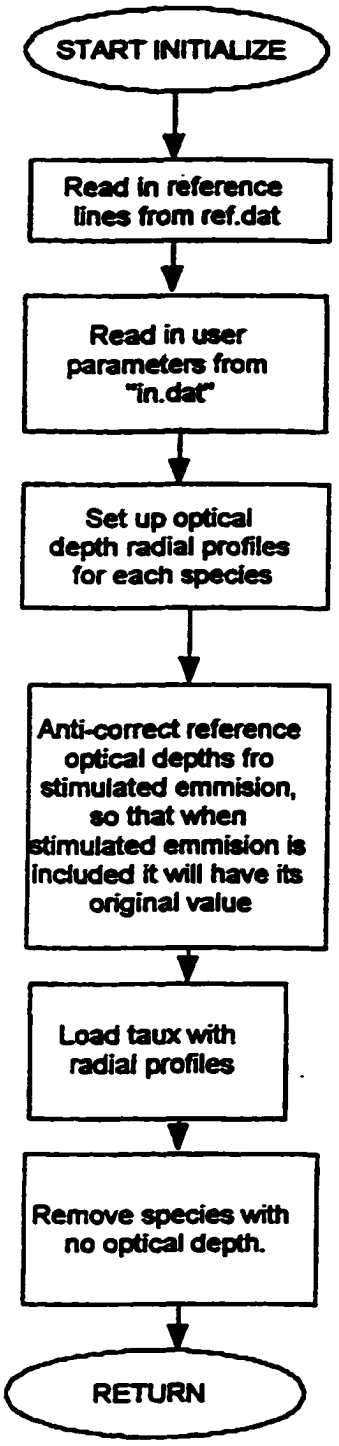
START INITIALIZE
Read in reference lines from ref.dat
Read in user parameters from "in.dat"
Set up optical depth radial profiles for each species
Anti-correct reference optical depths fro stimulated emmision, so that when stimulated emmision is included it will have its original value
Load taux with radial profiles
Remove species with no optical depth.
RETURN

SECTION 3 BB

i	looping variable

SECTION 4 THETA

crit	cosine of the angle between the tangent to the photosphere and the center of the supernova for this radial zone
pi	3.14159...
rad	the width of a radial zone divided by the radius of the photosphere
step	looping variable

SECTION 5 FILE

i,isto	dummy variables
tex	dummy variable

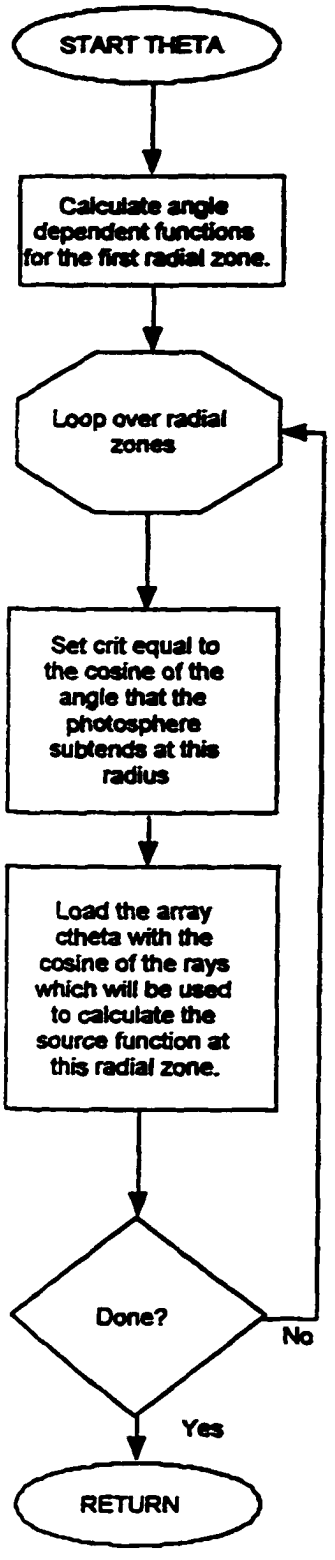
START THETA
Calculate angle dependent functions for the first radial zone.
Loop over radial zones
Set crit equal to the cosine of the angle that the photosphere subtends at this radius
Load the array ctheta with the cosine of the rays which will be used to calculate the source function at this radial zone.
Done?
No
Yes
RETURN

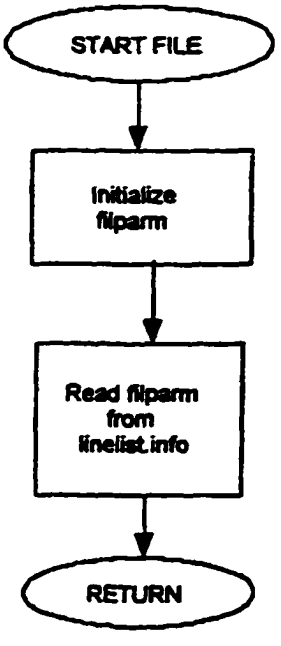
START FILE
Initialize fiparm
Read fiparm from linelist.info
RETURN

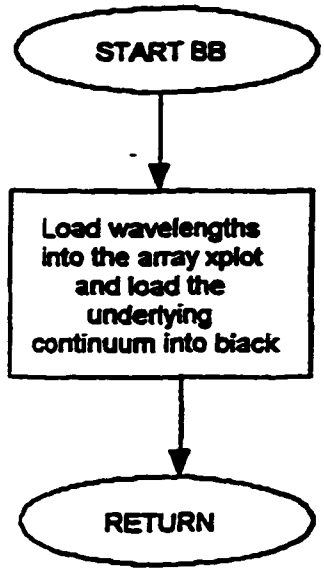
START BB
Load wavelengths into the array xplot and load the underlying continuum into biack
RETURN

SECTION 6 GETBIN

filename	contains path to linelist file
i	dummy variable
IEL	bits 0-11 of IIII containing energy level information
IIII	variable containing compressed from linelist file
IGF	bits 12-23 of IIII containing oscillator strength information
isto*	dummy variables
IWL	bits 24-31 of IIII containing wavelength information
j	dummy variable
wavelength(i)	contains wavelength of wavelength bin i
wk	dummy variable

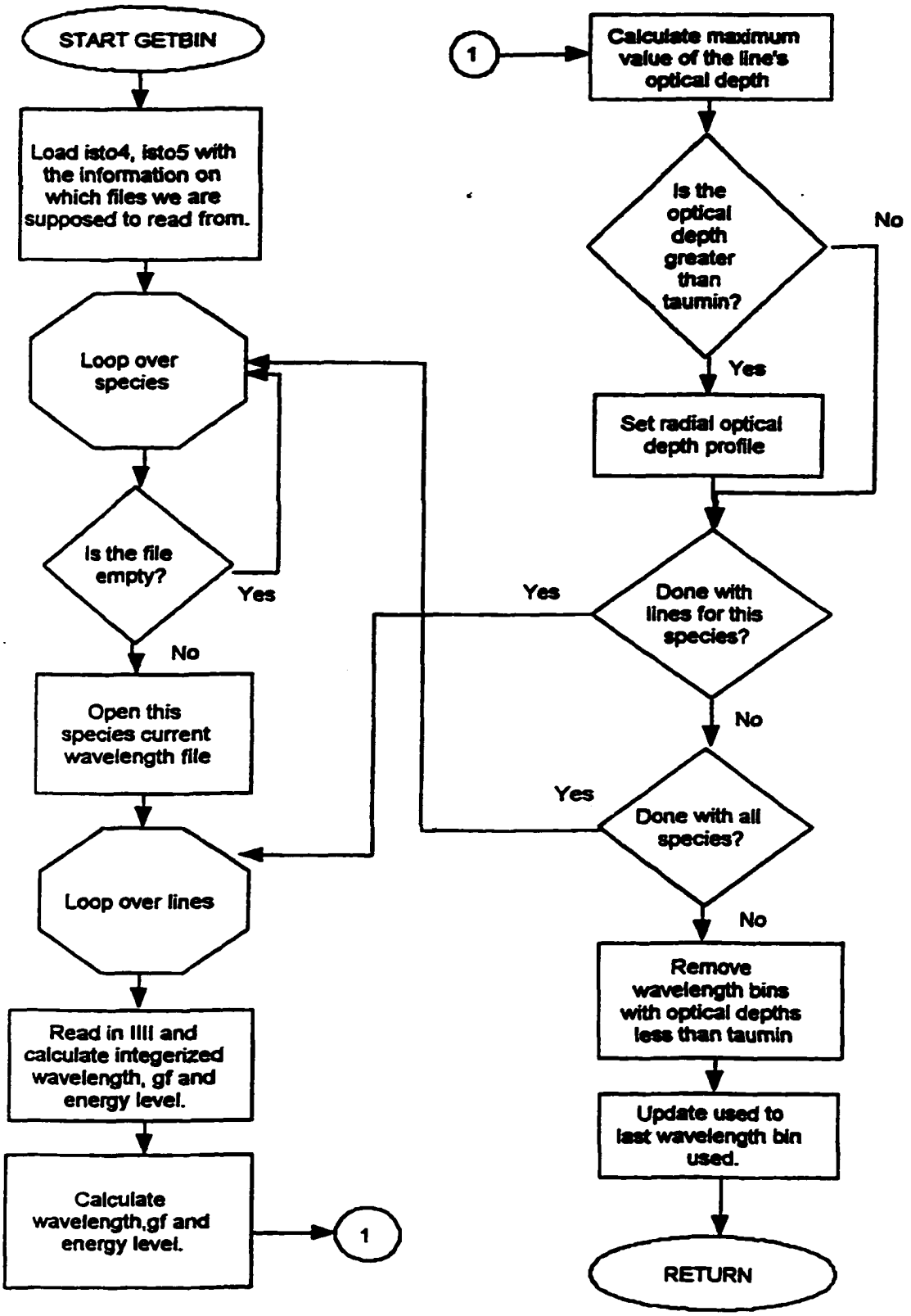
START GETBIN
Load isto4, isto5 with the information on which files we are supposed to read from.
Loop over species
Is the file empty?
Yes
No
Open this species current wavelength file
Loop over lines
Read in IIII and calculate integerized wavelength, gf and energy level.
Calculate wavelength,gf and energy level.
1
1
Calculate maximum value of the line's optical depth
Is the optical depth greater than taumin?
No
Yes
Set radial optical depth profile
Done with lines for this species?
Yes
No
Done with all species?
Yes
No
Remove wavelength bins with optical depths less than taumin
Update used to last wavelength bin used.
RETURN

SECTION 7 SOURCE

dr	velocity difference between line and thisline divided by vphot
factor	the correction factor for stimulated emission
in	the flux in the incoming ray
line	wavelength bin of line that is affecting this line
rm	used in calculating if the interacting line is between vphot and vmax
sp	the source function produced by rays beginning in the photosphere
so	the source function produced by rays beginning outside the supernova
sav	the interpolated source function for a line
tav	the interpolated optical depth for a line
u	cos(q) of the ray being calculated

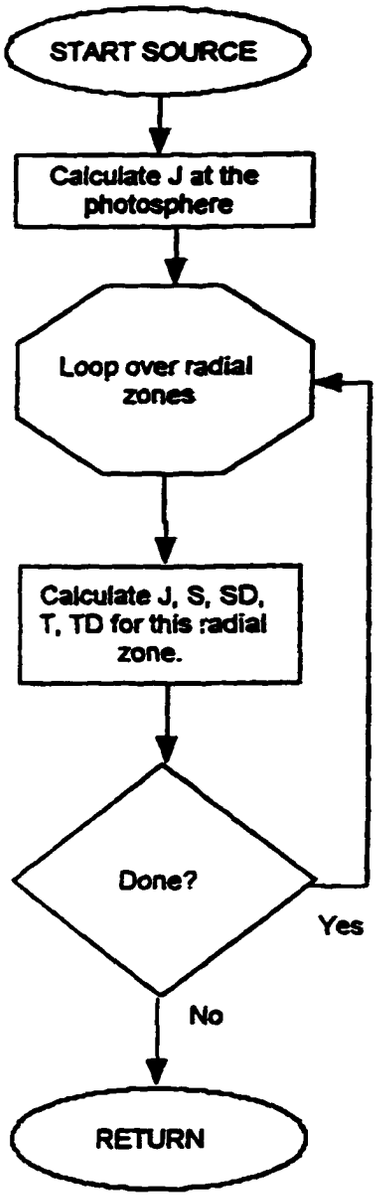
START SOURCE
Calculate J at the photosphere
Loop over radial zones
Calculate J, S, SD, T, TD for this radial zone.
Done?
Yes
No
RETURN

SECTION 8 SPECTRUM

acc	number of spectral rays per radial zone (real number)
iacc	number of spectral rays per radial zone (integral number)
drm	dummy variable
ii	dummy variable
in	flux in one ray
jp	dummy variable
krm	dummy variable
p	impact parameter for a ray
rm	radial location of current line for this ray
tot	summation of flux rays
wk	dummy variable
xp	it is the z coordinate where the ray intersects the photosphere
z	it is the current z position along the ray

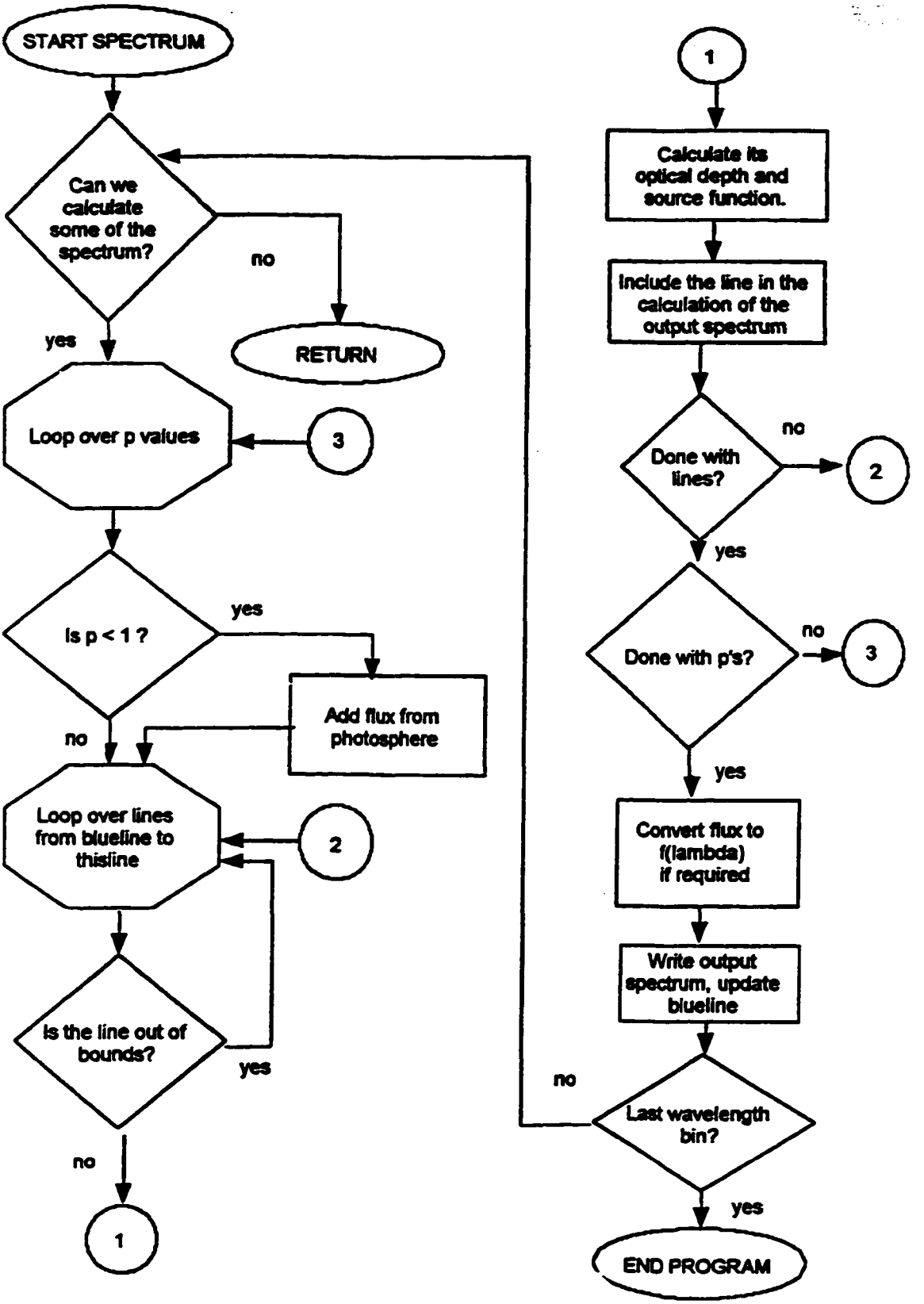
START SPECTRUM
Can we calculate some of the spectrum?
no
RETURN
yes
Loop over p values
3
Is p < 1 ?
yes
Add flux from photosphere
no
Loop over lines from blueline to thisline
2
Is the line out of bounds?
yes
no
1
1
Calculate its optical depth and source function.
Include the line in the calculation of the output spectrum
Done with lines?
no
2
yes
Done with p's?
no
3
yes
Convert flux to f(lambda) if required
Write output spectrum, update blueline
Last wavelength bin?
no
yes
END PROGRAM

APPENDIX 3 - EXAMPLE DATA FILES

Section 1 - in.dat

```
$parms

  vphot   = 13000.0
  vmax    = 35000.0
  tbb     = 14000.0
  ea      = 2000.0
  eb      = 9000.0
  nlam    = 5000
  flambda = .false.
  taumin  = 0.01
  grid    = 64
  stspec  = 3000.
  pwrlaw  = .false.
  pwrlawin = 10.
  zeta    = 1.0

  numref  = 4
  an      =   8,    11,   12,    14
  ai      =   0,     0,    1,     1
  taul    =  0.5,  0.00,  1.5,  15.0
  vmine =  16.0, 14.0, 15.5,  14.0
  vmaxe=  50.0, 50.0, 50.0,  30.0
  ve      = 2.40, 2.40, 2.40,  2.40
  temp    = 11.0, 11.0, 11.0,  11.0

$END
```

Anything down here is just for the users use it is not read by synow. Users are incouraged to use this space to record a history of their runs.

Section 2 - ref.dat

```
  656.2797  .710  1  0  10.21
  587.5615  .409  2  0  20.99
  468.5698 1.181  2  1  48.43
  670.7761 -.009  3  0   0.00000000
  548.4466 -.294  3  1  59.095
  457.2665  .591  4  0   5.284
  467.3422  .767  4  1  12.176
  614.1750 -.827  4  2 121.803
  821.1904 0.000  5  0   5.941
  703.0198 0.173  5  1  16.110
  783.5246 -.096  5  2  22.370
```

449.9400 -.943 5 3 203.06832886
940.5730 .225 6 0 7.69442320
426.7261 .769 6 1 18.06866455
464.7418 .078 6 2 29.572
580.1313 -.199 6 3 37.59567642
868.0282 .236 7 0 10.34888363
567.9558 .280 7 1 18.50635910
409.7355 -.016 7 2 27.472
638.0753 -.595 7 3 48.272
460.3737 -.283 7 4 56.624
777.1944 .324 8 0 9.15758514
732.0664 -8.432 8 1 3.32828021
436.3209 -8.340 8 2 2.517
479.8275 -.080 8 3 59.472
511.4057 -.682 8 4 69.676
685.6026 .420 9 0 12.712
402.4727 .190 9 1 22.701
640.2246 .360 10 0 16.63995552
588.9951 .117 11 0 .00000000
518.3604 -.180 12 0 2.72005367
448.1126 .740 12 1 8.87479210
309.2710 -.187 13 0 .01391125
704.2083 .350 13 1 11.33081627
700.5880 -.980 14 0 5.99152946
634.7109 .297 14 1 8.13122845
455.2622 .181 14 2 19.04022598
979.6828 .220 15 0 6.99400520
650.7979 .622 15 1 10.90000153
921.2863 .420 16 0 6.53269863
545.3855 .557 16 1 13.68874454
425.3589 .400 16 2 18.26670456
837.5943 .460 17 0 8.93291092
811.5311 .407 18 0 11.56286621
294.2893 -.630 18 1 17.16156578
766.4911 .130 19 0 .00000000
426.3445 0.070 19 1 20.23800087
422.6728 .265 20 0 .00000000
393.3663 .151 20 1 .00000000
391.1815 .560 21 0 .02089773
552.6790 .064 21 1 1.77040029
365.3496 .522 22 0 .04802654
334.9408 .586 22 1 .04884164
298.4744 .154 22 2 5.17716789
437.9230 .592 23 0 .30101219
327.6117 .500 23 1 1.12940204

357.8684	.472	24	0	.00000000
283.5629	.572	24	1	1.55130816
322.8089	.440	25	0	2.11687112
344.1988	-.244	25	1	1.77841234
358.1195	.404	26	0	.86007494
501.8440	-1.400	26	1	2.89465094
301.3131	-0.961	26	2	10.32077980
687.2388	-1.589	27	0	2.01053166
416.0673	-1.828	27	1	3.41193938
281.1708	-1.566	27	2	8.80575943
301.1998	.149	28	0	.42330810
406.7031	-1.835	28	1	4.03449154
273.3475	-1.622	28	2	10.20090675
553.5480	0.200	56	0	0.00000000
455.4027	0.190	56	1	0.00000000

Section 3 - linelist.info

This file is much too long to be presented here. Therefore a couple of lines from it are presented. From left to right the fields represent the atomic number, the ionization stage, the wavelength file number, the maximum and minimum values of the ln(gf) in that file, the maximum and minimum values of the excitation of the lower level in that file and the number of transitions in that file.

```
2 0 5 -0.14190E+01 -0.18671E+02  0.16628E+06  0.15986E+06      164
2 1 5  0.43300E+00 -0.30300E+00  0.39014E+06  0.39014E+06        3
```

Appendix 4 Auxiliary programs

Section 1 REDD

REDD is an auxialiary program that is run nearly every time SYNNEW is run. REDD reads the output spectrum from the file fort.11. REDD reddens the output spectrum, renormalizes the spectrum at a user defined wavelength and flux which are contained in the file fort.77.

```
c THIS PROGRAM REDDENS when avmag is positive and dereddens when avmag is
negative

      REAL avmag,xplot(10005),f(10005)
      REAL  aa,a,b,rv,x,y
      INTEGER h,i,j,k,l

C  THIS ROUTINE BASED ON ApJ (345) Oct 1, 1989 pg 245, Cardelli, Clayton,
Mathis
C
C  Rv is a parameter that is the extinction in the visual divided by the
C  B-V color excess
C  Rv has values around 3.1, but can vary from 2.60 to 5.30
C  x= 1./Lambda in inverse microns.
      READ (77,*) avmag
      READ (77,*) wavn,fluxn
      ia=1
   1  READ (11,*,end=2) xplot(ia),f(ia)
      if (xplot(ia).lt.wavn) ii=ia
      ia=ia+1
      GOTO 1

   2  Rv=3.1

C   DO VERY FAR UV

      do  5 h=1, ia-1
      x=10000./xplot(h)
      if (x.lt.8.) goto 6
      y=x-8.
      a=-1.073-.628*y+.137*y*y-.070*y*y*y
```

```
      b=13.670+4.257*y-.420*y*y+.374*y*y*y
      aa=avmag*(a+b/rv)
      f(h)=f(h)*10**(-aa/2.512)

 5    enddo
 6    do 10 i=h, ia-1

      x=10000./xplot(i)
C  NOW DO FAR UV
      if (x.lt.5.9) goto 11

      a=-0.04473*(x-5.9)*(x-5.9)-.009779*(x-5.9)*(x-5.9)*(x-5.9)
      b=.2130*(x-5.9)*(x-5.9)+.1207*(x-5.9)*(x-5.9)*(x-5.9)
      a=a+1.752-.316*x-.104/((x-4.67)*(x-4.67)+.341)
      b=b-3.090+1.825*x+1.206/((x-4.62)*(x-4.62)+.263)

      aa=avmag*(a+b/rv)
       f(i)=f(i)*10**(-aa/2.512)
10    enddo

11    do 20 j=i,ia-1
      x=10000./xplot(j)

C  NOW DO UV
      if (x.lt.3.3) goto 21

      a=+1.752-.316*x-.104/((x-4.67)*(x-4.67)+.341)
      b=-3.090+1.825*x+1.206/((x-4.62)*(x-4.62)+.263)
      aa=avmag*(a+b/rv)
      f(j)=f(j)*10**(-aa/2.512)

20    enddo

21    do 30 k=j,ia-1
      x=10000./xplot(k)

C  NOW DO OPTICAL
      if (x.lt.1.1) goto 31
      y=x-1.82
      a=1.+.17699*y-.50447*y*y-.02427*y*y*y+.72085*y*y*y*y
      a=a+.01979*y*y*y*y*y-.77530*y*y*y*y*y*y+.32999*y*y*y*y*y*y*y
      b=1.41338*y+2.28305*y*y+1.07233*y*y*y-5.38434*y*y*y*y
      b=b-.62251*y*y*y*y*y+5.30260*y*y*y*y*y*y-2.09002*y*y*y*y*y*y*y

      aa=avmag*(a+b/rv)
```

```
      f(k)=f(k)*10**(-aa/2.512)

 30   enddo

 31   do 40 l=k,ia-1
C  NOW DO INFARED
      x=10000./xplot(l)

      if (x.lt.0.3) goto 40

      a=.574*x**1.61
      b=-.527*x**1.61

      aa=avmag*(a+b/rv)
      f(l)=f(l)*10**(-aa/2.512)

 40   enddo

      do i=1,ia-1
      WRITE (10,*) xplot(i),f(i)*fluxn/f(ii)
      enddo
      END
```

Section 2 *run*

Run is a simple shell script that does routine maintainence for SYNNEW runs. First *run* copies a temporary copy of the in.dat file that was used on the last run to a file named old.dat for direct comparison with in.dat. *Run* then removes the old ouput files containing the output files that might be left around from previous runs. *Run* then runs SYNNEW, copies the in.dat file to a temporary file and moves the old output spectrum to a file called old.syn. *Run* then runs REDD and moves the current output spectrum to spectrum.syn. Finally, *run* runs a script called *vu* that launches a graphical viewer with the observed spectrum, the current spectrum, and the spectrum from the previous run. An example *run* script is provided below

```
cp temp.dat old.dat
rm fort.11 fort.10
synnew
cp in.dat temp.dat
mv spectrum.syn old.syn
echo ^G
redd
mv fort.10 spectrum.syn
echo ^G
echo ^G
vu &
```

Section 3 *runmore*

The purpose of *runmore* is to quickly allow the user to move through a series of spectra, usually of the same supernovae. The example below covers my SN1991T spectra. Each spectra has its own directory. The names of these directories are stored in the array i. Then each directory is visited by *runmore*. When *runmore* looks in a directory, it looks to see if this run has begun, then it looks to see if the run is complete. If it is complete, *runmore* launches *vu* to display the results of that run and launches a textedit window to allow the user to edit the appropriate in.dat file. When the user close the textedit window, *runmore* enters that directory into the later file which is used by the script *cmaster* to find a computer to do this run on. The text of a *runmore* script for SN1991T is presented below.

```
#!/bin/csh
#

set a  = '/home2/bubba/fisher/back/91T'
set i = ($aV91Tap $aVapr18 $aVapr19 $aVapr20 $aVmay05
$aVmay06 $aVmay07 $aVmay08)($aVmay11 $aVmay12 $aVmay14
$aVmay15 $aVmay16 $aVmay17 $aVmay18 $aVmay19)($aVjun8
$aVjun16 $aVjul12)

foreach j ($i)
echo $jVspectrum.syn
rm retard
grep $j /home2/bubba/fisher/master/later > retard
if (-z retard) then
if (-e $jVfort.11) then
  tail $jVfort.11
 else
  chdir $j
  vu &
```

```
  textedit note &
  textedit -Ws 1000 531 -Wp 10 10 in.dat
  if (-z /home2/bubba/fisher/master/later) then
    echo $j/run  >/home2/bubba/fisher/master/later
  else
    echo $j/run >>/home2/bubba/fisher/master/later
  endif

endif
else
echo in queue
endif
end
cat /home2/bubba/fisher/master/late
```

Section 4 *cmaster*

Cmaster is a c-shell script that was designed to allow a more optimal use of computational resources available for this project. *Cmaster* consists of two lists, the first list is a list of machines available for runs. The second list is contained in the file later. Later consists of a list of directories where jobs are ready to be run. *Cmaster* searches the list of computers for running jobs, and when there is an available machine it takes the first entry in later and runs it there. After looping through all the machines, *cmaster* waits five minutes for jobs to complete and then loops again. The most common use of cmaster is when the computational facilities are overloaded and jobs begin to back up. The secondary use of *cmaster* is to map out wide ranges of parameter space. A set of directories containing slightly different in.dat files can quickly be set up, then *cmaster* can accomplish the needed runs as efficiently as possible. On our network of approximately thirty Sun workstations,

cmaster efficiently can accomplish hundreds or thousands of runs per day, without human interaction. The text of *cmaster* is listed below.

```
#!/bin/csh
#
set b = ( palantir dimension brigit steve particle turks pixel2 bubba
sarex \
 m2sun phyast dyno sideout pixel chris qft watsonsun merlin adagio )

set a  = '/home2/bubba/fisher/master'
date
echo master looping

#   Search rsh's foreach computer
cd /home2/bubba/fisher/master
foreach i ($b)
echo $i
  rm file
  ps -u fisher -f|grep rsh |grep -v grep |grep $i >file
  if (-z file) then
     echo $i is unoccupied
     rm next
     set temp="nice -19 csh "
     set temp2=`head -1 later`
       echo $temp $temp2 $i > next
      chmod +x next
      /home2/bubba/fisher/master/next $i &
     sleep 5
     cat /home2/bubba/fisher/master/next
     mv later moving
     tail +2 moving > later
     rm moving
  endif
  if (-z /home2/bubba/fisher/master/later) break
end

if (-z /home2/bubba/fisher/master/later) then
```

```
  echo master program has emptied the buffer
  date
else
  cat later
  sleep 300
  /home2/bubba/fisher/master/cmaster &
endif
```

Section 5 *runalot*

The shell script runalot is handy when a large number of similar runs need to be accomplished. An example *runalot* is given below. This runalot steps over excitation temperatures for the iron peak elements.

```
#!/bin/csh
#
foreach i ( 7 8 9 10 11 12 13 14 15)
rm in.dat
cat << eof >in.dat
  \$parms

  vphot   = 4000.0
  vmax    = 18000.0
  tbb     = 25000.0
  ea      =  3300.0
  eb      =  6000.0
  nlam    =  4000
  flambda  = .false.
  taumin   =   0.01
  grid    = 32
  stspec   = 4300.
  pwrlaw   = .false.
  pwrlawin = 10.
  zeta    =   1.0

  numref   =   14

  an  =    8,  11,  2,  14,   20,   16,   22,    24,    6,   26,  26,   28,   27,  27
  ai  =    1,   0,  0,   1,    1,    1,    1,     1,    1,    1,   2,    1,    1,   2
  tau1 =  1.0,2.00, 0.0, 0.0,  70.0,  0.0,  00.0, 5000.0,  0.0,  20.0,  0.0,  0.0,  10.0,  0.0
  vmine=  13.0,10.0, 0.0,12.0,  9.0,  12.0,  00.0,   0.0,  8.0,  0.0,  0.0,  0.0,  0.0,  0.0
```

```
  vmaxe=  50.0,13.0,50.0,50.0,  16.0, 17.0,  50.0,   12.,  50.0,   12., 17.0,  50.0,   12.,
17.0
  ve  =  6.40,2.40,2.40,2.40,  2.90, 2.00,  2.90,  2.90,  8.90,  3.00, 9.90,  2.90,  3.00,
2.90
  temp =   7.0,11.0, 7.0, 7.0,  10.0,  7.0,  7.0,  $i.0,  30.0,  $i.0,  9.0,   6.0,  $i.0,  7.0

 \$END

eof
nice -19 run
mv spectrum.syn t$i
continue
end
```

You are probably thinking that it looks like an in.dat file with some junk around it. You are right. *Runalot* loops over each item contained within the parenthesis on the top line. It executes the rest of the script once for each entry given. The next line erases the old in.dat file, if it exists. The next line loads all the lines that follow into an in.dat file, while replacing any $i variables with the current item. Then *runalot* executes a *run* script. Finally, runalot moves the output spectrum to a filename that depends on $i so that the output files are not written over the top of one another. This routine is good for mapping out a grid of models, or for searching through all the species to identify a previously unknown line. Beware, it is very easy to set up a *runalot* script that can take longer than the age of the universe to finish running.

Section 6 READER

READER is a program designed to search the linelist. The user can run READER on a particular in.dat file and every transition that is greater than taumin will be put into the file lines.syn. This program is handy whenever the user needs to know what optical depth a certain line has or what line is producing a particular feature.

This routine used to be part of SYNNEW, but it was removed to decrease run time, decrease unnecessary network trafic and save disk space. The user is strongly warned to watch READER closely, as it can quite easily generate files that are 100 Megabytes or more.